PHENOMENA IN THE PROPAGATION OF ULTRASONIC VIBRATIONS IN NICKEL WIRE

by

JOHN DALLAWAY COULTER
B.Sc. (Electrical) Engineering, Cape Town

Submitted to the University of Cape Town
in partial fulfilment of the requirements
for the degree of Master of Science
in Engineering
September 1987

ABSTRACT

A wave-train-echo technique, with repeated forward-and-return travels of the signal, was used to study the propagation of ultrasonic waves in nickel wire. In particular, the origin of often observed anomalous waves in nickel wire was investigated. A possible explanation of an aspect of the phenomenon was devised.

During continuing investigation of the phenomenon of anomalous waves, an unexpected effect of stress on the attenuation of ultrasonic waves in annealed nickel wire was observed. Attention was transferred to the new phenomenon, and extensive experimental work carried out to measure the effects of direct and flexural stress on the attenuation. The effect was found to occur with torsional stress also.

Computer-aided determinations of attenuation were made from the experimental readings of signal strength for variations of stress and signal frequency.

A detailed study and documentation of known processes of attenuation of acoustic vibrations in solids was made.

Indications of the nature of the mechanism of stress-dependent attenuation have been sought, and a tentative conclusion arrived at.

ACKNOWLEDGEMENTS

I wish to thank Professor J.F.W. Bell for assistance provided in the choosing of a topic for research, and for much valuable guidance given during the extended period for which the work continued.

My thanks are due also to the Department of Electrical and Electronic Engineering of the University of Cape Town, and to the Council for Mineral Technology, for facilities provided.

CONTENTS

CHAPTER 1

INTRODUCTION

1-1. Magnetostriction Effects, and Their Use in the Production and Detection of Mechanical Vibrations in Wires

Ferromagnetic materials, subjected to a magnetic field, exhibit a change in physical dimensions, an effect known as magnetostriction. Conversely, those materials, strained by an external force, exhibit a change in magnetic properties. All such changes, which take a number of well defined forms, are termed magnetostriction effects.

The Joule effect takes the form of change in dimension of a body along lines parallel to the lines of magnetic induction when the magnetization is varied, and is the effect used in the production of longitudinal vibrations in wires. The changes in transverse dimensions, and in volume, which also occur, are unimportant here. The curves of Figure 1-1-1 illustrate the Joule effect.

The Villari effect, in which the magnetization of the material in a magnetic field varies when a strain is induced by an external force, is used in detecting, and in measuring the relative intensity of, longitudinal vibrations in wires. The curves of Figure 1-1-2, and those of Figure 1-1-3, which were derived from the curves of Figure 1-1-2, illustrate the Villari effect.

Magnetostriction (the Joule effect) is of small magnitude: in the alloy of iron and cobalt known as permendur, one of the most strongly magnetostrictive materials, the change in length per unit length at magnetic saturation is a little greater than 50×10^{-6}. Nickel, the 45%-nickel nickel-iron alloy of the permalloy range, cobalt and iron, in that order, exhibit magnetostriction in decreasing degree.

In magnetostriction, for a given material, the sign of the change in length is independent of the polarity of the magnetization; the relationship between change in length and flux density approximates a square law, as shown in Figure 1-1-1b. However, the sign of the change in length is dependent on the material. In permendur, and in 45%-nickel permalloy, magnetization causes an increase in length, while in nickel and in annealed cobalt it causes a reduction. In iron, magnetization increasing from zero causes a sharp initial

increase in length, followed by a gradual decrease to less than the original length.

Magnetostriction is explained physically as deformation of the lattice of a crystal resulting from changes in interatomic forces; the deformation occurs during the two stages of magnetization. In the first stage, which lasts until saturation begins, at the knee of the magnetization curve, boundaries of the magnetic domains within the crystal shift as vectors of magnetization of crystal unit cells near the boundaries of some domains switch from one direction of easy magnetization to another, thus becoming aligned with those of unit cells in adjacent domains. In the second stage, which begins as saturation begins, vectors of magnetization of unit cells in the now combined domains switch from directions of easy to directions of more difficult magnetization, which are better aligned with the magnetizing field. (Crawford, 1955, pp. 86 and 87; Brailsford, 1968, p. 1 et seq.; Brailsford, 1960, p. 34 et seq.)

For the experimental work on the propagation of mechanical vibrations in wires carried out in these investigations, nickel wire was used because of the relatively large magnetostriction effects that are obtained with it, and because of its ready availability.

In Figure 1-1-4 is shown a magnetostriction transducer for the excitation of longitudinal vibrations in a nickel wire and for the generation of electrical signals by such vibrations, as a means of detecting them. The transducer coil, which would have, typically, some hundreds of turns of thin wire, is wound on a thin-walled former having an internal diameter only slightly larger than that of the nickel wire, so that as little leakage flux (flux not passing through the nickel wire) as possible will be induced in the coil. The capacitance of the decade capacitor is set to a value for which the combination of coil and capacitor resonates at the frequency of the applied alternating-voltage wave shown. Since magnetostrictive contraction of the nickel wire is independent of the polarity of the applied field, application of only the alternating field of the transducer coil to the nickel wire would result in the same contraction of the wire at each half-cycle, and therefore in longitudinal vibration of the nickel wire at double the frequency of the alternating field. To prevent frequency

doubling, and to improve the sensitivity of the transducer, a steady polarizing field is applied to the transducer by means of the biasing permanent magnet shown. The effect of such a polarizing field can be shown algebraically by consideration of the flux produced (Hueter and Bolt, pp. 172 and 173). With reference to Figure 1-1-1b, let the relative change in length $\frac{\Delta \ell}{\ell}$, the strain, be given by the quadratic equation

$$\frac{\Delta \ell}{\ell} = kB^2 \qquad (1\text{-}1\text{-}1)$$

where B is the flux density in the nickel wire, and k is a constant of proportionality, dependent on the material, having the dimensions tesla^{-2}. It is seen that, if B varies about zero, the value of $\frac{\Delta \ell}{\ell}$ is independent of the sign of B, and becomes relatively very small for small values of B. Suppose now that the nickel wire is given a steady polarizing flux of density B_o, by which a static strain x_o is produced. Then

$$\frac{\Delta \ell}{\ell} = x_o = kB_o^2 \qquad (1\text{-}1\text{-}2)$$

A substantially linear effect will now be obtained if a small varying flux of density B is superimposed on the polarizing flux of density B_o. Differentiation of the middle and right-hand parts of Equation 1-1-2 with respect to B_o gives

$$\frac{dx_o}{dB_o} = 2kB_o$$

whence

$$dx_o = 2kB_o dB_o \qquad (1\text{-}1\text{-}3)$$

Putting x for dx_o, and B for dB_o, in Equation 1-1-3, leads to the basic magnetostrictive strain equation

$$x = 2KB_oB = \beta B \qquad (1\text{-}1\text{-}4)$$

where $\beta = 2kB_o$ is a magnetostrictive strain constant having the dimensions tesla^{-1}. If the ends of the bar are now clamped, so that stress is developed in it, the relationship between the incremental stress X and the incremental flux density B can be expressed as

$$X = \Lambda B \qquad (1\text{-}1\text{-}5)$$

where Λ is the magnetostrictive stress constant in newtons per weber. Application of Hooke's law gives

$$X = xE \qquad (1\text{-}1\text{-}6)$$

where E is Young's modulus. Substituting, for x in Equation 1-1-6, the expression given by Equation 1-1-4, gives

$$X = 2kB_oBE \qquad (1\text{-}1\text{-}7)$$

and substituting, for X in Equation 1-1-5, the expression given by Equation 1-1-7, and rearranging, yield

$$\Lambda = 2kB_oE \qquad (1\text{-}1\text{-}8)$$

Equations 1-1-4, 1-1-5 and 1-1-7 are not exact; however, the error will be small for $B \ll B_o$. Equations 1-1-4 and 1-1-7 indicate that, for the presence of a polarizing flux (of density B_o), the incremental strain x for a free bar or the incremental stress X, for a bar of which the ends are clamped, is proportional to the density B of the small varying flux, and that the coefficients of proportionality vary as B_o, for constant values of k and E.

In the reverse action of the transducer, the use of a biasing field is necessary for the provision of a magnetic flux in the nickel wire within the coil that can be caused to vary by varying stress in the nickel wire, and so to induce an electromotive force in the coil.

In the operation of launching longitudinal waves in the nickel wire, the position of the transducer coil on the wire is adjusted so that the distance from the centre of the coil to the left-hand end of the wire, as seen in Figure 1-1-4, is one quarter of the wavelength of the signal. For that condition, the wave propagating from the centre of the coil to the left undergoes a phase shift of 180° in travelling the path of a total length of half a wavelength, as well as a phase shift of 180° on reflection at the end of the line. Hence the reflected wave, on its return to the centre of the coil, is in phase with the wave being propagated to the right, and combines with it to increase its amplitude.

In the action of the transducer in abstracting energy from the line, the wave travelling from the right and its reflected wave, travelling in the opposite direction, are in phase at the centre of the transducer coil; there they together cause a larger voltage to be induced in the coil than would the incoming wave alone.

For a line of which the end is fixed, so that displacement of the end does not occur, reflection of the wave takes place without reversal of phase; the distance between the centre of the transducer coil and the end of the line is then made equal to half the wavelength of the signal, for greatest reinforcement by the reflected wave.

Correct positioning of the coil on the wire is effected by adjustment of position for greatest output from the transducer.

1-2. Propagation of Longitudinal, Plane Waves in a Thin Bar

The following mathematical analysis was compiled with reference to Hueter and Bolt, 1955; Kinsler and Frey, 1950; and Bell, notes.

1-2-1. For a Bar Having Negligible Loss. For a bar stressed uniformly by forces F_x and $-F_x$ at its ends, acting parallel to its axis, the x axis, as shown in Figure 1-2-1, Hooke's law, by which |strain| is proportional to |stress|, is valid; hence

$$\frac{F_x}{A} = -E\frac{d\xi}{dx}$$

where A is the cross-sectional area of the bar

ξ is the displacement of a transverse plane

$\frac{d\xi}{dx}$ is the longitudinal strain

E is Young's modulus

On rearrangement, the equation becomes

$$F_x = -EA\frac{d\xi}{dx} \qquad (1\text{-}2\text{-}1)$$

Figure 1-2-2 shows a segment of a thin bar, that is, a bar having lateral dimensions small compared with the wavelength of the vibrations that will be propagated in it. The cross-sectional area of the bar is A, the density of the material is ρ and the length of the segment, unstressed, is dx. The force at the section at x is F_x, and that at the section at $x + dx$ is $F_x + dF_x = F_x + \frac{\partial F_x}{\partial x}\,dx$. Partial differential coefficients of F_x and ξ are to be used since F_x and ξ are functions of both x and time t. The net force to the right, $-dF_x$ (negative since it is tensile) is given by

$$-dF_x = F_x + \frac{\partial F_x}{\partial x}\,dx - F_x$$

so that

$$dF_x = -\frac{\partial F_x}{\partial x}\,dx \qquad (1\text{-}2\text{-}2)$$

Substituting, for F_x on the right-hand side of Equation 1-2-2, the expression given by Equation 1-2-1, gives

$$dF_x = EA\,\frac{\partial^2 \xi}{\partial x^2}\,dx \qquad (1\text{-}2\text{-}3)$$

The mass of the segment of length dx is $\rho A dx$; the acceleration $\frac{\partial^2 \xi}{\partial t^2}$ of the segment will be determined by the equation

$$\rho A dx \frac{\partial^2 \xi}{\partial t^2} = EA\,\frac{\partial^2 \xi}{\partial x^2}\,dx \qquad (1\text{-}2\text{-}4)$$

whence

$$\rho\,\frac{\partial^2 \xi}{\partial t^2} = E\,\frac{\partial^2 \xi}{\partial x^2} \qquad (1\text{-}2\text{-}4a)$$

so that

$$\frac{\partial^2 \xi}{\partial t^2} = \frac{E}{\rho}\,\frac{\partial^2 \xi}{\partial x^2} \qquad (1\text{-}2\text{-}4b)$$

Putting

$$c^2 = \frac{E}{\rho} \qquad (1\text{-}2\text{-}5)$$

leads to the relation

$$\frac{\partial^2 \xi}{\partial t^2} = c^2\,\frac{\partial^2 \xi}{\partial x^2} \qquad (1\text{-}2\text{-}6)$$

Equation 1-2-6 represents one-dimensional propagation of longitudinal waves.

A complex exponential solution of Equation 1-2-6, providing for the propagation, in the direction of increasing x, of vibrations having simple harmonic motion, is

$$\xi = \xi_o e^{j\omega\left(t-\frac{x}{c}\right)}$$

in which ξ_o is the amplitude, ω is the angular velocity and

$c = \sqrt{\frac{E}{\rho}}$ is the velocity of propagation of the vibrations. Multiplying out by ω the terms in brackets in the exponent, and putting

$$\beta = \frac{\omega}{c} \tag{1-2-7}$$

lead to the relation

$$\xi = \xi_o e^{j(\omega t - \beta x)} \tag{1-2-8}$$

β is termed the wavelength constant, since $\beta = \frac{\omega}{c} = \frac{2\pi}{\lambda}$, where λ is the wavelength.

From Equations 1-2-8 and 1-2-1 can be derived expressions for the particle velocity u and the force F_x in the bar, and for the characteristic impedance Z of the bar and the wave power P being transmitted by the bar. The particle velocity, uniform over any cross-section of the bar, is obtained by differentiation of Equation 1-2-8 with respect to t: thus

$$\begin{aligned} u &= \frac{\partial \xi}{\partial t} \\ &= \frac{\partial}{\partial t} \xi_o e^{j(\omega t - \beta x)} \\ &= j\omega \xi_o e^{j(\omega t - \beta x)} \end{aligned}$$

so that

$$u = j\omega\xi \tag{1-2-9}$$

and the force acting at a cross-section of the bar, given by Equation 1-2-1 is, in terms of a partial differential coefficient,

$$F_x = -EA \frac{\partial \xi}{\partial x} \tag{1-2-10}$$

Differentiation of Equation 1-2-8 with respect to x gives

$$\frac{\partial \xi}{\partial x} = -j\beta \xi_o e^{j(\omega t - \beta x)}$$

so that

$$\frac{\partial \xi}{\partial x} = -j\beta\xi \tag{1-2-11}$$

Substituting, for $\frac{\partial \xi}{\partial x}$ in Equation 1-2-10, the expression given by Equation 1-2-11, gives

$$F_x = EAj\beta\xi \qquad (1\text{-}2\text{-}12)$$

The characteristic impedance Z is given by

$$Z = \frac{F_x}{u} \qquad (1\text{-}2\text{-}13)$$

Substituting, for F_x and u in Equation 1-2-13, the expressions given by Equations 1-2-12 and 1-2-9, gives

$$Z = \frac{EAj\beta\xi}{j\omega\xi}$$

$$= \frac{EA\beta}{\omega} \qquad (1\text{-}2\text{-}14)$$

Substituting, for β in Equation 1-2-14, the expression given by Equation 1-2-7, gives

$$Z = \frac{EA}{c} \qquad (1\text{-}2\text{-}15)$$

Substituting, for c in Equation 1-2-15, the expression $\sqrt{\frac{E}{\rho}}$ derived from Equation 1-2-5, gives

$$Z = \sqrt{E\rho}\,A \qquad (1\text{-}2\text{-}16)$$

and substituting, for E in Equation 1-2-15, the expression ρc^2 derived from Equation 1-2-5, gives

$$Z = \rho cA \qquad (1\text{-}2\text{-}17)$$

The instantaneous wave power P is given by

$$P = F_x u \qquad (1\text{-}2\text{-}18)$$

Substituting, for F_x and u in Equation 1-2-18, the expressions given by Equations 1-2-12 and 1-2-9, gives

$$P = EA\beta\omega(j\xi)^2$$

Substituting, for β in the equation, the expression $\frac{\omega}{c}$ given by Equation 1-2-7, gives

$$P = \frac{EA}{c} \omega^2 (j\xi)^2$$

whence, by substitution of Z for $\frac{EA}{c}$ in accordance with Equation 1-2-15, is obtained

$$P = Z\omega^2 (j\xi)^2 \qquad (1\text{-}2\text{-}19)$$

The average wave power P_{av} will be given by

$$P_{av} = \tfrac{1}{2} Z\omega^2 \xi_o^2 \qquad (1\text{-}2\text{-}20)$$

Also, substituting, for u in Equation 1-2-18, the expression derived from Equation 1-2-13, gives

$$P = \frac{F_x^2}{Z} \qquad (1\text{-}2\text{-}21)$$

Thence, the average wave power P_{av} will be given by

$$P_{av} = \frac{F^2 x_o}{2Z} \qquad (1\text{-}2\text{-}22)$$

where F_{xo} is the amplitude of F_x.

1-2-2. <u>For a Bar Having Significant Frictional Loss.</u> If it is assumed that the dissipative forces in the bar are proportional to the velocity of particles in the bar, the resulting loss of energy of the waves can be represented by an extra term in Equation 1-2-4a, which then becomes

$$\rho \frac{\partial^2 \xi}{\partial t^2} + R' \frac{\partial \xi}{\partial t} = E \frac{\partial^2 \xi}{\partial x^2} \qquad (1\text{-}2\text{-}23)$$

where R′ is a damping constant in newtons per cubic metre per unit velocity. Division of Equation 1-2-23 by ρ gives

$$\frac{\partial^2 \xi}{\partial t^2} + \frac{R'}{\rho} \frac{\partial \xi}{\partial t} = \frac{E}{\rho} \frac{\partial^2 \xi}{\partial x^2} \qquad (1\text{-}2\text{-}23a)$$

and, by substitution of c^2 for $\frac{E}{\rho}$ as before

$$\frac{\partial^2 \xi}{\partial t^2} + \frac{R'}{\rho} \frac{\partial \xi}{\partial t} = c^2 \frac{\partial^2 \xi}{\partial x^2} \qquad (1\text{-}2\text{-}24)$$

If a solution to Equation 1-2-24 of the usual form

$$\xi = B^* e^{j(\omega t + \gamma x)} \qquad (1\text{-}2\text{-}25)$$

is assumed, where the amplitude B* may be complex, it is seen that

$$-\omega^2 + j\omega \frac{R'}{\rho} = -c^2 \gamma^2 \qquad (1\text{-}2\text{-}26)$$

The propagation constant γ is hence not equal to $\beta = \frac{\omega}{c}$, but is given by

$$\gamma = \pm \frac{\omega}{c} \sqrt{1 - j \frac{R'}{\rho \omega}} \qquad (1\text{-}2\text{-}27)$$

For small loss, for which $\frac{R'}{\rho\omega} \ll 1$, $\left(1 - j \frac{R'}{\rho\omega}\right)^{\frac{1}{2}}$ can be expanded by the binomial theorem and all but the first two terms neglected. Then

$$\gamma = \pm \frac{\omega}{c} \left(1 - j \frac{R'}{2\rho\omega}\right)$$

$$= \pm \left(\frac{\omega}{c} - j \frac{R'}{2\rho c}\right)$$

so that

$$\gamma = \pm \left(\beta - j \frac{R'}{2\rho c}\right) \qquad (1\text{-}2\text{-}28)$$

Substituting, for γ in Equation 1-2-25, the expression given by Equation 1-2-28, gives

$$\xi = B^* e^{j\{\omega t - (\beta - j \frac{R'}{2\rho c}) x\}}$$

$$= B^* e^{\{j(\omega t - \beta x) - \frac{R'}{2\rho c} x\}}$$

from which

$$\xi = B^* e^{-\alpha x} e^{j(\omega t - \beta x)} \qquad (1\text{-}2\text{-}29)$$

where

$$\alpha = \frac{R'}{2\rho c} \qquad (1\text{-}2\text{-}30)$$

α is the attenuation constant.

The particle velocity u is obtained by differentiation of Equation 1-2-29 with respect to t: thus

$$u = \frac{\partial \xi}{\partial t}$$

$$= \frac{\partial}{\partial t} B^* e^{-\alpha x} e^{j(\omega t - \beta x)}$$

$$= j\omega B^* e^{-\alpha x} e^{j(\omega t - \beta x)}$$

so that, as for the lossless line

$$u = j\omega\xi \qquad (1\text{-}2\text{-}31)$$

and the force F_x is given by

$$F_x = -EA \frac{\partial \xi}{\partial x} \qquad (1\text{-}2\text{-}10)$$

Differentiation of Equation 1-2-29 with respect to x gives

$$\frac{\partial \xi}{\partial x} = -(\alpha + j\beta)\xi \qquad (1\text{-}2\text{-}32)$$

and substitution of the right-hand side of Equation 1-2-32 for $\frac{\partial \xi}{\partial x}$ in Equation 1-2-10 gives

$$F_x = EA(\alpha + j\beta)\xi \qquad (1\text{-}2\text{-}33)$$

The characteristic impedance Z, as for the lossless line, is given by

$$Z = \frac{F_x}{u} \qquad (1\text{-}2\text{-}13)$$

Substituting, for F_x and u in Equation 1-2-13, the expressions given by Equations 1-2-33 and 1-2-31, gives

$$Z = \frac{EA(\alpha + j\beta)\xi}{j\omega\xi}$$

$$= \frac{EA(\alpha + j\beta)}{j\omega} \qquad (1\text{-}2\text{-}34)$$

Rearrangement of Equation 1-2-5 gives

$$E = \rho c^2 \qquad (1\text{-}2\text{-}35)$$

Substituting, for E in Equation 1-2-34, the expression given by Equation 1-2-35, gives

$$Z = \frac{\rho c^2 A(\alpha + j\beta)}{j\omega}$$

$$= \rho cA(-j\frac{c\alpha}{\omega} + \frac{c\beta}{\omega}) \qquad (1\text{-}2\text{-}36)$$

Substituting, for $\frac{c}{\omega}$ in Equation 1-2-36, the expression $\frac{1}{\beta}$ derived from Equation 1-2-7, gives

$$Z = \rho cA(1-j\frac{\alpha}{\beta}) \qquad (1\text{-}2\text{-}37)$$

and substituting, for α and β in Equation 1-2-37, the expressions given by Equations 1-2-30 and 1-2-7, gives

$$Z = \rho cA(1-j\frac{R'}{2\rho\omega}) \qquad (1\text{-}2\text{-}38)$$

Without any loss of generality, the complex force amplitude constant $EA(\alpha + j\beta)B^*$ of Equation 1-2-33 may be replaced with F_{xo}, a real constant equal to the force amplitude of such a wave at $x = 0$. Then

$$F_x = F_{xo}e^{-\alpha x}e^{j(\omega t-\beta x)} \qquad (1\text{-}2\text{-}39)$$

Correspondingly, particle velocities of the wave may be represented by

$$u = \frac{F_x}{Z}$$

$$= \frac{F_{xo}}{\rho cA(1-j\frac{\alpha}{\beta})}e^{-\alpha x}e^{j(\omega t-\beta x)}$$

Rationalization of the denominator gives

$$u = \frac{F_{xo}(1+j\frac{\alpha}{\beta})}{\rho cA(1+\frac{\alpha^2}{\beta^2})} e^{-\alpha x} e^{j(\omega t-\beta x)} \qquad (1\text{-}2\text{-}40)$$

The instantaneous wave power is given by the product of the real parts of F_x and u, while the average wave power P_{av} is equal to half the product of the real parts of the amplitudes of F_x and u: thus

$$P_{av} = \tfrac{1}{2} \frac{F_{xo}e^{-\alpha x}F_{xo}e^{-\alpha x}}{\rho cA(1+\frac{\alpha^2}{\beta^2})}$$

$$= \frac{F^2_{xo}\, e^{-2\alpha x}}{2\rho cA(1+\frac{\alpha^2}{\beta^2})} \qquad (1\text{-}2\text{-}41)$$

The factor $e^{-2\alpha x}$ in Equation 1-2-41 represents an attenuation of αx nepers, and a rate of attenuation of α nepers per unit length (per metre in S.I.). The attenuation in decibels is given by the relation

$$\text{attenuation in decibels} = \frac{20}{\log_e 10} \times (\text{attenuation in nepers}) \qquad (1\text{-}2\text{-}42a)$$

whence is obtained

$$\text{attenuation in decibels} = 8{,}686 \times (\text{attenuation in nepers}) \qquad (1\text{-}2\text{-}42b)$$

Rate of attenuation may be expressed otherwise as nepers or decibels per unit time, as logarithmic decrement (often referred to simply as decrement), or as a loss factor $\frac{1}{Q}$. If the rate of attenuation is α nepers per unit length, then

$$\text{rate of attenuation} = \alpha c \text{ nepers per unit time} \qquad (1\text{-}2\text{-}43)$$

where c is the velocity of propagation of the vibrations; in practice, the unit is usually nepers per microsecond. Logarithmic decrement is equal to the number of nepers of attenuation per wavelength, that is, per cycle, so that

$$\text{logarithmic decrement} = \alpha\lambda \qquad (1\text{-}2\text{-}44)$$

and is a dimensionless quantity. From the following approximations relating to damped resonance

$$\text{logarithmic decrement} = \frac{1}{2} \frac{\text{energy lost per cycle}}{\text{energy stored}} \qquad (1\text{-}2\text{-}45)$$

and

$$Q = 2\pi \frac{\text{energy stored}}{\text{energy lost per cycle}} \qquad (1\text{-}2\text{-}46)$$

is obtained

$$\frac{1}{Q} = \frac{1}{\pi} \times \text{logarithmic decrement} \qquad (1\text{-}2\text{-}47)$$

Whence, by substituting for logarithmic decrement in Equation 1-2-47 the expression given by Equation 1-2-44, is obtained

$$\frac{1}{Q} = \frac{\alpha\lambda}{\pi} \qquad (1\text{-}2\text{-}48)$$

1-3. Sources of Attenuation of Longitudinal Waves in a Thin, Magnetostrictive Bar

Longitudinal, plane waves propagated in a thin, magnetostrictive bar are subject to a rather large number of different processes of attenuation (Mason, 1958, pp. 181 to 285; Pollard, 1977, pp. 203 to 301). In Figure 1-3-1 such processes are listed and classified, in a chart developed from a brief one given by Sharp (1974, p. 75). The processes may be divided broadly into two kinds, namely, those processes in which the energy remains in the form of acoustic waves, but suffers a change in the direction or mode of propagation, or both, and those processes in which the energy is converted immediately in form (Pollard, 1977, p. 203). Processes of the second kind are classified as internal friction, and the forms into which the energy may be converted are thermal motion and the motions of other constituents of the crystal lattice, such as dislocations, electrons and nuclei (Pollard, 1977, p. 203). Of the processes of redirection of energy, scattering is probably the most important in propagation in a thin bar, though its effect is not large. By far the most significant part of the attenuation of longitudinal waves in a thin bar is the result of internal friction.

It is seen in Figure 1-3-1 that conversion of energy by internal friction takes place by processes of four main types, which involve, according to type, viscosity effects, relaxation, resonance and hysteresis, respectively. In the next chapter, the mechanisms of those processes will be described.

1-4. Aims of the Project

The project was originally conceived as a study of phenomena in the reversible exchange of electrical and mechanical energies; the practical field for study was the exchange of energy, by magnetostriction effects, between an electric circuit and an acoustic transmission line conveying a repeatedly reflected train of waves. The field was broadened to include study of phenomena in the propagation of waves in the line.

The first phenomenon investigated was that of the anomalous waves familiar in wave-train-echo work, which constitute noise that obscures weak, wanted signals; an explanation of the origin of such anomalous waves was needed.

A second phenomenon, that of stress-dependent attenuation in the line, a seemingly little known phenomenon, became apparent in the course of experimental work; that phenomenon too was investigated, with the object of determining its characteristics and, if possible, understanding its physical mechanism.

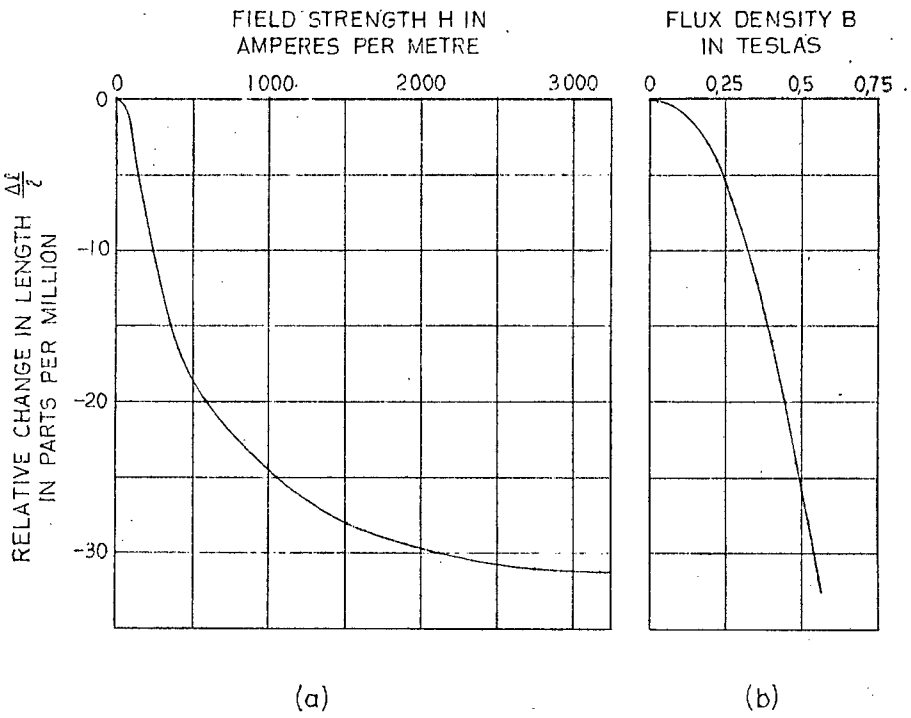

Figure 1-1-1. Magnetostrictive characteristics of nickel.

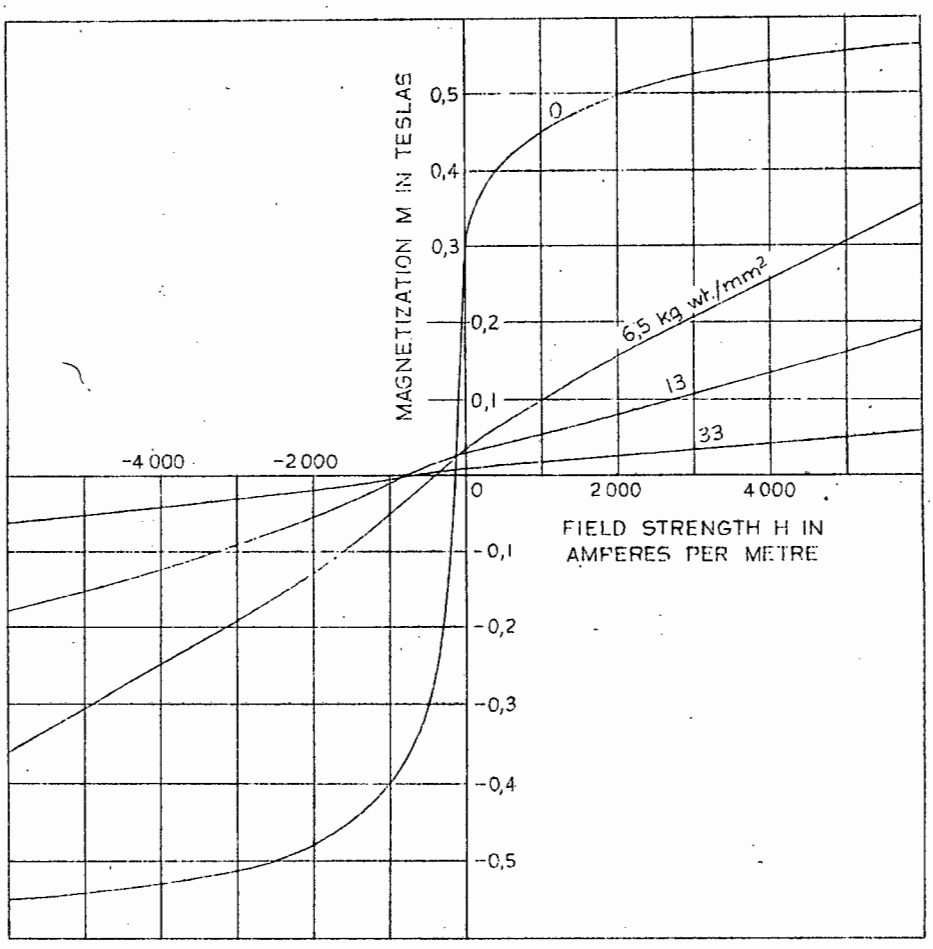

Figure 1-1-2. Half hysteresis loops, showing the effect of tensile stress on the magnetization of annealed nickel wire (after Brailsford, 1960, p. 67).

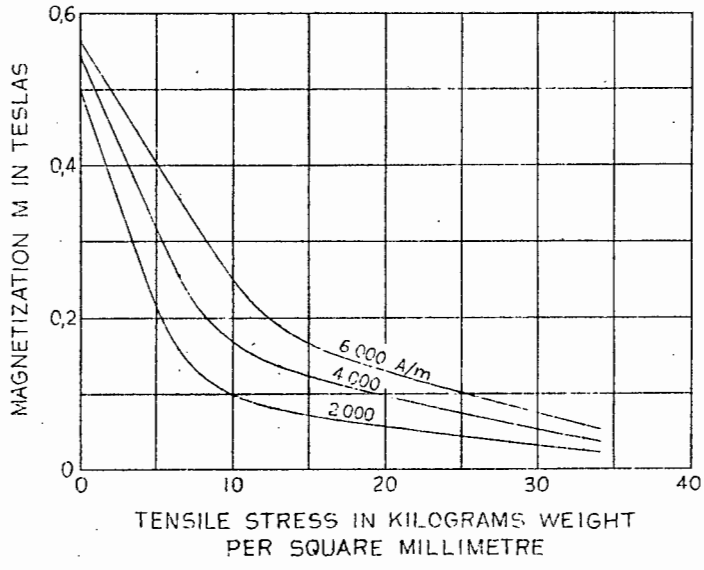

Figure 1-1-3. Curves showing the variation of magnetization M of annealed nickel wire with increasing tensile stress for constant values of field strength H.

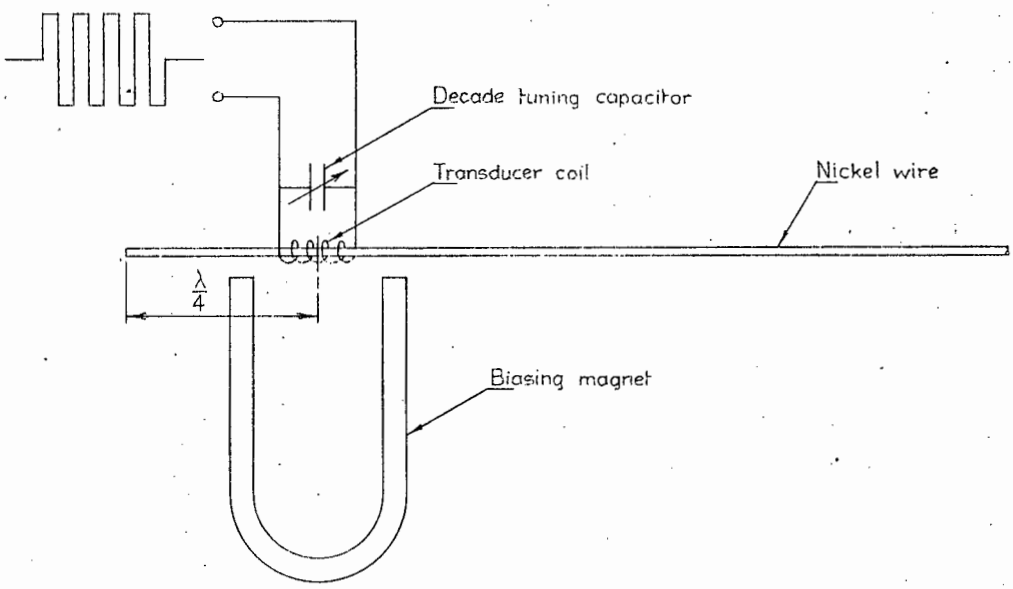

Figure 1-1-4. A magnetostriction transducer for use in the excitation and detection of longitudinal vibrations in nickel wire. The waveform of an applied drive voltage is shown.

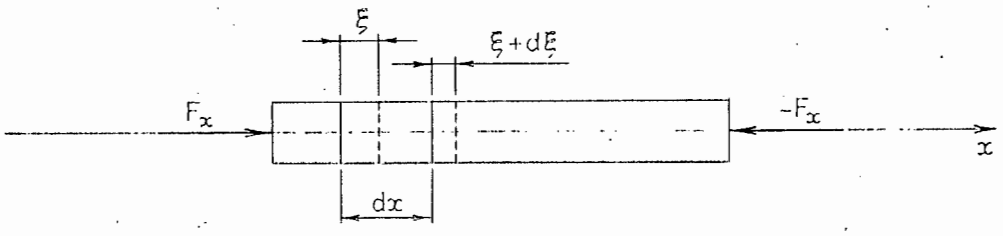

Figure 1-2-1. A bar stressed longitudinally, uniformly.

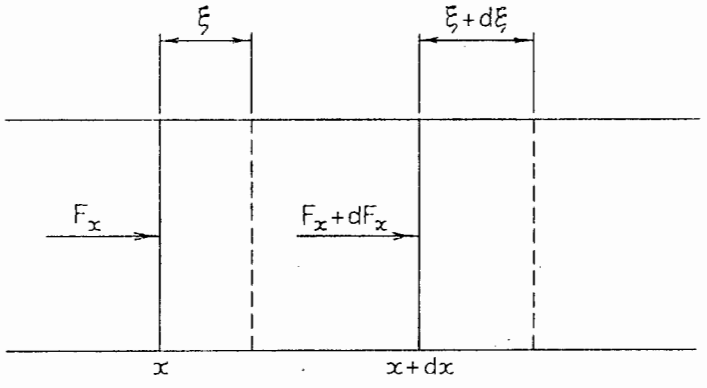

Figure 1-2-2. Forces and displacements in a longitudinal wave in a thin bar.

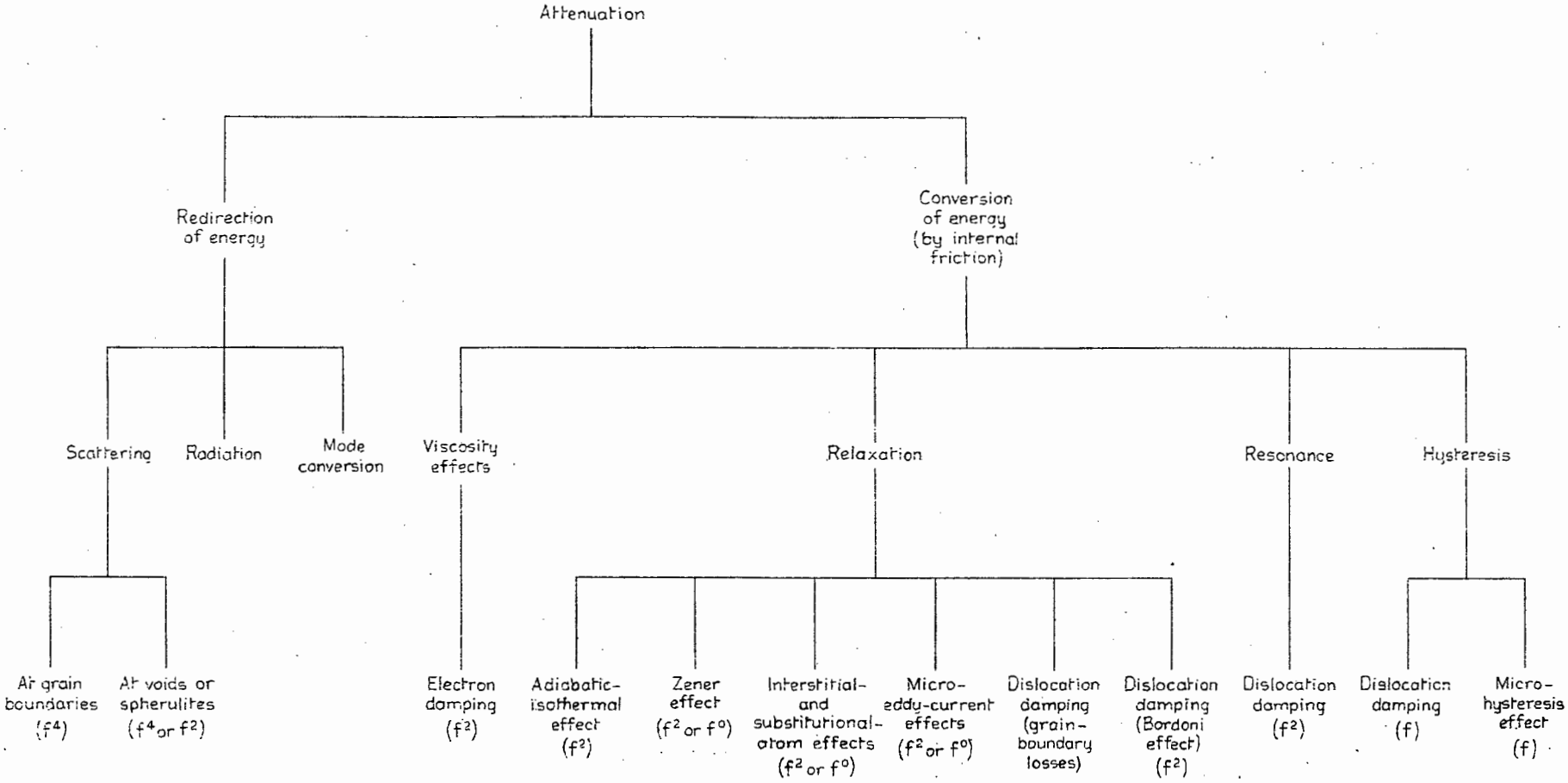

Figure I-3-1. Classification chart of possible processes of attenuation of longitudinal acoustic waves in a thin magnetostrictive bar. The symbols in brackets express the frequency dependence of the attenuation.

CHAPTER 2

MECHANISMS OF ATTENUATION

The classification chart of Figure 1-3-1 and this chapter were compiled by the author to aid his study of the phenomenon of stress-dependent attenuation, described in Section 4-5-4 and treated further in Chapter 5, and to provide for the reader a source of accessible information on mechanisms of attenuation that can be referred to in enquiring into the phenomenon.

2-1. Scattering

In an investigation into scattering of acoustic waves by the grains of polycrystalline media, including nickel (Papadakis, 1968), theoretical values of attenuation of the waves were calculated for Rayleigh scattering (for which $\lambda > 2\pi D$, where D is the average diameter of the grains) with the use of the relation

$$\alpha = Tf^4S \qquad (2\text{-}1\text{-}1)$$

where α is the attenuation in decibels per centimetre
T is the average volume of a grain in cubic centimetres
f is the frequency of the wave in megahertz
S is a theoretically derived scattering coefficient dependent on elastic anistropy of crystals, density of material and velocity of propagation.

For nickel, S = 896 for longitudinal waves, and for specimens of nickel annealed at 700°C for 3 hours, $T = 1{,}10 \times 10^{-5}$. Evaluation of Equation 2-1-1 for the mid-range frequency, 60 kHz, for the investigation of attenuation in this project, on the assumption that the same value for T is appropriate, gives the result

$$\alpha = 1{,}10 \times 10^{-5} \times (0{,}06)^4 \times 896$$
$$= 1{,}28 \times 10^{-7} \text{ (dB/cm)}$$

The attenuation in decibels per metre would be $1{,}28 \times 10^{-5}$.

If it is assumed that, as a result of grain growth, the diameter of the grains approximates 1 mm (nearly the diameter, 1,52 mm, of the nickel wire used), and that the average volume of a grain is 0,001 cm^3, then

$$\alpha = 1 \times 10^{-3} \times (0,06)^4 \times 896$$
$$= 1,16 \times 10^{-5} \text{ (dB/cm)}$$

The attenuation in decibels per metre would be $1,16 \times 10^{-3}$

Even the second value of attenuation is negligible in relation to the smallest value of attenuation at 60 kHz (about 1,91 dB/m) observed in the annealed nickel wire of which the attenuation was investigated.

2-2. Radiation

Loss by radiation from an end of an acoustic transmission line can be estimated by consideration of the reflection coefficient of the discontinuity between the material of the line and the atmosphere. If the reflection coefficient of the discontinuity is r, then

$$r = \frac{F_{xro}}{F_{xio}} \qquad (2\text{-}2\text{-}1)$$

where F_{xro} and F_{xio} are the force amplitudes of the reflected and incident waves respectively. If Z_ℓ is the acoustic impedance of the transmission line, the ratio of reflected and incident powers $\frac{P_r}{P_i}$ is given by

$$\frac{P_r}{P_i} = \frac{\frac{F_{xro}^2}{2Z_\ell}}{\frac{F_{xio}^2}{2Z_\ell}}$$

whence

$$\frac{P_r}{P_i} = \left(\frac{F_{xro}}{F_{xio}}\right)^2 \qquad (2\text{-}2\text{-}2)$$

Thence, by substitution of r for $\frac{F_{xro}}{F_{xio}}$ in accordance with Equation 2-2-1

$$\frac{P_r}{P_i} = r^2 \qquad (2\text{-}2\text{-}3)$$

If the specific acoustic impedance ρc of the material of the line is Z'_ℓ and the specific radiation impedance of the end face of the line is Z'_{rad} then

$$r = \frac{\frac{Z'_{rad}}{Z'_\ell} - 1}{\frac{Z'_{rad}}{Z'_\ell} + 1}$$

or

$$r = - \frac{1 - \frac{Z'_{rad}}{Z'_\ell}}{1 + \frac{Z'_{rad}}{Z'_\ell}} \qquad (2\text{-}2\text{-}4)$$

Substituting, for r in Equation 2-2-3, the expression given by Equation 2-2-4, gives

$$\frac{P_r}{P_i} = \left(- \frac{1 - \frac{Z'_{rad}}{Z'_\ell}}{1 + \frac{Z'_{rad}}{Z'_\ell}} \right)^2 \qquad (2\text{-}2\text{-}5)$$

Since $Z'_{rad} \ll Z'_\ell$, Equation 2-2-5 can be written

$$\frac{P_r}{P_i} \approx 1 - 4 \frac{Z'_{rad}}{Z'_\ell}$$

or

$$\frac{P_i}{P_r} \approx 1 + 4 \frac{Z'_{rad}}{Z'_\ell} \qquad (2\text{-}2\text{-}6)$$

Now

$$\text{loss in decibels by radiation at an end of the line} = 10 \log_{10} \frac{P_i}{P_r} \qquad (2\text{-}2\text{-}7)$$

Substituting, for $\frac{P_i}{P_r}$ in Equation 2-2-7, the expression given by Equation 2-2-6, yields

$$\text{loss in decibels by radiation at an end of the line} \approx 10 \log_{10} \left(1 + 4 \frac{Z'_{rad}}{Z'_\ell} \right) \qquad (2\text{-}2\text{-}8)$$

In the experiments performed, two forms of termination of the line were used. One was simply the free end of the nickel wire, while the other was a quarter-wavelength-long mild-steel stub, much larger in diameter than the nickel wire, in which the end of the nickel wire was rigidly held. Propagation of waves in the stub is likely to approximate that in an infinite medium, so that the specific acoustic impedance for the stub will be about $4{,}63 \times 10^7$ kg/m² s as compared with $4{,}24 \times 10^7$ kg/m² s for the nickel wire. The reflection coefficient at the boundary with air will therefore be greater for the mild-steel stub and, if other conditions are the same, the loss by radiation for the mild steel stub will be smaller. Moreover, reflection at the junction of the nickel wire and the stub will further diminish the loss by radiation.

If, therefore, Equation 2-2-8 is evaluated for the greatest possible value for Z'_{rad}, which is equal to ρc for air, a value will be obtained for the loss by radiation at an end of the line that cannot have been exceeded in the experiments. Taking ρc for air as 420 (kg/m² s) and for nickel as $4{,}24 \times 10^7$ (kg/m² s), and putting those values for Z'_{rad} and Z'_{ℓ} respectively in Equation 2-2-8, give, for the greatest possible loss,

$$\text{loss by radiation at an end of the line} \approx 10 \log_{10} \left(1 + 4 \frac{420}{4{,}24 \times 10^7}\right)$$

$$\approx 0{,}00017 \text{ dB}$$

The greatest possible loss, per round of travel of a wave on the line, resulting from radiation at the ends of the line would therefore be approximately 0,00034 dB. That loss would be negligible in relation to even the smallest loss (4,62 dB per round) observed in the annealed nickel wire.

2-3. Mode Conversion

A longitudinal wave, incident on the boundary between two isotropic solids, will give rise in general to both a longitudinal and a transverse reflected wave, together with a longitudinal and a transverse transmitted wave; for a normally incident longitudinal wave, there is no reflected or transmitted transverse wave. More generally, a plane elastic wave incident on a plane boundary between two anisotropic solids will give rise to three reflected waves and three

transmitted waves. The production of a wave having a mode of vibration different from that of the incident wave is termed mode conversion. (Pollard, 1977, pp. 67 and 68)

In a more restricted version of the first case, a longitudinal wave in an isotropic solid, falling on a boundary with a vacuum (or with air), will in general give rise to a reflected longitudinal wave and a reflected transverse wave; as before, for a longitudinal wave incident normally, there is no reflected transverse wave. (Pollard, 1977, pp. 59 and 60)

The last conditions specified, for normal incidence, approximate those of reflection at the end face of the nickel-wire transmission line; mode conversion therefore will not occur on reflection at the ends of the line.

With regard to scattering, theoretical and experimental work has shown that most (80%) of the scattered energy from an incident longitudinal wave is carried off by transverse waves for scattering particles much smaller in diameter than the wavelength (Papadakis, 1968). Such mode conversion will not affect the attenuation in the present investigations, since the scattered energy is in any case lost by the signal.

2-4. Electron Damping

At very low temperatures, at which the mean free paths of electrons become quite large in relation to their magnitudes at room temperature, the electrons can acquire momentum from collisions with the acoustically vibrating crystal lattice that is not immediately distributed amongst other electrons (Mason, 1958, p. 319). Measurements have shown (Mason, loc. cit.) that such electrons can cause attenuation of both longitudinal and transverse ultrasonic waves that increases in proportion to the mean free path and, for a mean free path that is less than the wavelength, increases in proportion to the square of the frequency. The effect is measurable only for signals in the megahertz range (Mason, loc. cit.). It is clear, therefore, that for the conditions of temperature and frequency that existed for the measurements in the present investigations, the effect would be negligible.

2-5. Adiabatic-isothermal Effect

In the compression of a solid, part of the mechanical energy is converted into heat, so that the compressed parts become warmer;

similarly, extended parts of a solid become cooler. As a result, the modulus of elasticity for adiabatic conditions is greater than that for isothermal conditions. Accordingly, in a longitudinal wave, flow of heat between parts at different temperatures results in the transfer of less energy by reconversion from potential to kinetic form than by conversion from kinetic to potential form. That process of relaxation causes attenuation of the wave. For longitudinal waves, the thermal path becomes shorter as the frequency increases, so that the attenuation per cycle, that is, per wavelength, increases in proportion to the frequency. The attenuation per unit length, therefore, increases in proportion to the square of the frequency.

Mason (1958, pp. 198 to 200) derives an expression for the propagation constant Γ for longitudinal plane waves subject to damping through the adiabatic-isothermal process. He finds

$$\Gamma = A + jB$$

$$\approx \frac{2\pi^2 f^2 \left[\chi + 2\eta + \left(\frac{\lambda^\sigma - \lambda^\theta}{\lambda^\sigma - 2\mu}\right)\frac{K}{C_v}\right]}{\rho V^3} + j\,\frac{\omega}{V} \qquad (2\text{-}5\text{-}1)$$

where f is the frequency of the signal

χ is the compressional viscosity

η is the shear viscosity

λ^σ is the adiabatic Lamé elastic constant

λ^θ is the isothermal Lamé elastic constant

μ is the Lamé shear modulus of elasticity

K is the thermal conductivity

C_v is the specific heat at constant volume per unit mass

ρ is the density

$V = \sqrt{\frac{\lambda^\sigma + 2\mu}{\rho}}$ is the velocity of propagation

For nickel, Mason (1958, p. 201) gives

$$\frac{A}{f^2} = 3{,}8 \times 10^{-17} \qquad (2\text{-}5\text{-}2)$$

where A is in nepers per metre and f is in hertz.

Hence, for nickel

$$A = 3{,}8 \times 10^{-17} f^2 \qquad (2\text{-}5\text{-}2a)$$

Putting for f in Equation 2-5-2a the value 60×10^3, the mid-range frequency, in hertz, for the investigation of attenuation in this project, gives

$$\begin{aligned} A &= 3{,}8 \times 10^{-17} \times (60 \times 10^3)^2 \\ &= 1{,}368 \times 10^{-7} \text{ (nepers per metre)} \end{aligned}$$

That attenuation, in decibels per metre, is $1{,}368 \times 10^{-7} \times 8{,}686 = 1{,}19 \times 10^{-6}$ and is negligible.

2-6. Zener Effect

Elastic anisotropy of the grains of polycrystalline materials, a characteristic that may be quite significant in certain metals, results in greater stiffness of some grains in the direction of motion of the waves than of others. Since the stiffer grains are compressed less than the more compliant ones, differences in temperature between grains will occur, with consequent flow of heat. For conditions such that the process becomes one of relaxation, there will be a loss, known as the Zener loss. The magnitude of the loss expressed as $\frac{1}{Q}$ has been shown to be (Mason, 1958, p. 205)

$$\frac{1}{Q} = \frac{C_p - C_v}{C_v} R \frac{f f_o}{f^2 + f_o^2} \qquad (2\text{-}6\text{-}1)$$

where C_p is the specific heat at constant stress

R is the fraction of the total strain energy associated with the fluctuation in dilatation

f_o is the inter-grain relaxation frequency.

Mason (1958, p. 202) gives

$$\rho(C_p - C_v) = 9B\alpha^2 T \qquad (2\text{-}6\text{-}2)$$

where B is the bulk modulus of elasticity

α is the linear temperature coefficient of expansion per degree Celsius

T is the temperature in Kelvins

Rearrangement of Equation 2-6-2 yields

$$C_p - C_v = \frac{9B\alpha^2 T}{\rho} \qquad (2\text{-}6\text{-}2a)$$

For nickel (Mason, 1958, pp. 358 and 201)

$$B = 19{,}0 \times 10^{10} \ (N/m^2)$$
$$\alpha = 13{,}3 \times 10^{-6} \ (\text{per } °C)$$
$$\rho = 8{,}90 \times 10^{3} \ (kg/m^2)$$
$$C_v = 440 \ (J/kg/°C)$$

Putting values for nickel for B, α and ρ, and room temperature (300, in kelvins) for T in Equation 2-6-2a), leads to

$$C_p - C_v = \frac{9 \times 19{,}0 \times 10^{10} \times (13{,}3 \times 10^{-6})^2 \times 300}{8{,}90 \times 10^{3}}$$

$$= 10{,}20 \ (J/kg/°C)$$

Hence

$$C_p = C_v + 10{,}20$$

Putting for C_v the value for nickel, yields

$$C_p = 440 + 10{,}20$$
$$= 450{,}2 \ (J/kg/°C)$$

Mason (1958, p. 205) gives the inter-grain relaxation frequency f_o as, approximately

$$f_o = \frac{D}{L_c^2} \qquad (2\text{-}6\text{-}3)$$

or as

$$f_o = \frac{K}{\rho C_p L_c^2} \qquad (2\text{-}6\text{-}4)$$

where D is the thermal diffusion constant

L_c is the mean diameter of the crystallites

C_p is the specific heat at constant stress

For nickel (Mason, 1958, p. 201)

$$K = 92 \ (W/m/°C)$$

$$\rho = 8,90 \times 10^3 \ (kg/m^3)$$

Putting for K and ρ in Equation 2-6-4 the values stated, for C_p the value derived, and for L_c, $5,54 \times 10^{-5}$ (m), corresponding to a volume T of $1,10 \times 10^{-11}$ (m^3) (Mason, 1968, p. 292) yields

$$f_o = \frac{92}{8,90x10^3 \, x0,45x10^3 \, x(5,54)^2 \, x10^{-10}}$$

$$= 7485 \ (Hz)$$

Mason (1958, p. 205) has tabulated values of R, the fraction of the total strain energy associated with the fluctuation in dilatation, for a number of metallic elements, but has not given a value for nickel. However, he mentions a relationship between R and the anisotropy factor (1958, p. 205) and has tabulated the anisotropy factors for the metallic elements referred to, including nickel (1958, p. 358). Table 2-6-1 shows the values given by Mason; the metals are arranged in the order of decreasing magnitude of the product $\frac{C_p - C_v}{C_v} R$:

Table 2-6-1

Metal by chemical symbol	Pb	Ag	Cu	Au	Ni	Fe	Al	W
Anisotropy factor	3,79	2,95	3,18	2,67	2,63	2,37	1,24	1,0
Fraction R	0,065	0,031	0,031	0,014		0,022	0,009	10^{-6}

Points have been plotted for corresponding values of the anisotropy factor and the fraction R, and an average curve drawn, from which a value for R for nickel has been obtained. Figure 2-6-1 shows the graph, and the value, 0,020, obtained for R for nickel.

Putting for $C_p - C_v$, R and f_o in Equation 2-6-1 the values derived,

for C_v the value stated, and for f 60×10^3, the mid-range frequency, in hertz, for the investigation of attenuation in this project, yields

$$\frac{1}{Q} = \frac{10,20}{0,44 \times 10^3} \times 0,020 \times \frac{60 \times 10^3 \times 7485}{(60 \times 10^3)^2 + 7485^2}$$

$$= \frac{10,20 \times 0,020}{0,44} \times \frac{60 \times 7485}{3,656 \times 10^9}$$

$$= 5,70 \times 10^{-5}$$

From the relations

$$\frac{\pi}{Q} = \alpha\lambda \qquad (1\text{-}2\text{-}48b)$$

and

$$\lambda = \frac{c}{f}$$

is derived

$$\alpha = \frac{\pi f}{c}\frac{1}{Q} \qquad (2\text{-}6\text{-}5)$$

Putting values for f, c (4 799, in metres per second) and $\frac{1}{Q}$ in Equation 2-6-5 yields

$$\alpha = \frac{\pi \times 60 \times 10^3}{4\ 799} \times 5,70 \times 10^{-5}$$

$$= 2,24 \times 10^{-3} \text{ (nepers per metre)}$$

The attenuation in decibels per metre would be $2,24 \times 10^{-3} \times 8,686 = 0,019$.

It is to be noted that combination of Equations 2-6-1 and 2-6-5 yields

$$\alpha = \frac{\pi}{c}\frac{C_p - C_v}{C_v} R \frac{f^2 f_o}{f^2 + f_o^2} \qquad (2\text{-}6\text{-}6)$$

which, for $f \gg f_o$, can be written

$$\alpha = \frac{\pi}{c}\frac{C_p - C_v}{C_v} R f_o \qquad (2\text{-}6\text{-}7)$$

Equation 2-6-7 shows that, for values of the signal frequency f high

enough that f_o^2 can be neglected in the sum $f^2 + f_o^2$, the attenuation can be considered to be independent of signal frequency.

2-7. Absorption by Moving Interstitial and Substitutional Atoms

Where the application of stress alters the relative preferability of different distributions of solute atoms in a crystal lattice, attenuation of acoustic vibrations can be caused by a resultant process of relaxation (Mason, 1958, p. 224). For example, in α-iron, which has a body-centred cubic structure, atoms of dissolved nitrogen or carbon can settle interstitially half-way along the edges of a unit cubic cell with equal preference for each of the x, y and z directions. However, if the crystal is subjected to, say, tensile stress in the x direction, with resultant extension in that direction and contraction in the y and z directions, positions of interstitial atoms on the y and z edges will be favoured less than those on the x edges. Atoms of the solute will therefore tend, with thermal agitation, to migrate from positions on the y and z edges to positions on the x edges. A specific quantity of energy is required for each atom to make the jump between positions, and the delay represented by the jump time is the source of the internal friction. It has been shown by experiment that diffusion of nitrogen in annealed iron wire can increase the loss factor $\frac{1}{Q}$ from about 0,003 to 0,03 for a relaxation frequency corresponding to a period of 4,9 seconds at a temperature a little above 0°C. A comparable result has been obtained for iron containing dissolved carbon (Mason, 1958, pp. 224 and 225).

The substitutional-atom solution represented by α-brass has shown the same kind of relaxation. The relaxation curve shows an increase in loss factor $\frac{1}{Q}$ from 0,0005 to 0,012 with change in temperature; the maximum loss occurs at about 415°C for a frequency of 620 Hz (Mason, 1958, p. 227)

The effects have been shown to conform to the relation

$$\frac{1}{Q} = \Delta \frac{\frac{\omega}{\omega_o}}{1 + \left(\frac{\omega}{\omega_o}\right)^2} \qquad (2\text{-}7\text{-}1)$$

that is

$$\frac{1}{Q} = \Delta \frac{f f_o}{f^2 + f_o^2} \qquad (2\text{-}7\text{-}2)$$

where Δ is the strength of the relaxation (Mason, 1958, p. 224).

Substituting, for $\frac{1}{Q}$ in Equation 2-6-6, the expression given by Equation 2-7-2, gives

$$\alpha = \frac{\pi}{c} \Delta \frac{f^2 f_o}{f^2 + f_o^2} \qquad (2\text{-}7\text{-}3)$$

which, for $f << f_o$, can be written

$$\alpha = \frac{\pi}{c} \Delta \frac{f^2}{f_o} \qquad (2\text{-}7\text{-}4)$$

and, for $f >> f_o$

$$\alpha = \frac{\pi}{c} \Delta f_o \qquad (2\text{-}7\text{-}5)$$

Equations 2-7-4 and 2-7-5 show that, depending on the relative magnitudes of f and f_o, α may vary as f^2 or may be constant.

2-8. Micro-eddy-current Effects

In a magnetostrictive material, a change in the modulus of elasticity with magnetization, known as the "ΔE" effect, occurs as a result of motions of the walls of magnetic domains in the material. A second effect, a relaxation loss resulting from the flow of micro-eddy currents, and having its strength set by the "ΔE" effect, and a third effect, a microhysteresis loss, are consequences of the same motions of the walls of domains. The "ΔE" effect and the related micro-eddy-current loss are considered here; the topics are well covered by Mason (1958, p. 209 et seq.).

A magnetic domain is a region within a crystal for which all the magnetic polarization is in one direction. In adjacent regions, or domains, the polarization, in the case of iron, is set in directions at either 90° or 180° to that of the first domain. Boundaries or walls, designated 90° or 180° boundaries (or walls) exist between pairs of domains differing in direction of polarization by 90° or 180° respectively. Magnetostriction in the domains, comprising a change in the dimensions of domains along the lines of polarization, and an opposite change perpendicular to the lines of polarization, gives rise to strain along 90° boundaries but, since magnetostriction is a square-law effect, gives rise to no

strain along 180° boundaries. Applied stresses can therefore affect 90° walls but not 180° walls, for which the effect of the stress is the same on each of the two oppositely polarized domains separated by the wall.

A tensile stress, applied to two domains of a negative magnetostrictive material separated by a 90° wall, reduces the magnetostrictive contraction of a domain polarized parallel to the stress, and increases by virtue of the Poisson's-ratio effect the magnetostrictive contraction of the domain polarized perpendicular to the stress. Accordingly, in material in tension, domains polarized perpendicular to the stress grow at the expense of those polarized parallel to the stress, so that the walls tend to move over towards the latter domains.

It is to be noted that in nickel, in which the differences between the directions of polarization of the domains are not 90° and 180°, but are 71° or 89° and 180°, the movement of walls of domains occurs in essentially the same manner as in iron.

The "ΔE" effect comes about because the movement of walls of domains results in the inclusion of more material in domains polarized in a direction perpendicular to the stress. For a negative magnetostrictive material, dimensions perpendicular to the lines of polarization increase with increasing magnetization, so that lengthening of the piece in tension occurs not only as elastic strain but also as magnetostrictive expansion. Since Young's modulus E is the ratio of stress to total strain, the value of E is lower than it would be if only elastic strain were contributing to elongation. For the same material in magnetic saturation, all former separate domains have become a single large domain, so that no walls of domains remain to be moved by stress. The value of E for the saturated material is therefore greater; the magnitude of the "ΔE" effect, $\frac{\Delta E}{E_o}$, is defined as

$$\frac{\Delta E}{E_o} = \frac{E_s - E_o}{E_o} \qquad (2\text{-}8\text{-}1)$$

where E_s and E_o are the Young's moduli for saturated and unsaturated material respectively. For nickel at 25°C, $\frac{\Delta E}{E_o} = 0{,}064$ (Mason, 1958, p. 211).

Micro-eddy-current loss for acoustic waves, like the "ΔE" effect, occurs only in magnetostrictive materials. Eddy currents

generated by the motions of the walls of the domains under the influence of applied stress give rise to losses in magnetization in the regions in which the direction of magnetism changes and in surrounding regions. At low frequencies, the loss per cycle is proportional to the frequency; as the frequency is increased, the motions of the walls of the domains follow the alternating stress to a diminishing degree, so that the loss caused by eddy currents decreases and finally vanishes. The phenomenon thus has the character of a relaxation effect. The relaxation frequency f_o is given (Mason, 1958, p. 217) by

$$f_o = \frac{R}{96 \chi_o \ell^2} \qquad (2\text{-}8\text{-}2)$$

where R is the electrical resistivity

χ_o is the initial susceptibility

ℓ is the thickness of a plate-like domain

The loss factor $\frac{1}{Q}$ is given (Mason, 1958, p. 217) by

$$\frac{1}{Q} = \frac{\Delta E}{E_o} \frac{\frac{f}{f_o}}{1 + \left(\frac{f}{f_o}\right)^2} \qquad (2\text{-}8\text{-}3)$$

Measurements of decrement $\delta = \frac{\pi}{Q}$ (Mason, 1958, p. 217) have indicated that the relaxation peak is much broader than one determined by Equations 2-8-2 and 2-8-3, for a single value of ℓ, would be; the reason for the broadening is shown by a photograph, having a magnification of 200, taken of the domains of a nickel crystal, in which the thickness ℓ of the plate-like domains is seen to range from about 0,01 mm to about 0,2 mm. The measurements showed also that the decrement δ of a polycrystalline nickel rod had a value of about 0,10 for a signal frequency of 60 kHz.

Combination of Equations 2-8-3 and 2-6-6 yields

$$\alpha = \frac{\pi f}{c} \frac{\Delta E}{E_o} \frac{\frac{f}{f_o}}{1 + \left(\frac{f}{f_o}\right)^2}$$

whence

$$\alpha = \frac{\pi}{c} \frac{\Delta E}{E_o} \frac{f^2 f_o}{f_o^2 + f^2} \qquad (2\text{-}8\text{-}4)$$

Equation 2-8-4 is of the same form as Equation 2-7-3 so that, as for α in Equation 2-7-3, α in Equation 2-8-4 may vary as f^2 or may be constant, depending on the relative magnitudes of f and f_o.

2-9. Grain-boundary Losses

This and the following three effects are ones of wave damping caused in different ways by dislocations, that is, by deviations from the regular structure of crystals. Before the effects are studied, the nature and properties of dislocations will be outlined.

The concept of dislocation, introduced independently by Taylor, Orowan and Polyani in 1934 (Pollard, 1977, p. 236), filled a need for an explanation of the fact that the limiting shearing stress, at which plastic flow began in very pure single metallic crystals, was so small a fraction of the shear modulus of elasticity of the crystal (Mason, 1958, p. 231). For a crystal free of imperfections, a limiting shearing stress of $\frac{1}{30}$ of the shear modulus was to be expected from existing theory, whereas in practice a value of perhaps only $\frac{1}{60\,000}$ of the shear modulus was obtained. A form of imperfection known as an edge dislocation was conceived to account for the difference; a second form, known as a screw dislocation, is also possible. (Mason, 1958, p. 233)

Figure 2-9-1a represents a crystal subjected to shearing forces. Some of the unit cells in the upper part of the crystal have been pushed forward by one full step, while others have not. A line of mismatch, D, called a dislocation, forms the boundary between the unit cells that have slipped and those that have not. As the shearing progresses, the dislocation moves through the crystal, so that the number of cells displaced increases. The continued generation and movement of such dislocations is the mechanism of plastic deformation of the material.

The part of the dislocation line that lies in the direction of the displacement, that is, parallel to the slip vector s, is a screw dislocation, and the part orthogonal to the direction of displacement is an edge dislocation. Those two components of the shear dislocation are shown in Figure 2-9-1 at b and c; the symbols $\S$ and $\perp$ are used respectively to designate them. Where the line of dislocation lies neither in nor orthogonal to the direction of displacement, the dislocation consists of a combination of edge and screw dislocations.

The "error of closure" b for a circuit round a dislocation is known as the Burgers vector for the dislocation.

Experiment has shown that dislocations are mobile, and that they move in planes in which the atoms are closely spaced, because in such planes less energy is needed for a change in the position of an atom. For the same reason, dislocations tend to move in those directions in a plane for which successive atoms are set closest (Mason, 1958, p. 233).

In a polycrystalline material, an area of mismatch occurs where adjacent crystals meet. Such boundaries between grains having different orientations are regions in which vacancies and considerable strain in the lattice may exist. At a grain boundary of a simple type, lying within the angle between the planes of two slightly misorientated cubic crystals, the crystals join in a series of edge dislocations; such a boundary can be caused to glide by the application of a shearing stress. At a tilt boundary, for which the obliquity with respect to the crystal planes is greater, two sets of edge dislocations, having widely divergent Burgers vectors, occur, while at a twist boundary, between grains mismatched by relative rotation about a common axis, screw dislocations occur.

A grain boundary having dislocations capable of mutual intersection is prevented from gliding by the intersections; movement of such a boundary is possible only by diffusion of atoms into adjacent vacancies. Movement of boundaries by diffusion, under the influence of applied stress, results in absorption of energy; measurements by Ké of the properties of polycrystalline aluminium (Mason, 1958, p. 283 et seq.), have shown the occurrence of a peak value of 0,09 for the loss factor $\frac{1}{Q}$ for the polycrystalline aluminium for a temperature of 290°C and a frequency of vibration of 0,7 Hz. No such peak occurs for single-crystal aluminium. Dependence of the frequency for maximum attenuation in polycrystalline aluminium on temperature has been shown to be in accordance with an equation of the form

$$\omega = \omega_o e^{-\frac{H}{RT}} \qquad (2\text{-}9\text{-}1)$$

where H is the activation energy for aluminium

R is the gas constant

T is the absolute temperature

Thermal energies of the atoms for high temperatures are necessary for the supply of the large activation energies for diffusion; even at higher temperatures, the process of diffusion is slow, so that grain-boundary losses tend to occur at low frequencies. Nickel, for which the Debye temperature (370 K) is roughly equal to that for aluminium (398 K), can be expected to show relaxation temperatures and frequencies roughly equal to those for aluminium (Hueter and Bolt, 1955, pp. 372 to 374).

Accordingly, the combinations of temperature and frequency of vibration for which grain-boundary losses occur in nickel would differ greatly from those for which the investigation of attenuation in nickel in this project was made, namely, combinations of room temperature and signal frequency in the range 20 kHz to 100 kHz. Grain-boundary losses are hence not of importance here.

2-10. Bordoni Relaxation

Measurements made at low temperatures on four metals having face-centred cubic crystal structures have indicated the ocurrence of a maximum of attenuation, of which the temperature of occurrence depends on the frequency of the signal. Information given by Mason (1958, p. 266) indicates that for the four metals lead, copper, aluminium and silver, the maxima, known as Bordoni peaks, occur at temperatures of about 35, 90, 100 and 65 kelvins respectively, for frequencies of 10,3, 30,3, 40 and 21,3 kilohertz respectively. Neither Mason (1958) nor Niblett (1966) gives information for nickel. The relationship between temperature and frequency for the peaks indicates that they are relaxation peaks; values of temperature and frequency for a given material have been found to be fitted by an equation of the form of Equation 2-9-1. The effect is substantially similar for single crystals and polycrystalline specimens and is not observed in fully annealed specimens, but appears as a result of cold work (Niblett, 1966, pp. 79 and 80; Pollard, 1977, p. 268).

Pollard (1977, p. 224) notes that the attenuation per unit length, α, for the Bordoni loss, varies as the square of the signal frequency f.

A number of theories based on movement of dislocations induced by thermal agitation have been devised to explain the occurrence of the Bordoni peak; difficulty has been found in explaining all aspects of observed phenomena.

The facts that Bordoni relaxation occurs at low temperatures, that it tends not to occur in annealed metal, and that the attenuation varies as f^2, make a connection between Bordoni relaxation and the attenuation investigated in the annealed nickel wire in this project unlikely.

2-11. Resonance and Hysteresis Forms of Dislocation Damping

Read, in a paper published in 1940, was the first to claim that the damping of ultrasonic waves in single crystals was the result of vibrations of dislocations. He had observed that the damping in a single crystal of copper appeared to consist of two parts, one of which was a function of the amplitude of the alternating strain, and the other a residual part that remained for small amplitudes of strain. (Pollard, 1977, p. 245)

Results of investigations by Hikarta et al. of the damping of longitudinal waves in polycrystalline aluminium in tension, published in 1956, suggest the existence of an additional source of strain in the crystals that contributes insignificantly to the elastic strain, but that sensibly increases the damping (Pollard, 1977, p. 245).

Granato and Lücke published in 1956 a comprehensive theory of dislocation damping, providing for losses both independent of and dependent on amplitude of vibration, which was based on the concept, introduced by Koehler in 1952, of the behaviour of a dislocation as a vibrating string. Granato and Lücke postulated a dislocation line, such as that illustrated in Figure 2-11-1, that had pinning points of two kinds, namely, strong nodal pinning points where dislocations intersect, and weaker intermediate pinning points comprising impurity atoms and other point imperfections. Two characteristic lengths of dislocation loop therefore resulted, as illustrated in Figure 2-11-2: those lengths are the network loop length, L_N, determined by the nodal pinning, and a shorter loop length, L_c, determined by the intermediate pinning. The effects of temperature, of interactions between dislocations and the crystal lattice, and of interactions between dislocations, were neglected in the theory. (Granato and Lücke, 1966, pp. 227 to 228, and p. 238; Pollard, 1977, pp. 247 to 249)

The external application of stress to the crystal causes, in addition to the elastic strain, a strain due to the dislocations,

called the dislocation strain. The solid-line graph of Figure 2-11-3 shows the law for stress as a function of dislocation strain for the process of Figure 2-11-2 in which distances L_c are equal. The effects of a gradual increase in an applied alternating stress are shown. As the amplitude of the stress is increased, the lines bow out with increasing amplitude of vibration, through the stage labelled b in Figure 2-11-2 and B in Figure 2-11-3 to the stage labelled c, C, at which catastrophic breakaway occurs from the intermediate pinning points, and the line is left vibrating between the nodal points. The effective modulus of the stress-dislocation-strain law is determined by L_c in that range. Between the stages c,C and d,D, a large increase in the dislocation strain occurs for no increase in the stress. For further increases in the stress, between the stages labelled d,D and e, E, the network length L_N bows out, so that the effective modulus is determined by the length L_N. Further increases in the applied stress may bring about multiplication of dislocations by the Frank-Read mechanism, as represented at the stages labelled f,F and g,G. Plastic strain would then occur. (Granato and Lücke, 1966, pp. 238 to 239; Pollard, 1977, p. 248)

The loss consists of two kinds. The first kind results from the fact that, in the dynamic process, the motion forced by the externally applied stress is resisted by some friction, so that there is a difference in phase between stress and strain. The loss, which is dependent on frequency and independent of amplitude, has the character of a resonance loss. (Granato and Lücke, 1966, p. 239)

Losses of the second kind result from the elastic collapse of the long loops, represented by progress along a path in Figure 2-11-3 determined by the length of the long loop, during the unloading part d,D to a,A of the stress cycle, with the formation of a hysteresis loop. On their complete collapse the loops are again pinned by the point defects, so that a path of the same type as before is followed in the other half-cycle. The loss is proportional to the area enclosed by the stress-dislocation-strain loop and is thus dependent on amplitude and independent of frequency. For stresses that are small enough, the loss does not occur. (Granato and Lücke, 1966, p. 239; Pollard 1977, p. 249)

The dashed-line graph of Figure 2-11-3 shows the stress-dislocation-strain law for the process of Figure 2-11-2 for the case in which the short loops are not of uniform length L_c, but have a distribution of lengths. (Granato and Lücke, 1966, p. 239)

Mason (1958, pp. 238 to 241) derives an expression for the loss factor $\frac{1}{Q}$ for the low-amplitude (resonance) process by solution of the equation for the vibration of a stretched string. He uses the equation in the form

$$M \frac{\partial^2 x}{\partial t^2} + B \frac{\partial x}{\partial t} - T \frac{\partial^2 x}{\partial y^2} = \text{force} = T_{13} b \qquad (2\text{-}11\text{-}1)$$

where, for a dislocation

$$M \approx \rho b^2 \qquad (2\text{-}11\text{-}2)$$

and

$$T = \frac{Gb^2}{2} \qquad (2\text{-}11\text{-}3)$$

and where x is the displacement of any point on the string at distance y from one end

M is the mass of the string per unit length

B is the damping constant

T is the tension

T_{13} is the shearing stress

b is the magnitude of the Burgers vector

p is the density of the material

G is the elastic shear modulus

Mason calculates a resonance frequency of dislocation loops, typical for many metals, of $1{,}2 \times 10^9$ Hz, and then derives the expression for the loss factor $\frac{1}{Q}$ as an approximation for the condition that the working frequency is small compared with the resonance frequency. He finds

$$\frac{1}{Q} \approx \frac{\bar{N} \ell^4 B \omega}{36 b^2 G} \qquad (2\text{-}11\text{-}4)$$

where $\bar{N}$ is the number of dislocations per square centimetre

ℓ is the length of a dislocation loop, all assumed to be equal

B is the damping constant

Two different formulae for the damping constant B have been derived, one by Eshelby, with reference to specific heats and thermal diffusivity, and the other by Leibfried, with reference to Boltzmann's constant. (Mason, 1958, pp. 238 to 239)

Substituting $2\pi f$ for ω in Equation 2-11-4 and combining the resultant equation with Equation 2-6-5 yield

$$\alpha = \frac{\pi^2 N \ell^4 B f^2}{18 c b^2 G} \qquad (2\text{-}11\text{-}5)$$

Equation 2-11-5 shows that, for low-amplitude (resonance) damping, α varies as f^2.

Loss of the second kind, the high-amplitude (hysteresis) loss, will be zero for stress amplitudes less than a critical value, corresponding to point C in Figure 2-11-3. For stress amplitudes greater than that value, the loss of energy w per half cycle, represented by the area ABCDA, will be constant. The decrement δ is given (Granato and Lücke, 1966, p. 245) by

$$\delta = \frac{w}{\frac{\sigma^2}{2G}} \qquad (2\text{-}11\text{-}6)$$

where σ is the shear stress and G is the shearing modulus; the decrement will be zero for stress amplitudes of up to the critical value, will rise abruptly to a maximum value at that stress amplitude, and then diminish as the inverse square of the stress amplitude for larger stresses. Breakaway of the dislocations from the pinning points will occur when the force exerted on a dislocation segment just exceeds that exerted on the segment by the pinning point; because there is a distribution of lengths of loop, breakaway will occur over a range of values of strain. The condition for breakaway may be written (Granato and Lücke, 1966, p. 245)

$$\frac{b\sigma(\ell_1 + \ell_2)}{2} = f_m \approx \frac{E_c}{b} \qquad (2\text{-}11\text{-}7)$$

where ℓ_1 and ℓ_2 are the lengths of two adjacent loops
f_m is the maximum force exerted by a pinning point
E_c is the pinning energy

It is evident that the longest pair of loops in a network segment will break away first, so that a catastrophic process, in which the entire network becomes unpinned, will result.

A calculation of the amplitude dependence of the decrement by Granato and Lücke (1966, p. 246) was based on the following assumptions:

1. All the network lengths L_N are of the same size
2. $L_N >> L_c$
3. At zero stress, the loop lengths ℓ are distributed randomly according to the Koehler distribution

$$N(\ell)d\ell = \frac{\Lambda}{L_c^2} e^{-\frac{\ell}{L_c}} \qquad (2\text{-}11\text{-}8)$$

where $N(\ell)d\ell$ is the number of loops of length between ℓ and $\ell + d\ell$

L_c is the average loop length

Λ is the dislocation density of the dislocation segments taking part in the breakaway process, that is, the total length of dislocation line per unit volume.

Those assumptions lead to the following relation for the decrement for hysteresis loss, δ_H, as a function of amplitude of strain

$$\delta_H = \frac{c_1}{\varepsilon_o} e^{-\frac{c_2}{\varepsilon_o}} \qquad (2\text{-}11\text{-}9)$$

where

$$c_1 = \frac{\Omega \delta_o \Lambda L_N}{\pi L_c} c_2 \qquad (2\text{-}11\text{-}10)$$

$$c_2 = \frac{K\eta b}{L_c} \qquad (2\text{-}11\text{-}11)$$

$$\delta_o = \frac{8Gb^2}{\pi^3 C} \qquad (2\text{-}11\text{-}12)$$

$$K = \frac{G}{4RE} \qquad (2\text{-}11\text{-}13)$$

$$C = \frac{2Gb^2}{\pi(1-\nu)} \qquad (2\text{-}11\text{-}14)$$

and where ε_o is the amplitude of the alternating strain

Ω is the orientation factor, the ratio of the square of the resolved shear stress on the slip system to the applied stress. (Granato and Lücke, 1966, p. 241)

η is Cottrell's misfit parameter, measuring the magnitude of the lattice dilatation at a point defect.

R is the resolved shear stress factor, defined by Granato and Lücke (Pollard, 1977, p. 257)

ν is Poisson's ratio

In correspondence with Equation 1-2-44

$$\delta_h = \alpha_h \lambda \qquad (2\text{-}11\text{-}15)$$

where α_h is the attenuation per unit length for hysteresis loss. Substitution of $\frac{c}{f}$ for λ in Equation 2-11-15 gives

$$\delta_h = \alpha_h \frac{c}{f} \qquad (2\text{-}11\text{-}16)$$

Substituting for δ_h in Equation 2-11-9 the expression given by Equation 2-11-16, and rearranging, yield

$$\alpha_h = \frac{f}{c} \frac{c_1}{\varepsilon_o} e^{-\frac{c_2}{\varepsilon_o}} \qquad (2\text{-}11\text{-}17)$$

Equation 2-11-17 shows that α_h varies as f, as is to be expected for hysteresis loss.

2-12. Microhysteresis Effect

The microhysteresis effect is, as mentioned in Section 2-8, one of three effects that result from motions of the walls of magnetic domains in ferromagnetic materials; the effect, one of attenuation, occurs because the relationship between the displacement of walls of domains and stress is not linear, but is represented by a hysteresis loop. Mason (1958, p.222) gives the power loss per unit volume, P_h, by the equation

$$P_h = \frac{4}{3} b T_{11}^3 f \qquad (2\text{-}12\text{-}1)$$

where T_{11} is the stress and b is the slope of the compliance-stress

curve, that is, where

$$b = \frac{d\left(\frac{1}{E_o}\right)}{d T_{11}} \qquad (2\text{-}12\text{-}2)$$

From Equation 2-12-1 is obtained, for the energy lost per cycle per unit volume, ΔW

$$\Delta W = \frac{4}{3} b T_{11}^3 \qquad (2\text{-}12\text{-}3)$$

and, in accordance with the principle of strain energy, the maximum energy stored per unit volume, W_{max}, is given by

$$W_{max} = \frac{1}{2} \frac{T_{11}^2}{E_o} \qquad (2\text{-}12\text{-}4)$$

Using the relation

$$\frac{1}{Q} = \frac{1}{2\pi} \frac{\Delta W}{W_{max}} \qquad (2\text{-}12\text{-}5)$$

and substituting, for ΔW and W_{max}, the expressions given by Equations 2-12-3 and 2-12-4, lead to

$$\frac{1}{Q} = \frac{4}{3} \frac{b E_o T_{11}}{\pi} \qquad (2\text{-}12\text{-}6)$$

Substituting, for $\frac{1}{Q}$ in Equation 2-6-5, the expression given by Equation 2-12-6, yields

$$\alpha = \frac{4}{3} \frac{f}{c} b E_o T_{11} \qquad (2\text{-}12\text{-}7)$$

Equation 2-12-7 shows that α varies as the frequency f.

Mason separates the microhysteresis loss (independent of frequency) from the micro-eddy-current loss (proportional to frequency) by taking the intercept at zero frequency in a graph of decrement δ against frequency for nickel; he obtains a value of 0,01 for δ and of about 0,003 for $\frac{1}{Q}$.

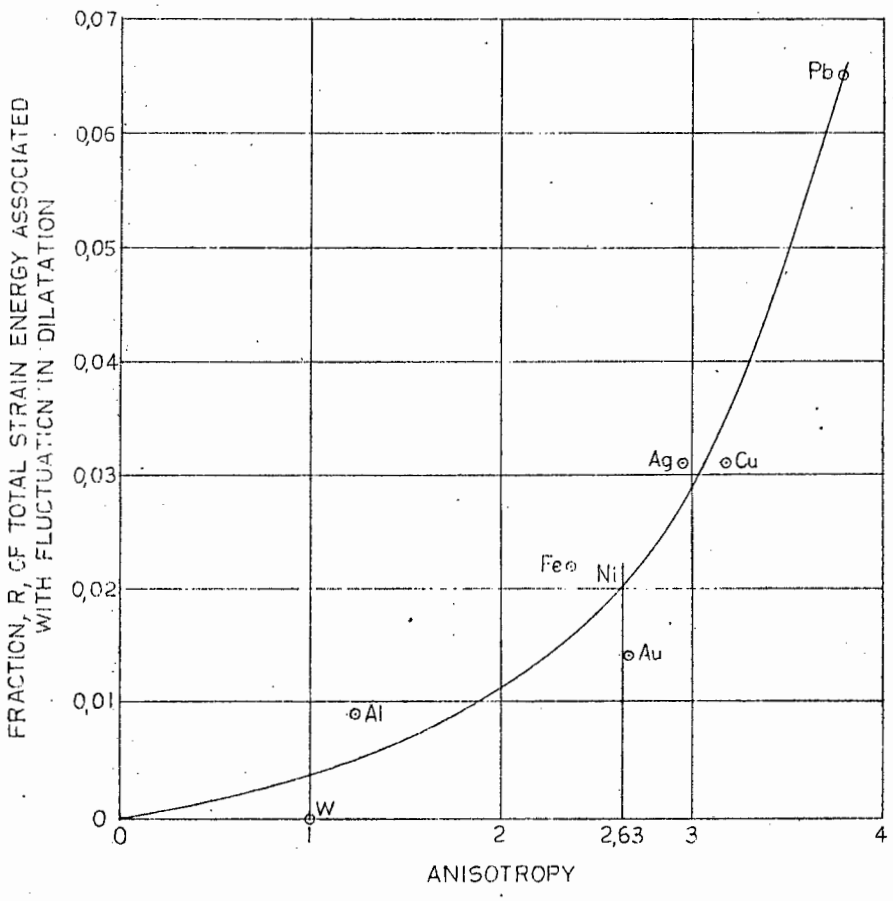

Figure 2-6-1. Graph used to determine the value of R, the fraction of the total strain energy associated with the fluctuation in dilatation, for nickel.

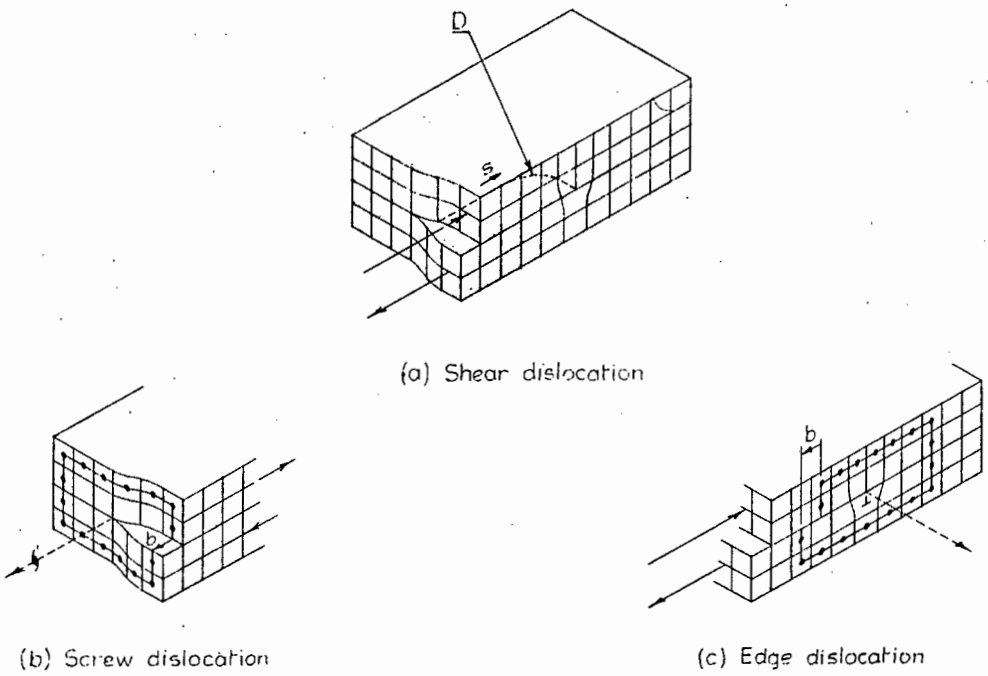

(a) Shear dislocation

(b) Screw dislocation

(c) Edge dislocation

Figure 2-9-1. A shear dislocation of a crystal, and the component dislocations (after van Vlack, 1970, p. 109).

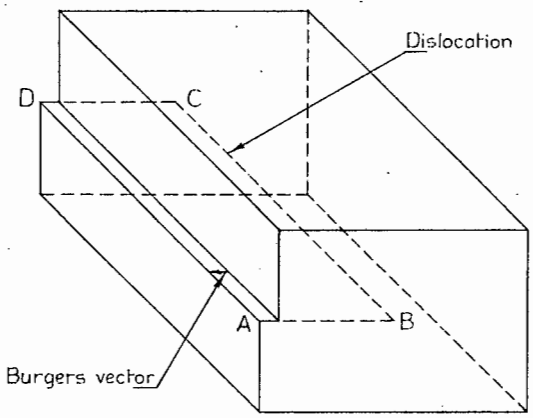

Figure 2-II-1. An edge dislocation in a crystal. The dislocation BC has been produced by unit slip over the area ABCD. (After Granato and Lücke, 1966, p. 230.)

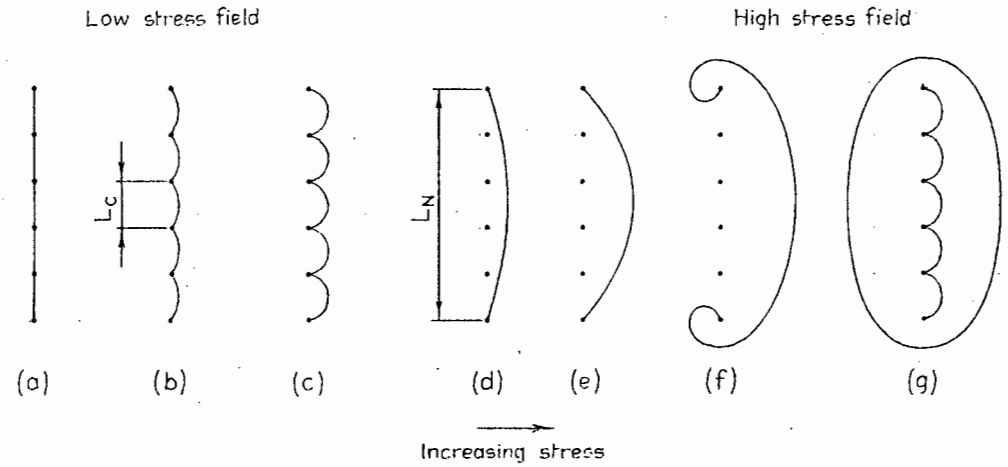

Figure 2-II-2. Successive diagrams indicating the bowing out and eventual reproduction of a pinned dislocation line under the influence of increasing stress (after Granato and Lücke, 1966, p. 238)

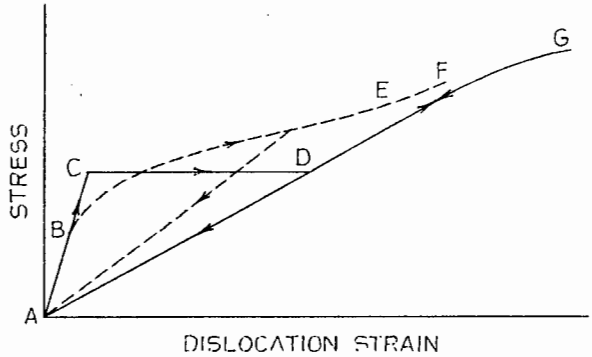

Figure 2-II-3. Graphs showing stress-strain laws for processes of the kind illustrated in Figure 2-II-2 (after Granato and Lücke, 1966, p. 239).

CHAPTER 3

EXPERIMENTAL APPARATUS

3-1. General Description

The apparatus used for the excitation and detection of longitudinal vibrations in nickel wire is shown diagrammatically in Figure 3-1-1. Trains or bursts of oscillations of voltage — the oscillations adjustable in number and frequency — are emitted by the signal-burst generator, at a rate of repetition of burst also adjustable, and applied to the transducer coil tuned to the oscillation, or signal, frequency. The voltage oscillations are transformed by the transducer, by the Joule effect, into longitudinal vibrations of the nickel wire in accordance with the theory described in Section 1-1, so that longitudinal acoustic waves are launched in the wire. The train of acoustic oscillations is propagated along the wire at a speed determined by the density and Young's modulus of the material of the wire in accordance with Equation 1-2-5, and is reflected at the far end so that it returns to the launching end where it again undergoes reflection, and at the same time induces in the transducer coil, by the Villari effect, a signal voltage, which is displayed by the oscilloscope. The train of oscillations continues to be propagated to-and-fro in the wire in a series of echoes, inducing in the coil a signal voltage each time it returns to the launching end, and suffering attenuation as it travels. Plate 3-1-1 shows a clipped drive burst of fourteen oscillations followed by four echoes of the signal, which suffers a rather large attenuation of about 9,5 decibels for a round of travel on the line.

Annealing, at red heat, of the end of the nickel wire at the transducer coil was found to result in an increase in the amplitudes of the echoes by a factor of 2 or 3.

3-2. Slide Wave-launching Unit

The slide wave-launching unit, depicted isometrically in Figure 3-2-1, and shown in Plates 3-2-1, 3-3-1 and 3-5-1, was constructed with the main aim of enabling the transducer coil to be supported clear of the nickel wire, while it is able to be moved

readily along the wire in finding the position for greatest signal strength as explained in Section 1-1. Clearance between the coil former and the nickel wire was considered desirable to prevent mechanical interference by the coil with acoustic waves in the wire.

The unit was constructed on a particle-board base of size 219 mm by 226 mm, the 219-mm edges being parallel to the nickel wire. On the base are two stretched rubber bands, which form supporting feet for the unit. At the front of the unit is the wire clamp, consisting of pads of polystyrene foam, which have a negligible effect on acoustic waves in the wire, compressed between boards of hardboard. The slide, the body of which is built up of hardboard, runs between guides of thick cardboard secured to the base at their ends with masking tape. On top of the body of the slide is the coil board of Veroboard, supported by three adjusting screws and pressed down by a retaining spring of thin steel wire. Cemented to the coil board is the transducer coil of about 445 turns of 0,051-mm-diameter enamelled copper wire wound on an alumina former having an internal diameter larger by about 0,5 mm than the diameter of the nickel wire.

A moveable anchor of polystyrene foam is used to restrict the deflection of the nickel wire under the pull of the biasing magnet, so that clearance between the coil former and the wire can be maintained.

Figure 3-2-2 shows in greater detail the construction of the transducer coil and its mounting.

3-3. Apparatus Used in an Investigation of the Phenomenon of the Anomalous Signal

Apparatus used in this investigation is seen in Plate 3-3-1; it consisted of the oscilloscope, frequency meter, decade capacitor, signal-burst generator and power supply, placed towards the back of the work-bench, and the baseboard carrying a nickel-wire transmission line and the slide wave-launching unit, placed towards the front of the bench. The line set up at the front edge of the bench was used in another investigation; the horseshoe magnet seen next to it was used with the slide wave-launching unit in this investigation. The arrangement corresponded to that shown in Figure 3-1-1. Short and long nickel-wire lines were used with the wave-

launching unit; a short line, about 1 235 mm long, is seen in Plate 3-3-1, while the greater part of the long line, formed into a spiral and supported by six slotted strips of polystyrene foam, is seen in Plate 3-3-2. The length of the long line was about 14 m.

For measurements for which termination of a transmission line in a high impedance was required, a stub, as illustrated in Figure 3-3-1, was used, soldered to the end of the nickel wire inserted into the hole in the stub. The stub was nominally a quarter-wavelength long and, at resonance, transformed the low impedance Z_2 at its far end to a high impedance Z_1 at the end joined to the transmission line according to the relation

$$Z_1 = \frac{Z_o^2}{Z_2} \qquad (3\text{-}3\text{-}1)$$

where Z_o is the characteristic impedance of the stub. Z_1 will be the impedance with which the transmission line is terminated; Z_1 is termed high if

$$Z_1 >> Z$$

where Z is the characteristic impedance of the transmission line. By substitution of the expression given by Equation 3-3-1 for Z_1 in the inequality above, it is seen to be necessary that

$$\frac{Z_o^2}{Z_2} >> Z$$

Because Z_o is easily made greater than Z, and because, since the far end of the stub is coupled only to air, Z_2 will be so small as to be negligible, the second inequality will be easily satisfied.

Where $Z_2 = 0$, as can be taken to be true here, and where the wavelength of the signal is variable, Z_1 is given by

$$Z_1 = jZ_o \tan 2\pi\frac{\ell}{\lambda} \qquad (3\text{-}3\text{-}2)$$

where ℓ is the length of the stub. Equation 3-3-2 shows that, for any value of λ different from the value for resonance, Z_1 varies directly as Z_o; hence the greater the value of Z_o, the greater will be the deviation in wavelength, from that for resonance, for which Z_1 falls to the smallest acceptable value, and so the greater

will be the bandwidth. Z_o, in accordance with Equation 1-2-17, is given by

$$Z_o = \rho c A$$

and so can be made large by choosing for the stub a material having a large value for ρc, such as tungsten or steel, and by making the cross-sectional area A of the stub large.

It is necessary to calculate the required length of a stub for optimum performance in a given range of frequencies. Equation 3-3-2 can be written

$$Z_1 = jZ_o \tan \frac{\pi}{2} \frac{4\ell}{\lambda} \tag{3-3-2a}$$

Now, if λ_{max} and λ_{min} are the wavelengths at the extremes of the frequency band to be covered, and if Z_1, which will be reactive, is to have magnitudes equal, but opposite in sign, for those wavelengths, then

$$jZ_o \tan \frac{\pi}{2} \frac{4\ell}{\lambda_{max}} = -jZ_o \tan \frac{\pi}{2} \frac{4\ell}{\lambda_{min}}$$

so that

$$\tan \frac{\pi}{2} \frac{4\ell}{\lambda_{max}} = -\tan \frac{\pi}{2} \frac{4\ell}{\lambda_{min}} \tag{3-3-3}$$

Now, for any angle θ

$$\tan \left(\frac{\pi}{2} - \theta\right) = -\tan \left(\frac{\pi}{2} + \theta\right)$$

or

$$\tan \frac{\pi}{2}(1 - \Delta) = -\tan \frac{\pi}{2}(1 + \Delta) \tag{3-3-4}$$

where $\Delta = \frac{\theta}{\frac{\pi}{2}}$

Equating corresponding arguments of Equations 3-3-3 and 3-3-4 gives

$$1 - \Delta = \frac{4\ell}{\lambda_{max}} \tag{3-3-5a}$$

$$1 + \Delta = \frac{4\ell}{\lambda_{min}} \tag{3-3-5b}$$

Adding Equations 3-3-5a and 3-3-5b and factorizing give

$$2 = 4\ell\left(\frac{1}{\lambda_{max}} + \frac{1}{\lambda_{min}}\right)$$

so that

$$1 = 2\ell\,\frac{\lambda_{min} + \lambda_{max}}{\lambda_{max}\,\lambda_{min}}$$

whence

$$\ell = \frac{1}{2}\,\frac{\lambda_{max}\,\lambda_{min}}{\lambda_{max} + \lambda_{min}} \qquad (3\text{-}3\text{-}6)$$

For a stub of mild steel, for which the bulk velocity c_b = 5 850 (m/s) (Hueter and Bolt, 1955, p. 26), and for the frequency range from 40 kHz to 100 kHz

$$\lambda_{min} = 58{,}5 \times 10^{-3} \text{ (m)}$$

$$\lambda_{max} = 146{,}3 \times 10^{-3} \text{ (m)}$$

whence

$$\ell = 20{,}9 \times 10^{-3} \text{ (m)}$$

3-4. Apparatus Used in Measurements of the Effect of Tensile Stress on Attenuation

The length of annealed nickel wire on which these measurements were made is seen in Plate 3-3-1 at the front edge of the work-bench, held in tension between the brass anchor bracket clamped to the bench, on the left, and the brass link connected to a spring balance, on the right. Mild-steel stubs like that illustrated in Figure 3-3-1, soldered to the ends of the wire, enabled tension to be applied to the wire, and tended to form with the wire a vibrating assembly that made contact with the faces of the anchor bracket and brass link in its nodal planes. The constructions at the ends of the wire are seen in greater detail in Plates 3-2-1 and 3-4-1. Frictional holding of the clamped anchor bracket to the bench was improved by the inclusion of a thin pad of rubber between it and the bench, while drag between the brass link and the bench was minimized by means of rollers. Adjustment of the tension in the wire was effected

by rotation of the nut on the eye-screw through the brass link, with the use of one or other of the two brass-wire links shown.

The total length of the annealed piece of nickel wire was 1 190,1 mm, and the length between the faces of the terminating stubs 1 180,7 mm.

The main parts of the apparatus, the brass anchor bracket and the brass link, which were formed of 3-mm-thick plate, were designed to withstand, in case the requirement arose, a load approximately equal to one that would induce yield-point tensile stress in the 1,52-mm-diameter annealed nickel wire. A value for the yield-point tensile stress for annealed nickel was not then available but, since iron and nickel have generally similar characteristics, the value of 10 tons/in^2 for wrought iron (Morley, 1940, p. 48) was used; expressed in S.1. units, the value is 1,55 x 10^8 N/m^2. The cross-sectional area of the wire is 1,81 x 10^{-6} m^2, so that the design load for the main parts was 1,55 x 10^8 x 1,81 x 10^{-6} N = 281 N. Other, smaller, parts were made strong enough to sustain a tensile force of 98 N, that is, 10 kg wt., the force for maximum scale reading of the spring balance used; sustaining of that force was the actual requirement.

The spring balance used in setting required values of tension was a precision balance made by Salter.

The transducer coil rested in contact with the nickel wire; for these measurements, that circumstance appeared to have little effect on accuracy.

The same arrangement of electronic apparatus was used for these measurements as was used in the investigation of the phenomenon of the anomalous signal.

3-5. Apparatus Used in Measurements of the Effect of Flexural Stress on Attenuation

The apparatus in which the annealed 1 190,1-mm-long piece of nickel wire was bent elastically, for part of its length, into arcs of circles having radii of from 10 m to 1 m is seen in Plate 3-5-1.

It consisted of the baseboard and slide wave-launching unit seen in Plate 3-3-1, together with a large white card set vertical and contiguous to the wire clamp of the wave-launching unit, and clipped to a supporting board of faced corrugated cardboard behind it.

The supporting board was equipped with an integral horizontal base, which was clipped to the baseboard, while vertical webs held the supporting board perpendicular to the base. On the card were set out, by means of x and calculated y co-ordinates, points on arcs of circles having radii of from 10 m to 1 m tangential, at the vertical edge of the card, to the horizontal line at the height of the centre of the wire clamp. Straight lines were drawn between the points for each arc. The nickel wire could be bent to cover, approximately, any of the sets of points for arcs by the generation of bending moments at its ends through the media of the fixed wire clamp and a moveable cross-bar carrying a strip of polystyrene foam into which the end of the wire was inserted. The weight of the wire prevented exact matching with the points, particularly when the radius of curvature was large, but the effect of the weight could be almost completely cancelled by the application of vertical support to the wire at one, two or three points along its length. Such support was applied by means of spring-loaded clamps of polystyrene foam that held the wire and that were suspended by threads held to the top edge of the board by clips, which enabled adjustment to be made. The purpose of this measure was to improve the uniformity of the bending moment in the part of the wire in flexure.

For simple bending of a beam (Morley, 1940, p. 140)

$$\frac{M}{I} = \frac{p}{y} = \frac{E}{R} \qquad (3\text{-}5\text{-}1)$$

where M is the bending moment

I is the second moment of area of the cross-section about its neutral axis

p is the fibre stress

y is the distance of the fibre from the neutral plane

E is Young's modulus

R is the radius of curvature of the neutral plane.

Equation 3-5-1 shows that M and p are proportional to $\frac{1}{R}$. Since it would seem reasonable to expect that any effects of bending would be simpler functions of M and p, and therefore of $\frac{1}{R}$, than of $\frac{1}{M}$ and $\frac{1}{p}$, the radii R of the arcs for which points were set out on the vertical card were chosen to make equal differences between successive values of $\frac{1}{R}$. In Table 3-5-1 are shown the values of $\frac{1}{R}$ for the chosen values of R.

Table 3-5-1

R in metres	10	5	$\frac{10}{3}$	2,5	2	$\frac{10}{6}$	$\frac{10}{7}$	1.25	$\frac{10}{9}$	1
$\frac{1}{R}$ in metres^{-1}	0,1	0,2	0,3	0,4	0,5	0,6	0,7	0,8	0,9	1

A signal-burst generator of modified design, which minimized unwanted interference with the received signal, was used for these measurements, instead of the one used previously. Differences in the design are described in Section 3-6.

3-6. Signal-burst Generators

Figure 3-6-1 is a block diagram of the signal-burst generator used in investigating the phenomenon of the anomalous signal and in measuring the effect of tensile stress on attenuation. The unit was an adaptation of a prototype constructed for a thesis by R. Gordon.

In the unit, a Type-74LS124 integrated circuit — a dual voltage-controlled oscillator — serves as a signal-frequency oscillator and as a burst-repetition-rate oscillator. The signal frequency can be varied by means of the signal-frequency control, a helical-track potentiometer, fitted to the front panel, while the range within which the frequency can be varied is determined by the value of the capacitor C_1 plugged in. An emitter-follower buffer between the frequency control and the integrated circuit minimizes the loss of linearity in the relationship between the potentiometer output voltage and control-shaft position caused by loading by the integrated circuit. The burst repetition rate can be varied by means of the burst-repetition-rate control, and the range of control by substitution of a capacitor C_2 of different value.

The square-wave output of the signal-frequency oscillator is passed or stopped in its path to the output amplifier by the AND gate; while the AND gate is enabled, the pulses passed are counted by the counters until a preset number have been counted, when a pulse from the counters triggers the monostable multivibrator, so causing the AND gate to be disabled. To ensure that enabling of the AND gate, which is effected cyclically by the free-running burst-repetition-rate oscillator, takes place at an instant such that the first pulse of signal passed is a whole pulse, the synchronizer is used. The synchronizer, a D-type edge-triggered flip-flop, is

fed with the square-wave signal and with a fixed-width command pulse at burst-repetition rate from the monostable multivibrator following the burst-repetition-rate oscillator. The synchronizer provides an output pulse that is almost a repetition of the command pulse: it begins at the first positive-going edge of the signal wave following the beginning of the command pulse, and ends at the first positive-going edge of the signal wave following the end of the command pulse.

The synchronized trigger signal that is the Q output of the synchronizer is converted by the following monostable multivibrator to a pulse of width smaller than the period of the signal at its highest frequency, so that the bistable multivibrator controlling the AND gate, once triggered, can be reset by a pulse from the counters after only one signal pulse has been counted.

The counters are decade (÷ 10) presettable up or down counters, worked in the down-count mode. The four-digit words with which the counters are to be loaded for the down-count are preset with the set-count switches. The range of counts available is from 1 to 15 x 10 + 15, that is, from 1 to 165.

Emitter-follower buffers provide a low-impedance source of continuous signal for the measurement of signal frequency, and a low-impedance source of the Q output of the synchronizer for triggering of the oscilloscope.

The output amplifier consists of a TIP37C transistor having its emitter earthed and its base driven by the signal at the mid-point of a voltage divider consisting of two 1,2-kΩ resistors in series, connected between the output terminal of the AND gate and earth. The tuned transducer coil is connected between the collector of the transistor and the +15-V supply.

The signal-burst generator described provided generally satisfactory signals for experiments, but had the disadvantage that, as a result of leakage or stray pick-up, a slight signal from the continuously running signal-frequency oscillator still reached the oscilloscope during the intervals between the generated bursts. The unwanted signal tended to obscure small echo signals, and so diminished the accuracy with which they could be measured. It was therefore decided, on completion of the measurements of the effect of tensile stress on attenuation, that for further work another signal-burst generator built in the Electronics Laboratory at the University, in which the signal-frequency oscillator was disabled during the intervals between bursts, should be used. Accordingly,

for the measurements of the effect of flexural stress on attenuation, the new signal-burst generator, which had, in addition, a push-pull output amplifier instead of the single-ended amplifier of the first generator, was used.

3-7. Annealer for Nickel Wire

The annealer, seen in Plate 3-7-1, consists of a tube of fused quartz of outside diameter 10 mm, inside diameter 8 mm and length 381 mm, supported by two legs of 1,61-mm-diameter tinned copper wire at each end. The tube carries an external winding of one layer, 295 mm long, of nickel-chrome wire, having a resistance of about 68 ohms. Two asbestos discs of diameter 50 mm, having central holes of such a size that the discs fit tightly on the quartz tube, are fitted to the tube, one near each end. The discs support a reflecting heat screen of aluminium, having the shape of an inverted U, composed, for convenience, of four thicknesses of aluminium foil. The complete assembly stands on a rectangular sheet of steel covered with aluminium foil.

The annealer was fed with a supply at variable voltage from an adjustable auto-transformer.

In Plate 3-7-1 are seen also a Fluke Type-8024B multimeter and a Fluke Type-K (chromel-alumel) thermocouple probe, which were used to measure the temperature within the quartz tube of the annealer. In the centre foreground is seen an iron-constantan thermocouple probe constructed by the author, which was used, with another digital multimeter set to indicate millivolts, for the same purpose.

A temperature of about 960°C within the quartz tube was attained for a supply voltage of about 240.

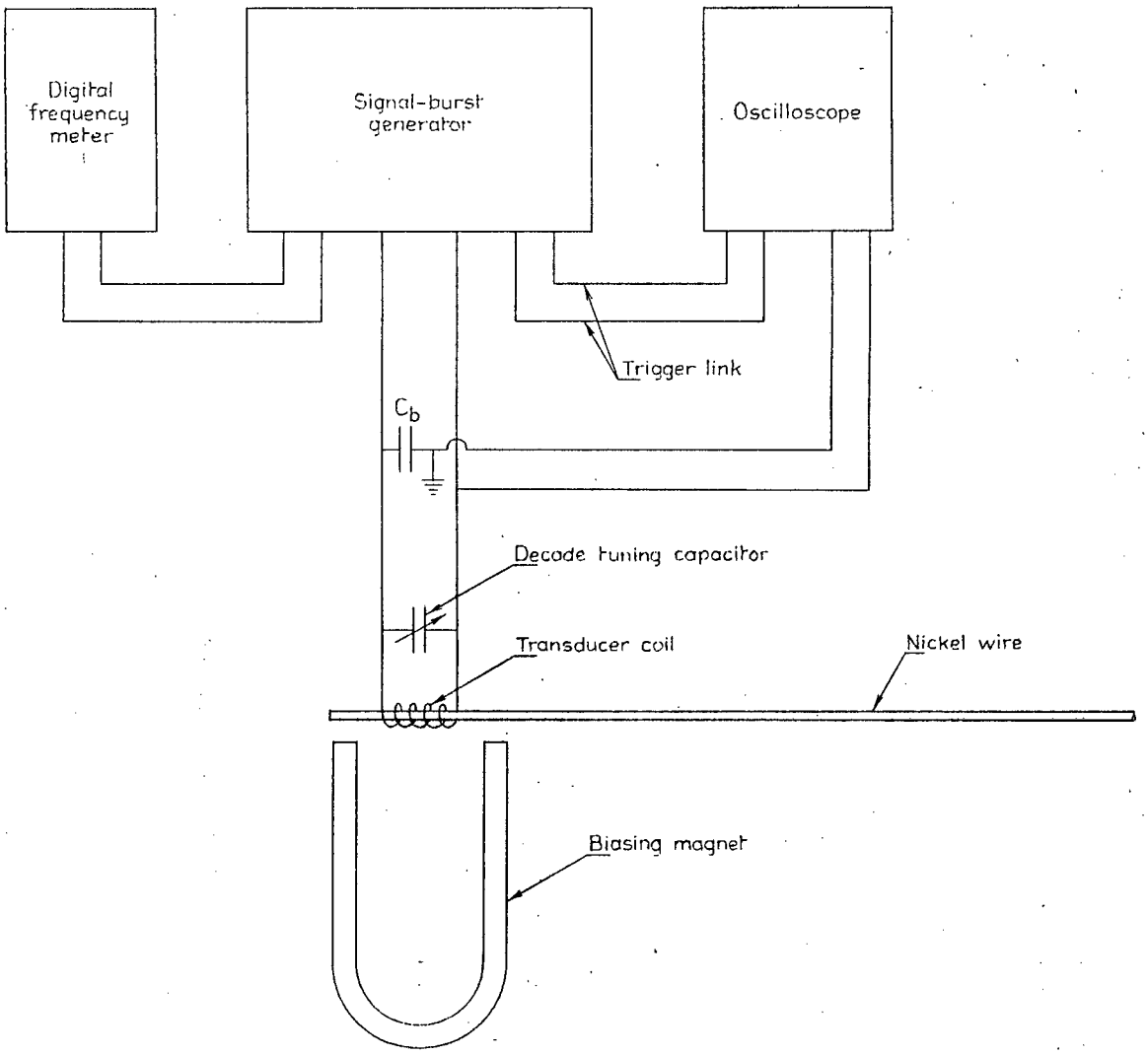

Figure 3-1-1. Apparatus for the excitation of longitudinal vibrations in nickel wire. The power supply for the signal-burst generator, providing supplies at +5 V, +15 V and −15 V, is not shown. The D.C.-blocking capacitor C_b is actually the smoothing capacitor for the +15-V supply.

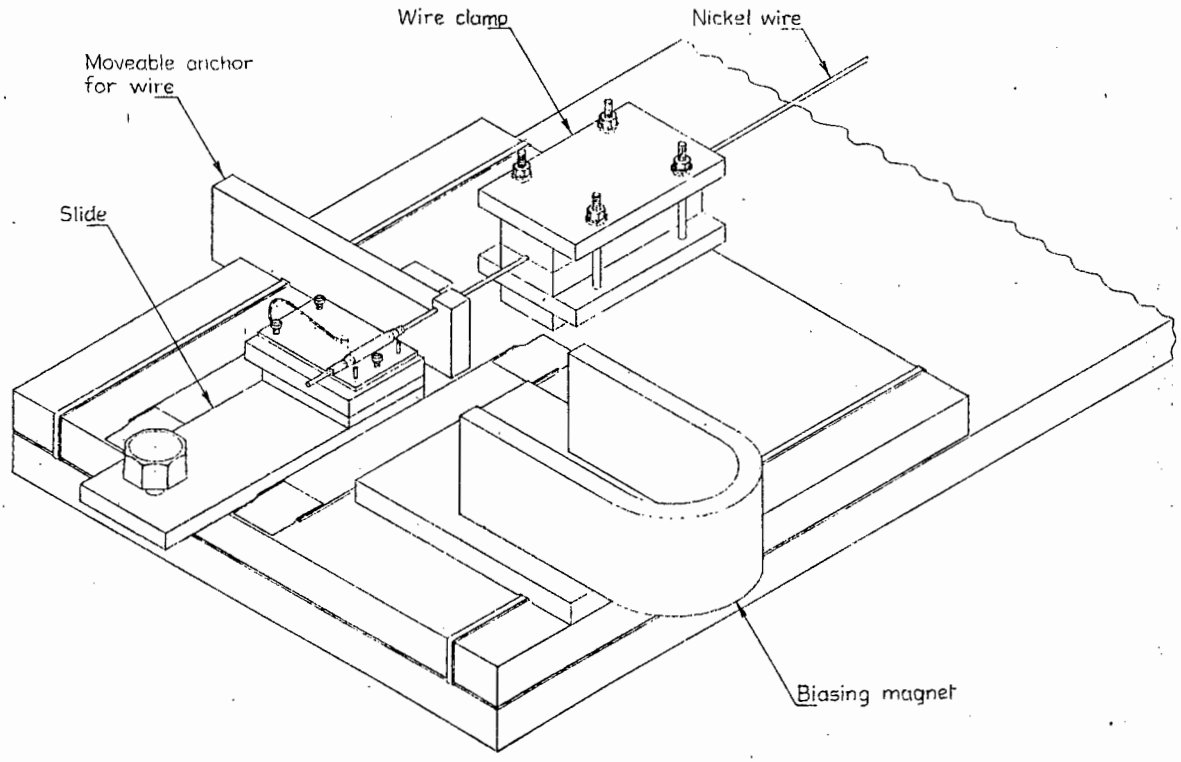

Figure 3-2-1. Slide wave-launching unit. For clarity, the biasing magnet is shown withdrawn from its working position nearer to the nickel wire.

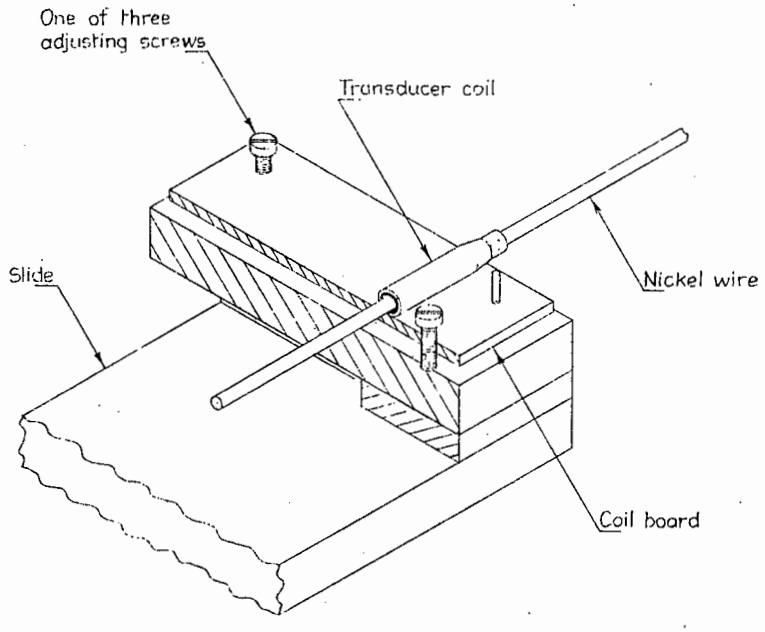

Figure 3-2-2. Sectional detail of the transducer coil and its mounting, in the slide wave-launching unit. The retaining spring for the coil board is not shown. Also, in this figure, as in Figure 3-2-1, the perforations of the Veroboard used for the coil board are not shown.

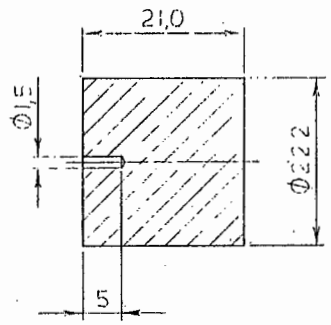

Dimensions are in millimetres

Scale 1:1

Figure 3-3-1. Sectional view of a cylindrical, mild-steel stub for high-impedance termination of the acoustic transmission lines.

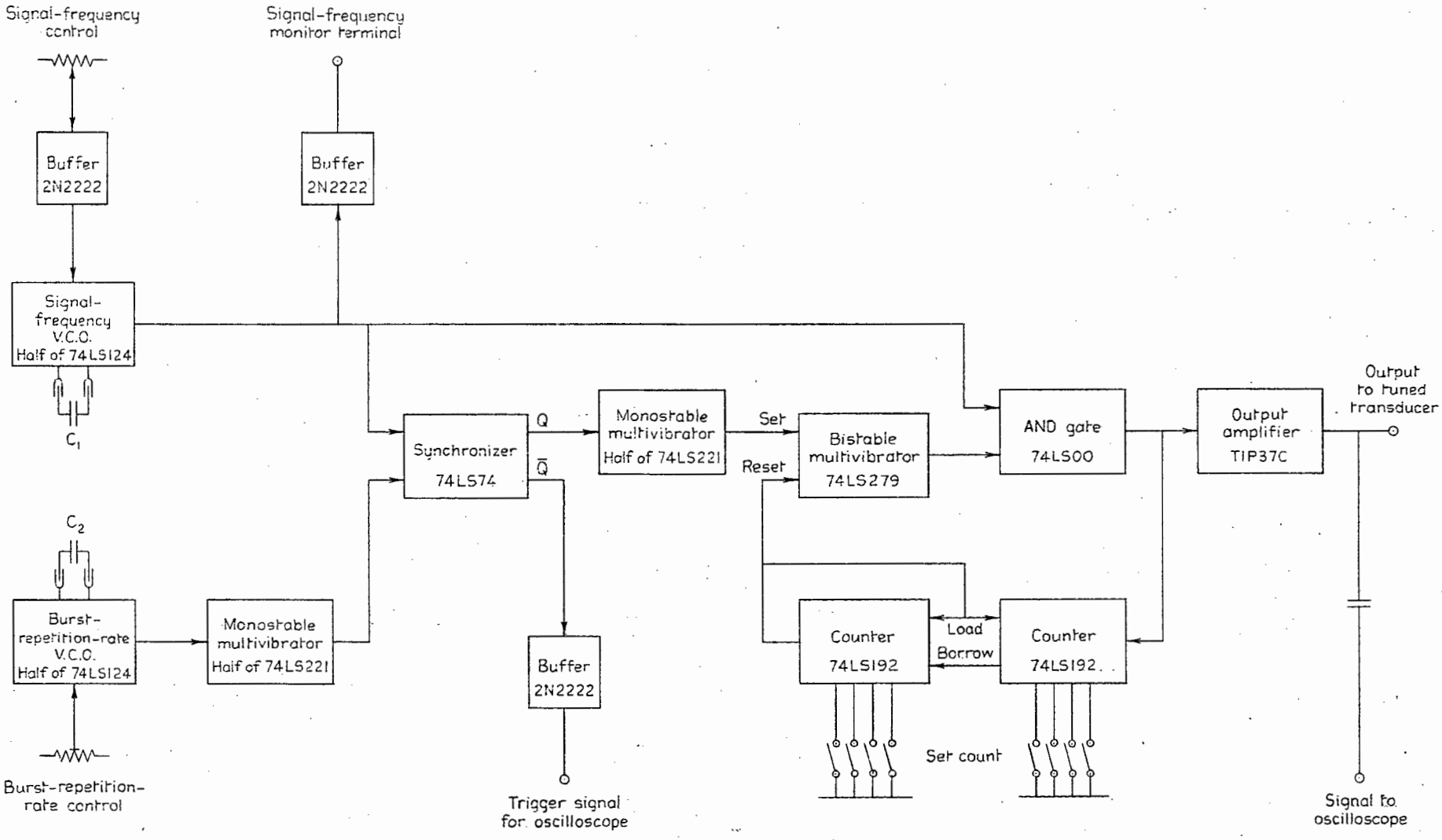

Figure 3-6-1. Block diagram of the signal-burst generator used at first in the investigations.

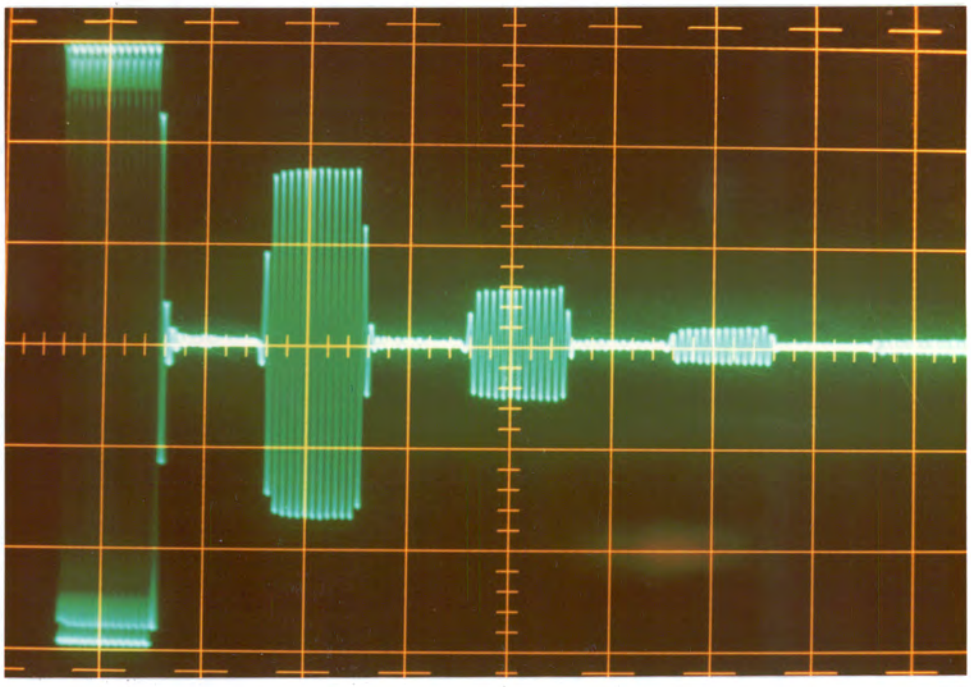

Plate 3-1-1. A clipped drive burst and four echo signals, at 50,78 kHz, for an annealed nickel wire, 1 190,1 mm long, in flexure to curvature of radius 10/9 m for 1 017,8 mm of its length.

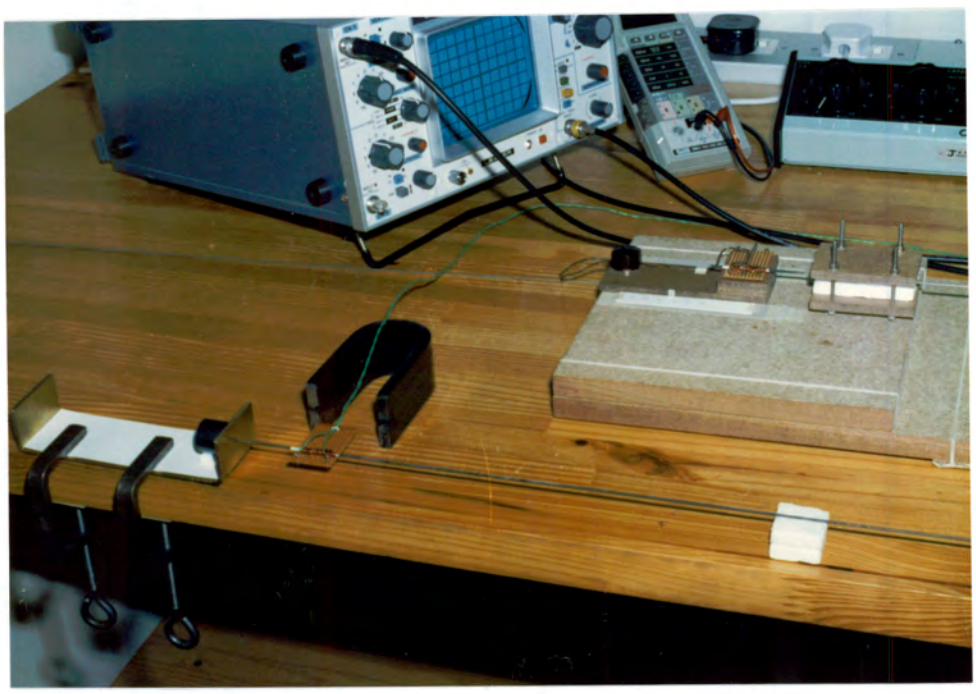

Plate 3-2-1. The slide wave-launching unit, and the transducer end of the line of annealed nickel wire on which measurements of the effect of tensile stress on attenuation were made.

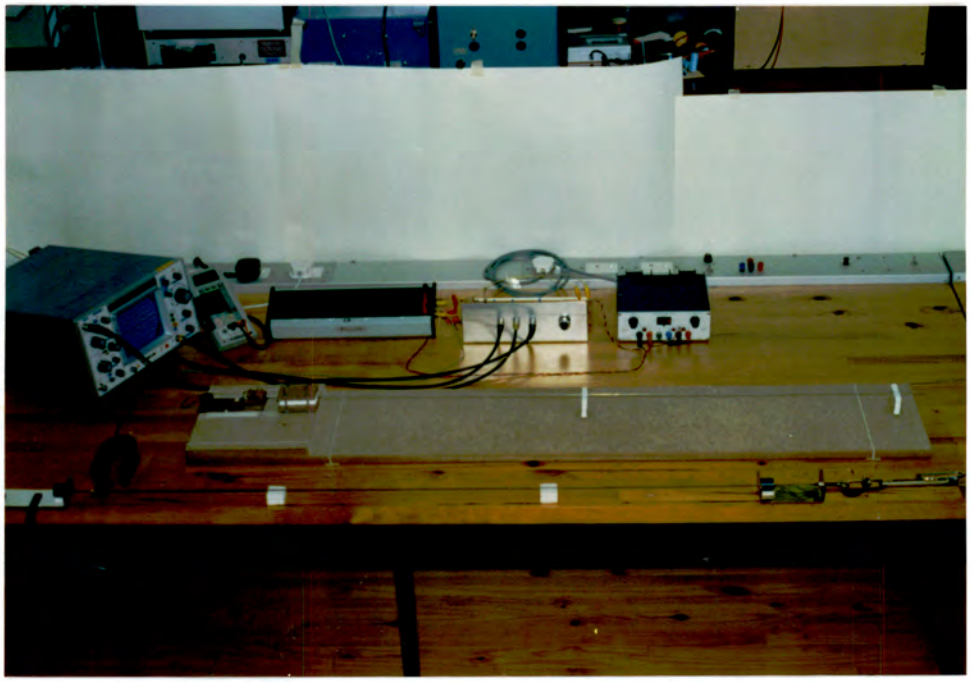

Plate 3-3-1. The electronic apparatus, a nickel-wire line used in the investigation of the phenomenon of the anomalous signal, and the annealed-nickel-wire line on which measurements of the effect of tensile stress on attenuation were made.

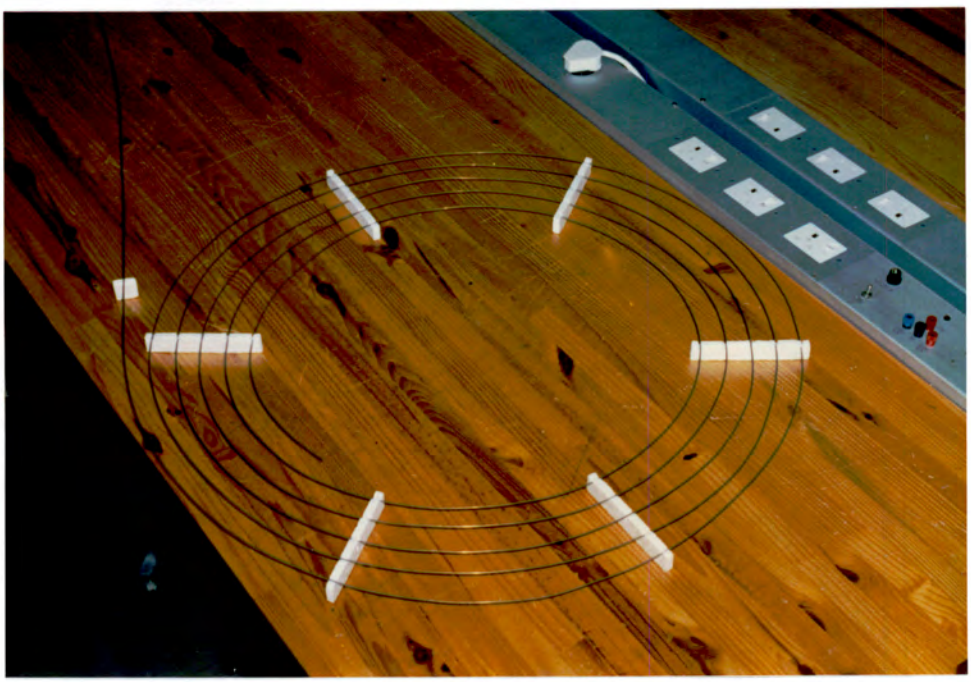

Plate 3-3-2. The greater part of the 14-m-long nickel-wire line.

Plate 3-4-1. In the foreground, construction at the far end of the line of annealed nickel wire on which measurements of the effect of tensile stress on attenuation were made.

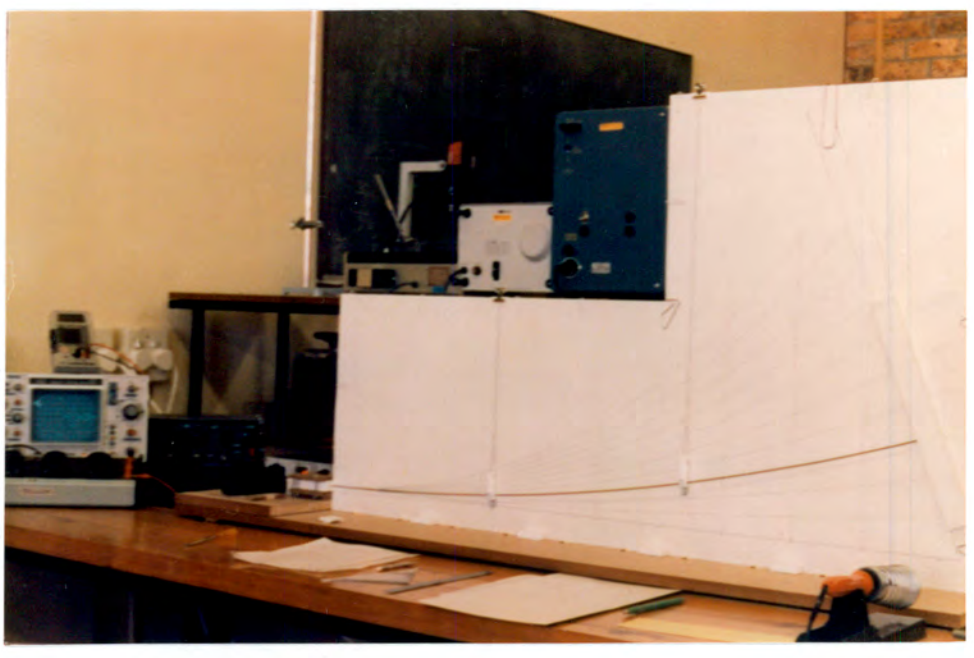

Plate 3-5-1. The apparatus used in measurements of the effect of flexural stress on attenuation.

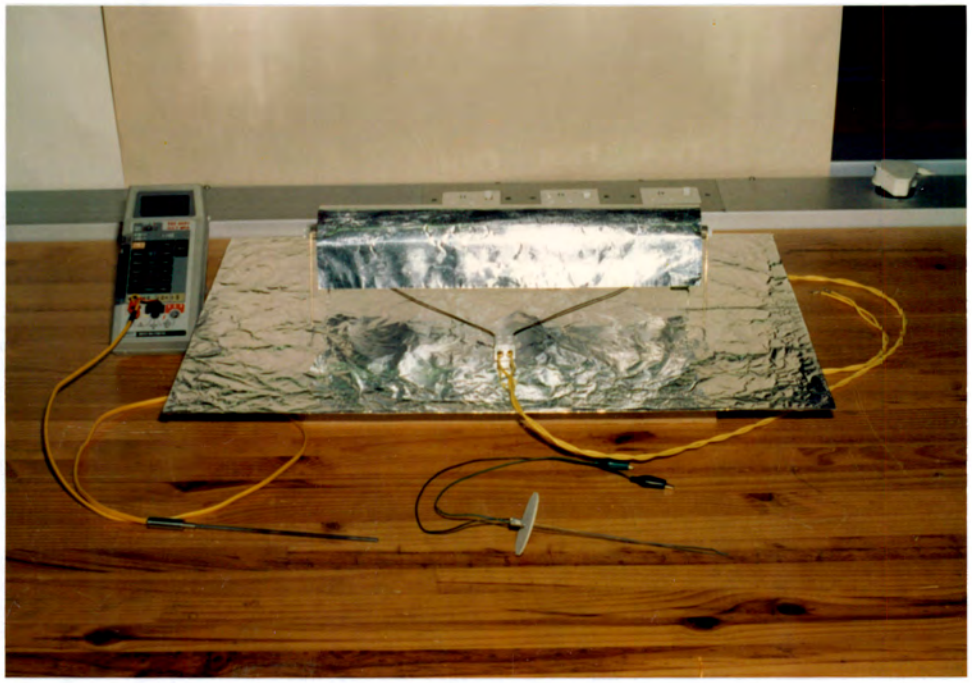

Plate 3-7-1. The annealer for nickel wire, and a meter and two thermocouple probes used for measurement of the temperature in the annealer.

CHAPTER 4

INVESTIGATION OF THE PHENOMENON OF THE ANOMALOUS SIGNAL

4-1. Occurrence of the Phenomenon

The wave-train-echo technique is one that has many different applications in fields of both research and measurement. In the example of a display of a wave train and its progressively attenuated echo signals shown in Plate 3-1-1, which was produced with signals of 59,78 kHz in a piece of annealed nickel wire 1 190,1 mm long, it will be observed that during the interval before the arrival of each echo signal only a very small, and relatively constant, signal exists, which is small enough to be neglected in relation to the echo signals. However, in the display illustrated in Plate 4-1-1, produced with signals of 20,04 kHz in the same piece of wire, it is seen that, while in the interval before the arrival of the second echo signal (third wave train) only a very small signal is displayed, in the following intervals a progressively increasing signal appears, which continues to increase until the seventh interval, after which it diminishes. This anomalous signal detracts from the definition of the weaker echo signals, and may also affect their amplitude. Such an anomalous signal, which is often encountered in wave-train-echo work, has been found to have maxima at a number of distinct frequencies in a given frequency range.

4-2. Preliminary Observations

Apparatus was set up as described in Section 3-3; a short length of nickel wire, of diameter 1,52 mm and length 1 291,4 mm, unannealed except for a few centimetres of its length at one end, within which distance the transducer coil would be positioned, was clamped in the slide wave-launching unit. Maxima of the anomalous signal were found to occur for signal frequencies of 57,3 kHz, 65,5 kHz and 78,2 kHz; for each frequency, the capacitive tuning of the transducer coil, the distance of the coil from the end of the nickel wire and the position of the biasing magnet were, in accordance with normal procedure, adjusted for greatest strength of the echo signals. The number of oscillations per train, or burst, was 11.

Tracings were taken of the oscilloscope displays of signals for the three frequencies for maxima of the anomalous signal.

Since the occurrence of anomalous signals during intervals between the echo signals proper suggested that reflection of signals was occurring at points in the nickel wire between the ends, the effect of introducing, artifically, points of reflection between the ends of the wire was tried. It was found that holding the wire with two fingers at certain points produced anomalous signals similar to those that occurred at other frequencies for the untouched line. A small piece of putty attached to the line had a similar effect. The magnitude of such artificially produced anomalous signals showed a sensitivity to signal frequency similar to that occurring in the untouched line.

4-3. A Suggested Mechanism for the Artifically Induced Phenomenon

Figure 4-3-1 is a time-displacement diagram in which the line ABCE represents part of the travel of a signal burst that is repeatedly passing up and down the transmission line by reflection at the ends. Two successive crossings of a discontinuity in the transmission line by the signal burst are represented by points B and E. The travels of waves reflected at the discontinuity are represented by the thinner lines.

It is assumed that the phase shift of the wave reflected at the discontinuity will be the same for travel of the incident wave in either direction. Hence, for $d_1 = d_2$, the indirect, that is, anomalous, waves travelling after the reflection at E will be in phase, since the phase shifts at C and D, and at B and E, will cancel.

For $d_1 \neq d_2$, and for the indirect waves after the reflection at E to be in phase, the difference between the lengths of the two tracks must be equal to an integral number of wavelengths. Hence

$$d_1 + 2d_2 - 3d_1 = n\lambda \qquad (4\text{-}3\text{-}1)$$

where λ is the wavelength and n an integer

Simplification of the equation gives

$$d_2 - d_1 = n\frac{\lambda}{2} \qquad (4\text{-}3\text{-}1a)$$

whence

$$\lambda = \frac{2(d_2 - d_1)}{n} \qquad (4\text{-}3\text{-}1b)$$

Now

$$f = \frac{c}{\lambda}$$

where f is the frequency and c the velocity of propagation; substitution of the right-hand side of Equation 4-3-1b for λ gives

$$f = \frac{c}{2(d_2 - d_1)} n \qquad (4\text{-}3\text{-}2)$$

By consideration of the part of the travel of the burst represented by the line CEGH, it can be shown similarly that, for the condition set by Equation 4-3-1a, all three indirect waves after the reflection at H will be in phase. It follows that all indirect waves after the subsequent reflections will be in phase.

Figure 4-3-2 shows, with a horizontal time axis, curves representing the amplitudes of the echo signals and anomalous signal for the maximum of the anomalous signal that occurred with the 1 291,4-mm-long nickel wire, untouched, for the signal frequency of 57,3 kHz. The middle of each echo signal is represented by a vertical line. If it is assumed that the anomalous signal is produced by reflections at a single discontinuity in the line then, since the anomalous signal acquires two contributions to its amplitude by reflection at the discontinuity for each forward-and-return journey of the signal burst, it can be stated that

$$\text{magnitude of reflection coefficient at discontinuity, } |r| \approx \frac{v_r}{v_i} \qquad (4\text{-}3\text{-}3)$$

where v_i is the amplitude of the signal burst and $2v_r$ is the increment in the amplitude of the anomalous signal per forward-and-return journey of the signal burst. From the tracing of the oscilloscope display, 0,025 in volts was read for $2v_r$ and 1,34 in volts for the corresponding value of v_i. Putting values for v_r and v_i in Equation 4-3-3 gives

$$|r| \approx \frac{\frac{1}{2} \times 0,025}{1,34}$$

$$\approx 0,0093$$

4-4. Further Observations, and an Attempted Verification of the Suggested Mechanism

4-4-1. Experimental Work, and Results. A second piece of nickel wire of diameter 1,52 mm, having a length of 1 234,7 mm, and being unannealed except for a few centimetres of its length at one end, was clamped near that end in the slide wave-launching unit. Maxima of the anomalous signal were found to occur for signal frequencies of 57,2 kHz and 46,2 kHz; it appeared as if there might be a maximum for a signal frequency near 37 kHz as well. The envelopes of the anomalous signals represented a less well defined pattern than those for the 1 291,4-mm-long wire.

It was thought that possible irregularities in the diameter of the nickel wire might be causing reflection, but measurements of the diameter of the 1 291,4-mm-long nickel wire in a large number (perhaps 50) of random positions with a 0 to 1-inch micrometer yielded no readings that could be observed to differ from 0,060 inch (1,524 mm). Bends in the wire gave rise to readings of up to 0,0605 inch (1,537 mm). A bent part of the wire between the gauge surfaces of the micrometer could be detected by observation of the surfaces and the outline of the wire against a bright background, in a line of sight coplanar with each surface in turn.

A third piece of nickel wire of diameter 1,52 mm, having a length of about 14 m, and being unannealed except for about 100 mm of its length at one end, was next used. Part of the wire, from the unannealed end to a point about 10 m from it, was formed into a flat spiral having an outside diameter of about 1 m; the spiral was placed on dishes of polystyrene foam for non-interfering support, while the remainder of the wire was extended tangentially from the spiral to the slide wave-launching unit, in which it was clamped near its end. Preliminary observations indicated the occurrence of about eight maxima of anomalous signal in the frequency range of 40 kHz to 100 kHz.

The spiral of nickel wire, supported on six improved supports in the form of slotted strips of polystyrene foam, is shown in Plate 3-3-2.

A conclusion was reached that frequencies for maxima of anomalous signal measured for high-impedance termination of the transmission line at its far end might, in accordance with the mechanism described in Section 4-3, occupy positions in the band

that interleaved with those of frequencies measured for a low-impedance (free-end) termination of the transmission line. With reference to Figure 4-3-1 and Equation 4-3-1, insertion of the term $-\frac{\lambda}{2}$ on the left-hand side of the equation, corresponding to an extra half-wavelength of travel in the track BCE, and so being equivalent in effect to a reversal of the sign of the reflection coefficient for the far end C, gives

$$d_1 + 2d_2 - 3d_1 - \frac{\lambda}{2} = n\lambda \qquad (4\text{-}4\text{-}3)$$

Simplification of the equation gives

$$d_2 - d_1 = \left(n + \frac{1}{2}\right)\frac{\lambda}{2} \qquad (4\text{-}4\text{-}3a)$$

whence

$$\lambda = \frac{2(d_2 - d_1)}{n + \frac{1}{2}} \qquad (4\text{-}4\text{-}3b)$$

Use of the relation

$$f = \frac{c}{\lambda}$$

leads to

$$f = \frac{c}{2(d_2 - d_1)}\left(n + \frac{1}{2}\right) \qquad (4\text{-}4\text{-}4)$$

Now, while Equation 4-3-2 shows that, for the transmission line terminated in a low impedance, frequencies for maxima of anomalous signal are given by a constant expression multiplied by n, Equation 4-4-4 shows that, for the transmission line terminated in a high impedance, the frequencies are given by the same constant expression multiplied by $\left(n + \frac{1}{2}\right)$. It is evident, therefore, that frequencies for the high-impedance termination will fall midway between those for the low-impedance termination.

Accordingly, a terminating stub designed as described in Section 3-3 for the frequency range of 40 kHz to 100 kHz, and illustrated in Figure 3-3-1, was turned from a piece of mild-steel rod. The far end of the 14-metre-long nickel wire was soldered in the stub with the aid of an electric hot-air blower, the surfaces of both the wire and the hole having been tinned previously. The depth

of insertion of the wire into the stub was 3,2 mm, according to a measurement made from the face of the stub to a datum-line previously scored round the wire 30 mm from the end.

Signal frequencies for maxima of the anomalous signal in the range of 40 kHz to 100 kHz, for signal bursts of 40, 100 and 160 oscillations, were then measured. The readings are set out in the first three lines of Table 4-4-1. The stub was next removed, and signal frequencies for maxima of the anomalous signal again measured. The nickel wire was then shortened by 3,2 mm by cutting at the far end, so that the length of the line without the terminating stub would be equal to the working length of the line terminated with the stub. Signal frequencies for maxima of the anomalous signal were again measured. The second and third sets of readings also are recorded in Table 4-4-1.

Some observations were next made of echoes of single-oscillation signals transmitted in one-way travel along the transmission line, which was terminated in an absorbing load consisting of a coating of soft putty about 950 mm in length, of which the first part, about 180 mm long, was tapered from negligibly small to full thickness, to make an outside diameter of about 6 mm. Echoes were received from points distributed along the length of the line. The straightening out of some of the small, irregular bends in the wire noticeably reduced the magnitudes of the echoes received from the positions of those bends.

Modifications were made to the signal-burst generator to extend the working range of signal frequencies downwards to include the frequency of 20 kHz. The group of readings of frequencies for maxima of the anomalous signal taken with the 14-m length of nickel wire shortened by 3,2 mm was then, for bursts of 40 and 100 oscillations, extended to include readings of lower frequency; the extra readings have been recorded in Table 4-4-1. It is to be noted that bursts of 160 oscillations, for signal frequencies of less than about 40 kHz, had durations so long that they occupied too great a part of the period of a round of travel for the 14-metre-long nickel wire.

In the plot of the readings for maxima of the anomalous signal for the 14-metre-long nickel wire shown in Figure 4-4-1, the extra readings taken in the lower-frequency part of the range for the wire shortened by 3,2 mm show a distribution having little conformity to that shown by the readings in the higher-frequency part of the range. It was thought that the interim experimentation with bends

in the wire might have caused changes in its condition that had affected the distribution, and so it was decided to make a new, complete set of measurements of frequencies to cover the whole range.

The new set of readings is recorded in Table 4-4-1. As before, for the final group of readings, the nickel wire was shortened by a distance equal to the depth to which it had been inserted into the terminating stub, namely 3,0 mm. The new set of readings is plotted with the previous set in Figure 4-4-1.

4-4-2. Discussion of the Results. In the first three groups of frequencies plotted in Figure 4-4-1, for the conditions labelled Line terminated in stub, Stub removed and Wire shortened by 3,2 mm, there is distinct evidence of interleaving of the frequencies for high- and low-impedance terminations of the line, which Equations 4-3-2 and 4-4-4 indicate will occur. The diminished degree of staggering for the high frequencies is probably the result of the lessening of the impedance of the stub as its resonance frequency, observed to be about 111,5 kHz, is approached.

In the second three groups of frequencies plotted, for the conditions labelled Line terminated in stub, Stub removed and Wire shortened by 3,0 mm, little, if any, definite evidence of interleaving of frequencies for high- and low-impedance terminations of the line is to be found.

An estimate should be made of the performance of the terminating stub for a signal frequency of 20 kHz, since it had been designed for the frequency range of 40 kHz to 100 kHz. For a frequency of 20 kHz and for c_b = 5 850 (m/s), λ = 0,2925 (m). Putting that value for λ, and the length of the stub for ℓ, in Equation 3-3-2, gives

$$Z_1 = jZ_o \tan 2\pi \frac{21 \times 10^{-3}}{0,2925}$$

$$= jZ_o \times 0,484 \qquad (4-4-5)$$

Let Z be the characteristic impedance of the nickel-wire transmission line, assumed to be lossless. Now let $|Z_1|$ = 10Z, which corresponds to an angle of the reflection coefficient at the stub of 11° [read from Smith Chart (Smith, 1939, 1944)] instead of the ideal value of 0° for $Z_1 = \infty$. Rearrangement of Equation 4-4-5, and substitution of 10Z for $|Z_1|$ give

$$Z_o = \frac{10Z}{0,484}$$

$$= 20,7Z$$

so that

$$\frac{Z_o}{Z} = 20,7$$

The ratio of ρcA (Equation 1-2-17) for the stub to ρcA for the nickel wire is likely to be greater than 20,7, so that $|Z_1|$ is likely to be greater than 10Z and the angle of the reflection coefficient less than 11°. At the low frequency of 20 kHz, therefore, the stub used should still provide a near enough approximation to a rigid termination.

The inconclusive result of the attempted verification of the suggested mechanism led to a decision to measure signal frequencies for maxima of the anomalous signal in a short transmission line of nickel wire for the line in turn open-ended and stub-terminated, then to anneal the wire at a temperature of not less than 450°C, and thereafter to make further measurements.

4-5. An Investigation of the Effect of Annealing of the Nickel Wire

4-5-1. Description of the Piece of Nickel Wire Used, and Initial Measurements. The piece of nickel wire, of diameter 1,52 mm and length 1 291,4 mm, that had been used in the preliminary observations, and which had, for incidental reasons, been shortened to a length of 1 199,3 mm, was used. The piece of wire, as well as having been shortened, had been made straighter by hand.

Frequencies for maxima of the anomalous signal, for the 1 199,3-mm-long nickel wire terminating in the stub, detached from the stub, and then shortened by a distance equal to the depth to which it had been inserted into the stub, were measured for signal bursts of 4, 8 and 16 oscillations. The readings are recorded in Table 4-5-1. Then, because incorrect longitudinal positioning of the nickel wire in the clamp of the slide wave-launching unit had prevented positioning of the transducer coil at a full quarter wavelength from the adjacent end of the line for some of the measurements at the lowest frequencies, the stub was resoldered to the wire, and another set of measurements made. The second set of readings is recorded in

Table 4-5-2. Finally, because the pattern of the last group of readings of the second set, for the condition labelled Wire shortened by 2,8 mm, did not match those of the groups of readings for the preceding two conditions, a group of measurements was made for the wire shortened by another 3,5 mm, to obtain an indication of any trend in the variation. The readings are recorded after the others in Table 4-5-2. The readings in both Table 4-5-1 and Table 4-5-2 are plotted in Figure 4-5-1.

The length of the nickel wire after the final shortening was 1 190,1 mm.

4-5-2. Annealing of the Nickel Wire. Two trial annealings of the 1 190,1-mm-long nickel wire were made. In the first, the nickel wire was passed at an estimated rate of 1 mm/s through a tube of mild steel having an internal diameter of 16 mm, a wall thickness of 2,25 mm and a length of 238 mm, that was heated in the flame of a large Bunsen burner. A faulty thermocouple probe prevented accurate measurement of the temperature within the tube at the time, but a later measurement with the iron-constantan probe, for conditions of heating judged to be nearly the same, gave the temperature of the hottest region in the tube as about 675°C. In the second trial annealing, the nickel wire was passed at about the same rate as before through a brass-sheathed mild-steel tube having an internal diameter of 10,5 mm, a wall thickness of 1 mm and a length of 301 mm, that was heated in the flame of the Bunsen burner to provide a temperature of the hottest region in the tube of about 725°C. Measurements made after each annealing showed that neither had caused any significant change in the frequencies for maxima of the anomalous signal or in the values of the maxima.

A third, and final, annealing of the 1 190,1-mm-long nickel wire was effected with the electrically heated annealer described in Section 3-7. The nickel wire was passed through the quartz tube of the annealer at a rate of about 1 mm/s; the temperature within the quartz tube, measured with a Fluke Type-8024B multimeter and a Fluke Type-K (chromel-alumel) thermocouple probe, was 819°C immediately before the passage of the nickel wire, and 831°C immediately after. The average temperature was 825°C.

4-5-3. Effects of the Annealing. Measurements made on the 1 190,1-mm-long nickel wire after the final annealing showed that, for a signal frequency of 50 kHz, the peak-to-peak magnitude of

the first echo signal was 0,22 V; the value for the unannealed wire had been 3,0 V. The peak-to-peak magnitude of the second echo signal after the final annealing was, for a signal frequency of 50 kHz, about one-twentieth of that of the first echo signal; for the unannealed wire, first and second echo signals had been nearly equal.

For signals of frequencies above about 30 kHz, a large anomalous signal was present in the interval between the drive burst and the first echo signal; the magnitude of the anomalous signal varied with frequency, and was, for signals of certain frequencies, comparable with that of the first echo.

4-5-4. Appearance of an Unexpected Effect. During the making of measurements, an increase in the magnitude of the first echo signal was noticed when pressure was applied, inadvertently with the arm, to the nickel wire between its points of support. Investigation showed that the effect was the result of elastic bending of the wire, and that it was a reversible effect: the first echo signal resumed its previous, smaller magnitude when the nickel wire was allowed to straighten. Evidently, the bending was causing a lessening of the attenuation of the signal travelling in the wire. It was found that an increase in the magnitude of the first echo signal to about four times as much could be brought about by pressing, with pieces of polystyrene foam, simultaneously at the centres of the two spans of the wire between the supports. An increase in the magnitude of the second echo signal was observed too, while the third and fourth echo signals, previously unobservable, became apparent. A still greater reduction in the attenuation in the nickel wire was brought about by bending the full length of the wire outside the slide wave-launching unit into an arc of a circle.

4-6. Discussion

The promising support for the suggested mechanism of the phenomenon of the anomalous signal seen in the first three groups of frequency readings for the 14-metre-long nickel wire plotted in Figure 4-4-1 is not followed by similar support in the second three groups of readings for the 14-metre-long wire plotted in Figure 4-4-1, nor in the seven groups of readings for the short

piece of nickel wire plotted in Figure 4-5-1. However, it is to be noted that the suggested mechanism was developed from consideration of a single point of reflection between the ends of a transmission line, and that experimental findings for a line in which there are a large number of points of reflection, as there may be in practice, are not easily predictable. Further mathematical treatment might help to resolve the problem.

The appearance of the phenomenon of the dependence of attenuation on stress was an interesting incidental result of the investigation of the phenomenon of the anomalous signal, and it was felt that to investigate the former phenomenon further might well be more profitable than to continue to work on the latter. The decision was therefore made to transfer attention to the phenomenon of stress-dependent attenuation.

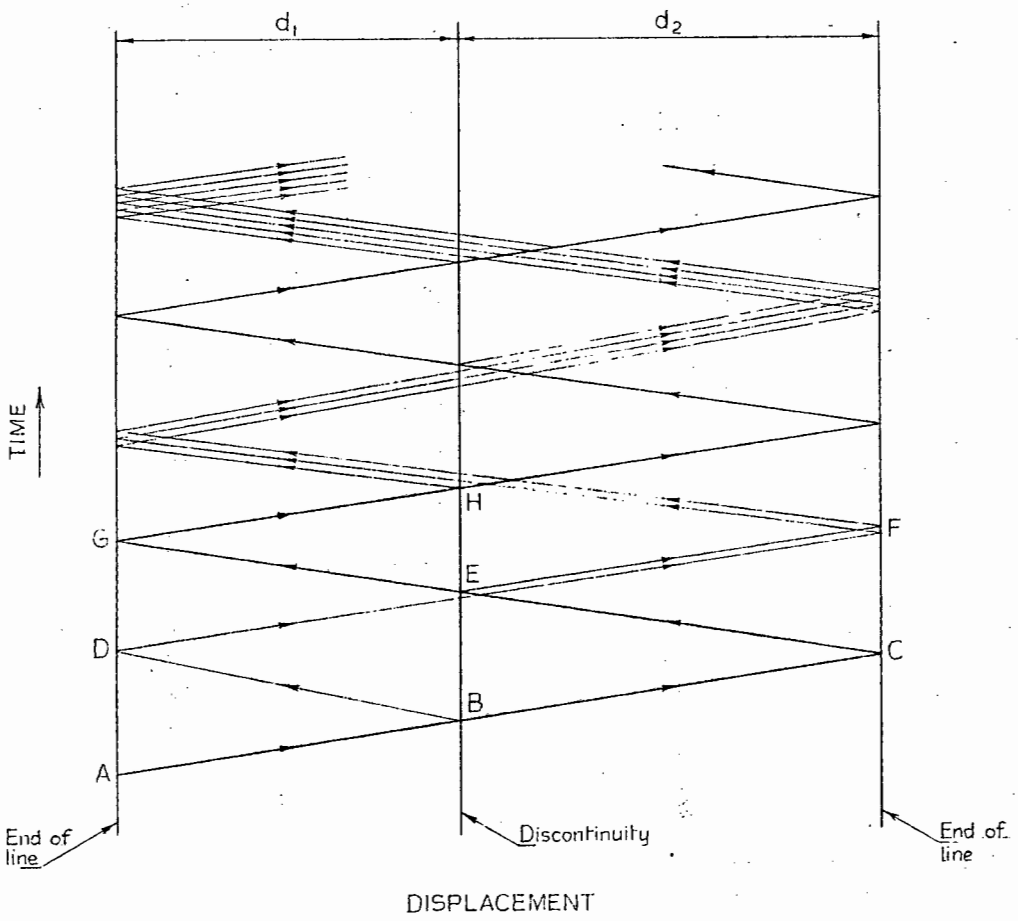

Figure 4-3-1. Time-displacement diagram for normal and anomalous waves in the transmission line.

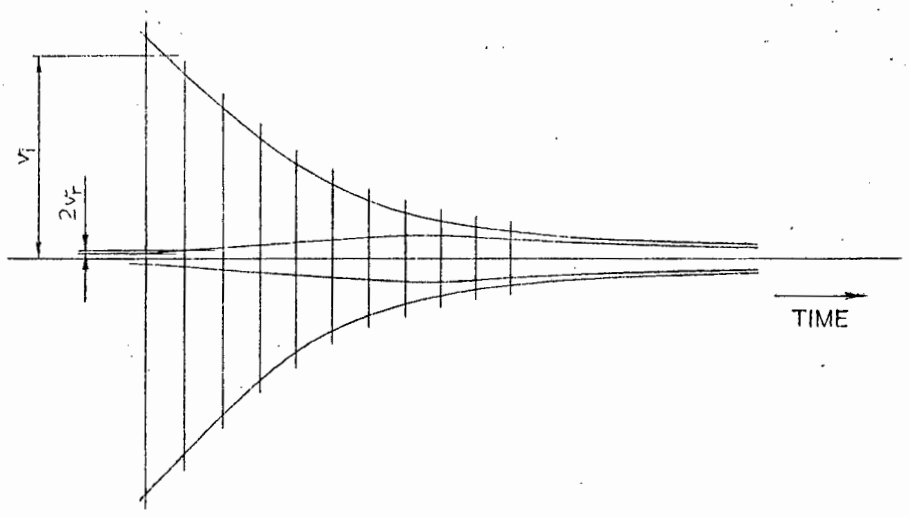

Figure 4-3-2. Envelopes of echo signals and anomalous signal for the 1190,1-mm-long transmission line, for a signal frequency of 57,3 kHz.

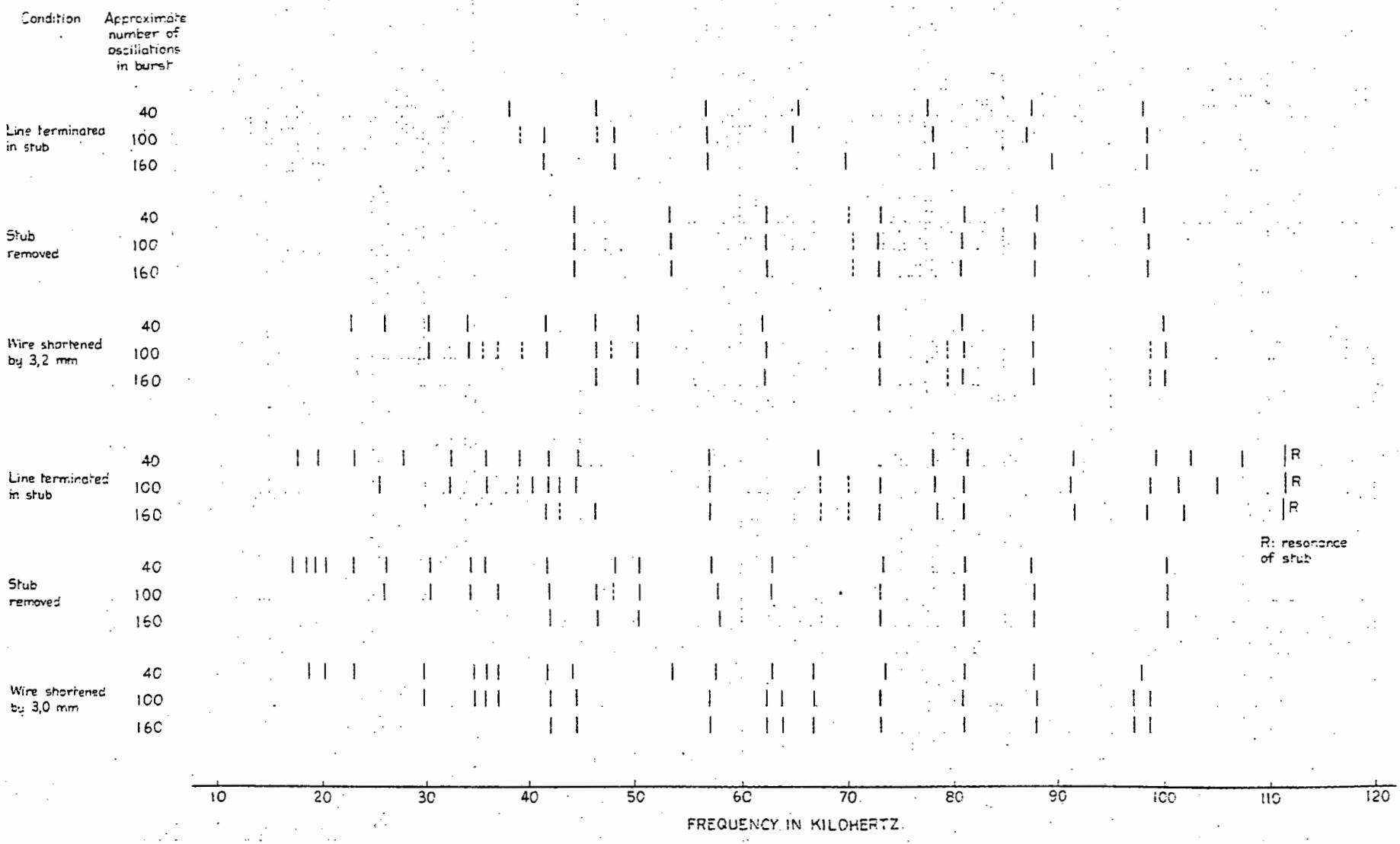

Figure 4-4-1. Signal frequencies for maxima of anomalous signal in the 14-m length of 1,52-mm-diameter nickel wire.

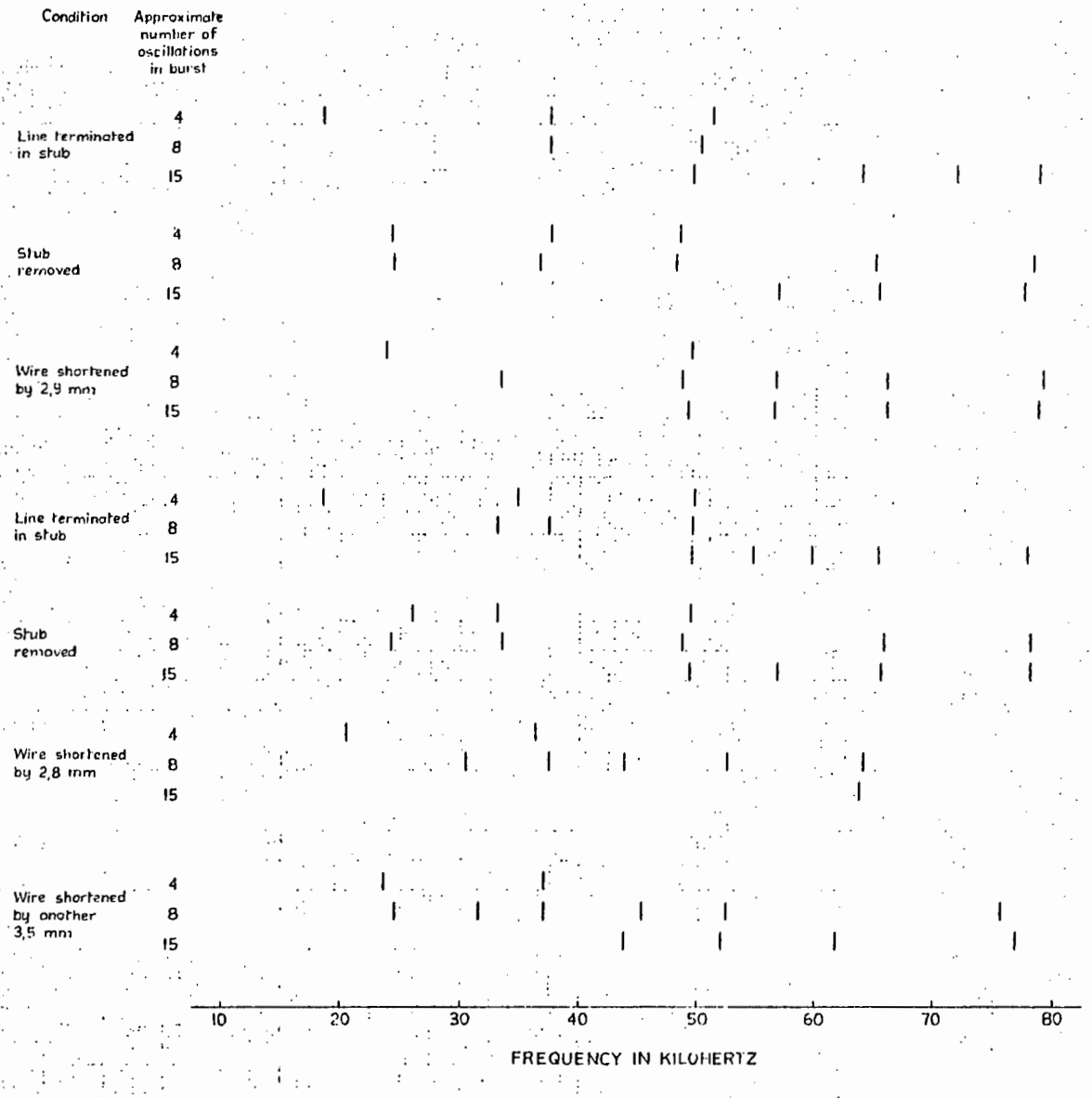

Figure 4-5-1. Signal frequencies for maxima of anomalous signal in a transmission line of 1,52-mm-diameter nickel wire. The length of the wire was 1199,3 mm initially, and 1190,1 mm finally.

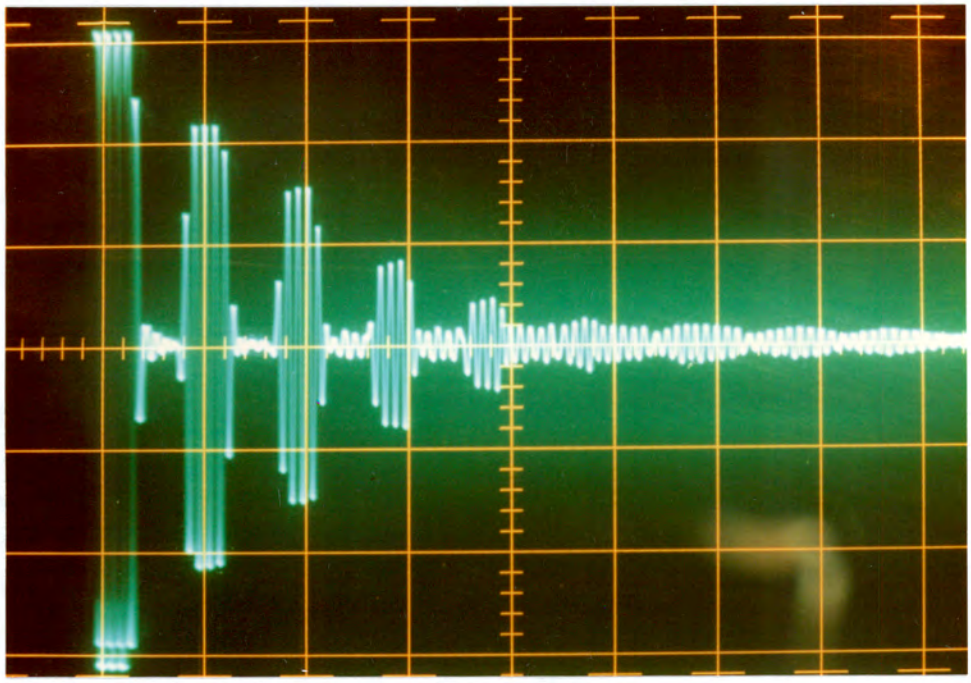

Plate 4-1-1. A clipped drive burst, echo signals and an anomalous signal, at 20,04 kHz, for the same annealed nickel wire, subjected to the same flexure, as for Plate 3-1-1.

Table 4-4-1

Condition	Approximate number of oscillations in burst	Signal frequencies, in kilohertz, for maxima of anomalous signal											
Line terminated in stub	40	98,2		87,8	77,7		65,6		56,9		46,7		38,5	
	100	98,6		87,3	78,2		65,1		57,0		48,4	46,8	41,8	39,6
	160	98,6		89,7	78,3		69,9		57,1		48,4		41,7	
Stub removed	40	98,3		88,2	81,2		73,2	70,2	62,5		53,4		44,6	
	100	98,7		88,0	80,9		72,9	70,6	62,4		53,6		44,6	
	160	98,6		88,0	80,8		73,0	70,5	62,5		53,6		44,6	
Wire shortened by 3,2 mm	40	100,1 41,8		87,8 34,3	80,9 30,4		72,9 26,2		62,1 23,0		50,5		46,5	
	100	100,3 41,9	98,8 39,6 37,2 35,7	87,8 34,4	81,1 30,4	79,5	73,0		62,4		50,4	48,0	46,6	
	160	100,2	98,7	87,8	80,9	79,5	73,0		62,3		50,4		46,6	
Line terminated in stub	40	111,5* 67,3 25,4		107,4 57,0 23,2	102,6 44,8 19,8		99,3 42,0 17,8		91,5 39,3		81,4 35,9		78,0 32,6	
	100	111,5* 73,0 70,0 25,6	67,4	105,1 57,1	101,4 44,6		98,7 43,0	41,9	91,2 40,4	39,1	81,0 36,0		78,2 32,4	
	160	111,3* 72,9 70,0	67,5	57,1	101,9 46,4		98,4 43,0	41,7	91,6		81,0		78,4	
Stub removed	40	62,9 30,4		57,2 26,2	50,5 23,1		100,3 48,3 20,4		87,5 41,8 19,5		81,1 35,8 18,6		73,3 34,5 17,3	
	100	62,8 34,4		57,8 30,4	50,5 26,0		100,3 48,1		87,8 46,5		81,0 42,0		73,0 37,1	
	160			57,9	50,4		100,3		87,7 46,6		80,9 42,1		73,0	
Wire shortened by 3,0 mm	40	66,7 37,1		62,8 35,9	57,6 34,7		97,8 53,5 29,8		87,7 23,1		81,0 44,2 20,3		73,5 41,8 18,8	
	100	66,8 37,1	63,7	62,3 35,8	98,6 57,0 34,8		97,1 53,4 29,8		88,0		80,8 44,6		72,9 42,1	
	160	66,7	63,8	62,3	98,6 57,1		97,1 53,5		87,9		80,9 44,6		73,0 42,1	

* Resonance frequency of stub

Table 4-5-1

Condition	Approximate number of oscillations in burst	Signal frequencies, in kilohertz, for maxima of anomalous signal								
Line terminated in stub	4					51,0	37,3		18,4	
	8					50,0	37,3			
	15	78,6	71,7	63,8		49,4				
Stub removed	4					48,3	37,4	24,1		
	8	78,2		65,0		48,0	36,5	24,3		
	15	77,5		65,3	56,7					
Wire shortened by 2,9 mm	4					49,4		23,7		
	8	79,1		66,0	56,6	48,6	33,3			
	15	78,7		66,0	56,4	49,1				

Table 4-5-2

Condition	Approximate number of oscillations in burst	Signal frequencies, in kilohertz, for maxima of anomalous signal												
Line terminated in stub	4						49,7			34,8				18,5
	8						49,6		37,4	33,1				
	15	77,8		65,3	59,7	54,7	49,5							
Stub removed	4						49,4				33,1	23,5		
	8	78,1		65,8			48,7				33,5	24,2		
	15	78,1		65,6	56,8		49,3							
Wire shortened by 2,8 mm	4								36,3					20,5
	8			64,1		52,5		43,8	37,4		30,4			
	15			63,7										
Wire shortened by another 3,5 mm	4								37,0			23,6		
	8	75,6				52,4		45,3	37,0		31,5	24,5		
	15	76,9		61,7		52,0		43,8						

CHAPTER 5

INVESTIGATION OF THE PHENOMENON OF STRESS-DEPENDENT ATTENUATION

5-1. Preliminary Work

Soon after the observation of the effect of flexure of the annealed nickel wire on the attenuation of ultrasonic waves travelling in it, as described in Section 4-5-4, work was begun on the design of apparatus with which the wire could be bent, for a large part of its length, to conform to arcs of circles of known radii. Besides that design work, tests were made to reveal roughly the ratios in which the magnitude of the first echo signal could be increased, at selected signal frequencies in the working range, by flexure of the annealed nickel wire. It was found that the ratio varied from about three for a signal frequency of 20 kHz to about thirty for a signal frequency of 100 kHz.

In a discussion with Associate Professor R.O. Heckroodt of the Department of Metallurgy and Materials Science (now Department of Materials Engineering) at the University of Cape Town, his opinion was expressed that the effect of the induction of direct, longitudinal stress in the nickel wire should be investigated. It was decided to follow the suggestion, and accordingly to suspend work on the design of apparatus for uniform flexure of nickel wire and to transfer attention to the design of apparatus for the measurement of attenuation in nickel wire subjected to direct, tensile stress.

Before the new design work was begun, a test was made to determine the effect of flexure on the magnitudes of echo signals in unannealed nickel wire. The 1 234,7-mm-long nickel wire, referred to in Section 4-4-1, of which a length of only about 60 mm at one end had been annealed for application in the transducer, was used in the test; it was found that virtually no change in the magnitudes of the echo signals occurred when it was deflected.

On completion of the designing and making of parts of the apparatus for measurement of the attenuation of ultrasonic waves in annealed nickel wire in tension, with the exception of the brass rollers and the anchor hook for the spring balance, the apparatus was set up substantially as seen in Plates 3-3-1, 3-2-1 and 3-4-1 and as described in Section 3-4. Preliminary observations of the

effects of increasing tension in the nickel wire indicated that little change occurred in the magnitude of the first echo signal but that increases occurred in the magnitudes of the following echo signals. The smallness of the change in the magnitude of the first echo signal appeared to result from near equality of the effects of reduction of attenuation in the nickel wire and reduction of efficacy of the transducer brought about by stress.

The effect of torsional stress in the nickel wire was noted: the wire was twisted, short of its limit of elasticity, for its full length, including the part functioning in magnetostriction; an appreciable diminution of attenuation resulted.

5-2. Measurements of the Attenuation of Ultrasonic Waves in Annealed Nickel Wire in Tension

5-2-1. Experimental Work. The apparatus used in this experimental work is described in Section 3-4. The annealed 1 190,1-mm-long piece of nickel wire, to the ends of which the terminating stubs were soldered, was used; the length of annealed nickel wire between the faces of the stubs was 1 180,7 mm.

The procedure adopted in making measurements of magnitudes for the determination of attenuation was to arrange a predetermined state of tension (the states included absence of tension) in the annealed nickel wire, and then to measure, at 10-kHz intervals, for signal frequencies of from 20 kHz to 100 kHz, the peak-to-peak magnitudes of the drive burst and the first five, or as many as were measurable, of the echo signals.

Trial runs of measurements were made for the nickel wire without tension and in tension of 10 kg wt., after which improvements were made in the apparatus, namely in the collinearity of the axes of the nickel wire and spring balance, in the security of the anchor hook for the spring balance and in the supporting of the terminating stubs and nickel-wire span. Then, with the apparatus set up as seen in Plates 3-3-1, 3-2-1 and 3-4-1, sets of measurements were made for the wire without tension and in tensions of from 1 to 10 kg wt., at intervals of 1 kg wt. A force of 10 kg wt. induces a stress of $5{,}41 \times 10^{7}$ N/m^2 in the 1,52-mm-diameter nickel wire, and a strain of $2{,}71 \times 10^{-4}$, calculated for $E = 2{,}0 \times 10^{11}$ (N/m^2).

The readings of peak-to-peak magnitudes of echo signals in millivolts, and calculated values in decibels with respect to one millivolt, for the readings, are recorded in Table 5-2-1.

5-2-2. Computation and Results. With the use of a Hewlett-Packard Type-85 desk-top computer and a linear-regression curve-fitting programme, plots were made of values of relative magnitude of echo signal in decibels with respect to one millivolt, against echo number. The mean attenuation of the echo signal per round of travel on the transmission line is given by the negative of the slope of the straight line most nearly fitting the points plotted; the value of the slope is printed out by the computer and the line drawn. Specimens of calculated values of slope (the numbers followed by the symbol X) and graphs are shown in Figure 5-2-1. The number designated YHAT is the y value of the stretch of the y axis intercepted between the x axis and the line. The negatives of the slopes, interpreted as mean values of attenuation of the echo signal per round of travel, are recorded in Table 5-2-2.

Figure 5-2-2a shows a family of curves of attenuation per round of travel in decibels as a function of signal frequency in kilohertz, where the parameter is tension in the nickel wire; Figure 5-2-2b shows a family of curves of attenuation per round of travel in decibels as a function of tension in the nickel wire, where the parameter is signal frequency. The curves were drawn from the values given in Table 5-2-2.

5-3. Measurements of the Attenuation of Ultrasonic Waves in Annealed Nickel Wire in Flexure

5-3-1. Experimental Work. The apparatus used in this experimental work is described in Section 3-5, and seen in Plate 3-5-1. The annealed 1 190,1-mm-long piece of nickel wire, after removal of the terminating stubs, was clamped in the slide wave-launching unit so that the length of the part projecting forward from the clamp was 1 017,8 mm.

In a procedure analogous to that followed for the measurements for annealed nickel wire in tension, the wire was set straight or was set, for the forward-projecting part of its length, to curvature of a predetermined radius, and measurements made, at 10-kHz intervals, for signal frequencies of from 20 kHz to 100 kHz, of the peak-to-peak magnitudes of the drive burst and the first five, or as many as were measurable, of the echo signals. The radii of the successive curvatures to which the forward-projecting part of the wire was set are given, with reasons for their choice, in Section 3-5. To enable the reversibility, on the

removal of stress, of the changes in attenuation to be investigated, measurements were begun for the straight wire, and then continued for the wire set, for the forward-projecting part of its length, to curvature of a radius of one metre; thereafter, measurements were continued for the wire set, for the forward-projecting part, to curvatures of increasing radius up to 10 m, and then completed for the wire again straight.

The deflection given to the wire was assumed, as a working approximation, to be equivalent to a constant curvature of the set value over the 1 017,8-mm length of the forward-projecting part. That assumption was based on the fact that constant, set curvature exists from the face of the clamp in the wave-launching unit to the face of the pad in the cross-bar; that, within the cross-bar pad, curvature exists, diminishing from set magnitude at the face at which the wire enters to zero at the opposite face; and that, in the clamp in the wave-launching unit, curvature exists, diminishing from set magnitude at the front face. The assumption is made that the effective loss of length at set curvature in the cross-bar is compensated by an effective gain of length at set curvature in the clamp.

For the 1,52-mm-diameter annealed nickel wire deflected to the curvature of the minimum radius of one metre, the greatest stress in the wire, occurring in the parts farthest from the neutral plane, is given by Equation 3-5-1: for $E = 2,0 \times 10^{11}\ (N/m^2)$, the value is $1,52 \times 10^{8}\ N/m^2$. The yield-point tensile stress for the annealed nickel wire was not known to any degree of exactness; however, no indication of permanent set in the wire was observed after flexure to curvature of the minumum radius.

The readings of peak-to-peak magnitudes of echo signals in millivolts, and calculated values, in decibels, with respect to one millivolt, for the readings, are recorded in Table 5-3-1.

5-3-2. Computation and Results. Graphs of relative magnitude of echo signal in decibels with respect to one millivolt, against echo number, were constructed with the use of a Hewlett Packard Type-35 desk-top computer, as described in Section 5-2-2. Specimens of calculated values of slopes, and graphs, are shown in Figure 5-3-1, while negatives of the slopes, interpreted as mean values of attenuation of the echo signal per round of travel, are recorded in Table 5-3-2.

Figures 5-3-2a and 5-3-2b show families of curves for annealed nickel wire in flexure, drawn from the values given in Table 5-3-2, corresponding to those for the same wire in tension, shown in Figures 5-2-2a and 5-2-2b.

5-4. Discussion of the Results.

The experiments performed have shown that the phenomenon of variation of attenuation of acoustic waves with stress, in nickel wire that has been annealed at about 825°C for about five minutes, is present for stress in any of three different forms, namely flexural stress, torsional (shear) stress and direct tensile stress. The experiments have shown that the phenomenon is absent for propagation in unannealed nickel wire.

The reversibility of the phenomenon, in the sense that a change in attenuation occurring on the induction of stress is reversed on the removal of the stress, has been established in the measurements made. Particular provision for the investigation of reversibility was not made in the arrangements for the measuring of variation of attenuation in the annealed nickel in tension; thus measurements for the wire unloaded were not repeated after the series of loadings. However, measurements for the same piece of wire, unstressed (without the terminating stubs, and hence 19,4 mm, that is, 1,6 per cent, longer as a transmission line) were later made in the first of the sets of measurements for the wire in flexure; comparison of the values of attenuation for infinite radius of curvature in Table 5-3-2 with those for absence of tension in Table 5-2-2 shows quite close agreement, and hence virtual reversibility. In the measurements for the wire in flexure, provision was made for the investigation of reversibility, as described in Section 5-3-1. The evidence of reversibility is confirmed: the initial and final sets of readings, both of them for the straight wire (infinite radius of curvature), in Table 5-3-2, taken respectively before and after the series of flexures, show reasonable agreement, and the two curves for $\frac{1}{R} = 0$ in the graph of Figure 5-3-2a, plotted from the same readings, are quite nearly coincident.

The graphs of Figures 5-2-2a and 5-3-2a show that the attenuation is quite closely proportional to the frequency of the signal. Proportionality of loss to frequency is characteristic of loss due to hysteresis, in which the fraction of the stored energy lost per cycle, or per wavelength, is constant. That relationship can

be deduced on combining Equations 1-2-44 and 1-2-45 and setting the fraction of the energy lost per cycle constant: thus

$$\text{logarithmic decrement} = \alpha\lambda = \frac{1}{2}\frac{\text{energy lost per cycle}}{\text{energy stored}} = \text{constant} \qquad (5\text{-}4\text{-}1)$$

so that

$$\alpha\lambda = \text{constant} \qquad (5\text{-}4\text{-}1a)$$

If ℓ is the length of the transmission line and A' the attenuation per round of travel in nepers

$$A' = 2\alpha\ell \qquad (5\text{-}4\text{-}2)$$

Multiplying and dividing the right-hand side of Equation 5-4-2 by λ give

$$A' = 2\alpha\lambda\frac{\ell}{\lambda}$$

Putting $\alpha\lambda$ = constant, in accordance with Equation 5-4-1a, gives

$$A' = 2 \times \text{constant} \times \frac{\ell}{\lambda}$$

whence, since $\lambda = \frac{c}{f}$, is obtained

$$A' = 2 \times \text{constant} \times \frac{\ell}{c} f \qquad (5\text{-}4\text{-}3)$$

or

$$A = 2 \times \frac{20}{\log_e 10} \times \text{constant} \times \frac{\ell}{c} f \qquad (5\text{-}4\text{-}3a)$$

where A is the attenuation per round of travel in decibels.
Equations 5-4-3 and 5-4-3a show that the attenuation per round of travel is proportional to the frequency f.

The length of the part of the annealed nickel wire that was subjected to tension was 1 180,7mm, while the length of the part subjected to flexure was 1 017,8 mm; the ratio of the lengths is 1,16. The graphs of Figures 5-2-2b and 5-3-2b show that the changes in attenuation for greatest tension are greater than for greatest

flexure; that relationship is found to remain true even if the changes for flexure are increased in the ratio of 1,16, to correct for the difference in length. Yet the greatest direct stress of $5{,}41 \times 10^7$ N/m² is only about one third of the maximum fibre stress of $1{,}52 \times 10^8$ N/m² at greatest flexure. Nevertheless, that circumstance may be expected, since, for flexure, stress varies from zero at the neutral plane to maxima in parts farthest from it, while, for direct tension, the stress in the wire is uniform.

The effect of compression on attenuation would appear to be similar to that of tension since, in flexure, halves of the wire on either side of the neutral plane are subjected to tension and compression respectively. At least, it is clear that the effects of tension and compression do not cancel.

A square-law relationship between stress and attenuation would seem possible, since that relationship would result in the occurrence of changes in attenuation of the same numerical magnitude, and of the same sign, for a given stress, whether tensile or compressive. With that possibility in view, it was thought to be of interest to attempt to discover a function implicit in the experimental curves; knowledge of such a function might help to provide insight into the physical mechanism of the phenomenon.

5-5. Development of an Empirical Equation for Attenuation of Ultrasonic Waves in Annealed Nickel Wire in Tension

The general resemblance of the curves of attenuation as a function of tension of Figure 5-2-2b to half-curves of resonance provided a starting-point. The equation for the current in a series inductive-capacitive-resistive circuit as a function of angular velocity was modified, with an approximation, to provide an equation in which the independent variable is the deviation from angular velocity for resonance instead of the angular velocity itself. The resulting equation is

$$I = I_{max} \frac{1}{\sqrt{1 + k(\Delta\omega)^2}} \qquad (5\text{-}4\text{-}4)$$

where I is the current

I_{max} is the maximum value of the current

k is a constant

$\Delta\omega$ is the deviation in angular velocity from the value for resonance

An equation having a form similar to that of Equation 5-4-4, designed, with appropriate symbols, to express the attenuation of waves in the annealed nickel wire as a function of frequency and static tension, can be written

$$A = af \frac{1}{\sqrt{1 + bt^2}} \qquad (5\text{-}4\text{-}5)$$

where A is the attenuation in decibels
f is the signal frequency in hertz
t is the tension in kilograms weight
a is a constant
b is a constant

Variations of Equation 5-4-5, in which A varies as other functions of t, are

$$A = af \frac{1}{1 + bt^2} \qquad (5\text{-}4\text{-}6)$$

$$A = af \frac{1}{\sqrt{1 + bt^4}} \qquad (5\text{-}4\text{-}7)$$

$$A = af \frac{1}{1 + bt^4} \qquad (5\text{-}4\text{-}8)$$

A previously constructed normalized curve of attenuation per round of travel as a function of tension for a signal frequency of 100 kHz, each value of attenuation for which was obtained as the average of the experimental value for 100 kHz, if recorded, and experimental values normalized for 100 kHz by proportion, was used in assessing the applicability of each of the four equations, Equations 5-4-5 to 5-4-8. A curve was drawn for 100 kHz for each of the four equations, for appropriate values of the constants a and b, and the curves compared with the normalized curve for 100 kHz. The curve for Equation 5-4-7 came most nearly to fitting.

Normalized values of attenuation and their averages were then calculated for the mid-range signal frequency of 60 kHz, from the values in Table 5-2-2; the values are shown in Table 5-4-1. A normalized curve of attenuation per round of travel as a function of tension was then drawn from the values, and comparison made with curves drawn for the four equations, for 60 kHz and for

appropriate values of the constants a and b. As before, the most nearly fitting curve was that for Equation 5-4-7. Finally, a small adjustment was made in the value of the constant b of Equation 5-4-7 to provide an optimum fit of the curve for that equation to the normalized experimental curve for 60 kHz; the curve for the equation was then redrawn. The two curves are shown in Figure 5-4-1. The equation for the best-fitting curve is

$$A = 5{,}33 \times 10^{-4} f \frac{1}{\sqrt{1 + 0{,}0043t^4}} \qquad (5\text{-}4\text{-}9)$$

The experimental and best-fitting curves are shown in Figure 5-4-1.

For values of t for which $0{,}0043t^4 \gg 1$, Equation 5-4-9 can be written

$$A = 5{,}33 \times 10^{-4} f \frac{1}{\sqrt{0{,}0043t^4}}$$

whence

$$A = 5{,}33 \times 10^{-4} f \frac{1}{0{,}066t^2} \qquad (5\text{-}4\text{-}10)$$

It is seen that, for values of t that satisfy the inequality $0{,}0043t^4 \gg 1$,

$$A \propto t^{-2}$$

Figure 5-4-2 shows graphs of experimental values of A plotted against values of t^{-2} for highest, median and lowest frequencies in the range, for values of t from 10 to 5, in kilograms weight. It is seen that, for $t^{-2} \leq 0{,}0028$, that is, for $0{,}0043t^4 \geq 5{,}48$, A is quite closely proportional to t^{-2} for all three frequencies.

It is significant that, in Equation 5-4-7, t occurs in an even-power term, since that implies that the attenuation is independent of the sign of a given numerical value of t, and therefore that, for a given degree of loading of the annealed nickel wire, the attenuation is the same whether the loading is tensile or compressive.

5-6. Indications of the Nature of the Mechanism of the Phenomenon

A notable characteristic of the phenomenon of stress-dependent attenuation, shown by the curves of Figures 5-2-2a and 5-3-2a, is the near proportionality of the attenuation per round of travel to the signal frequency. The attenuation per unit length, α, is therefore closely proportional to the signal frequency; that characteristic, as shown in Section 5-4, is one of loss due to hysteresis.

Of the twelve known processes of attenuation in the classification chart of Figure 1-3-1, only two have α proportional to the frequency f: they are dislocation damping of the hysteresis form and the microhysteresis effect.

An important characteristic of dislocation damping of the hysteresis form, accounted for by Granato and Lücke (1966) in their vibrating-string theory, is dependence of the loss on the amplitude of the vibration. (See Section 2-11 of this thesis.) In contrast to that, independence of attenuation on amplitude of vibration for annealed nickel wire, at least in the range of amplitude of the measurements, is strikingly shown in the linearity of the plots, for three or more points, of Figures 5-2-1 and 5-3-1, in which relative magnitude of echo signal in decibels is shown as a function of echo number; the nearly linear plots indicate almost complete independence of decrement on amplitude. Similar virtual independence of decrement on amplitude is shown in plots for other parts of the ranges of stress and frequency. That independence would seem to suggest that the stress-dependent attenuation is not the result of dislocation damping.

The microhysteresis effect, referred to in Section 2-8 and treated in Section 2-12, is one that occurs in magnetostrictive materials as a result of motions of the walls of magnetic domains. Bratina (1966) discusses such magnetomechanical damping and shows curves (1966, p. 235) for attenuation in decibels per microsecond in annealed 0,20% carbon steel for a frequency of 3 MHz, where the steel is subjected to both static strain and a magnetic field. For no magnetic field, an appreciable diminution of attenuation occurs with increasing static strain; as the external field is increased, the attenuation for zero static strain progressively diminishes, as does the rate of decrease of attenuation with increasing static strain diminish. For large magnetic fields,

the diminution of attenuation with small, increasing static strain reverses, to become an increase.

Bratina observes (1966, p. 238) that the decrease in attenuation in the annealed material with either field or stress must be due to change in domain configuration. It would therefore seem to be of value to make measurements on annealed nickel for applied mechanical loading and magnetic field, and to study the combined effects on the attenuation.

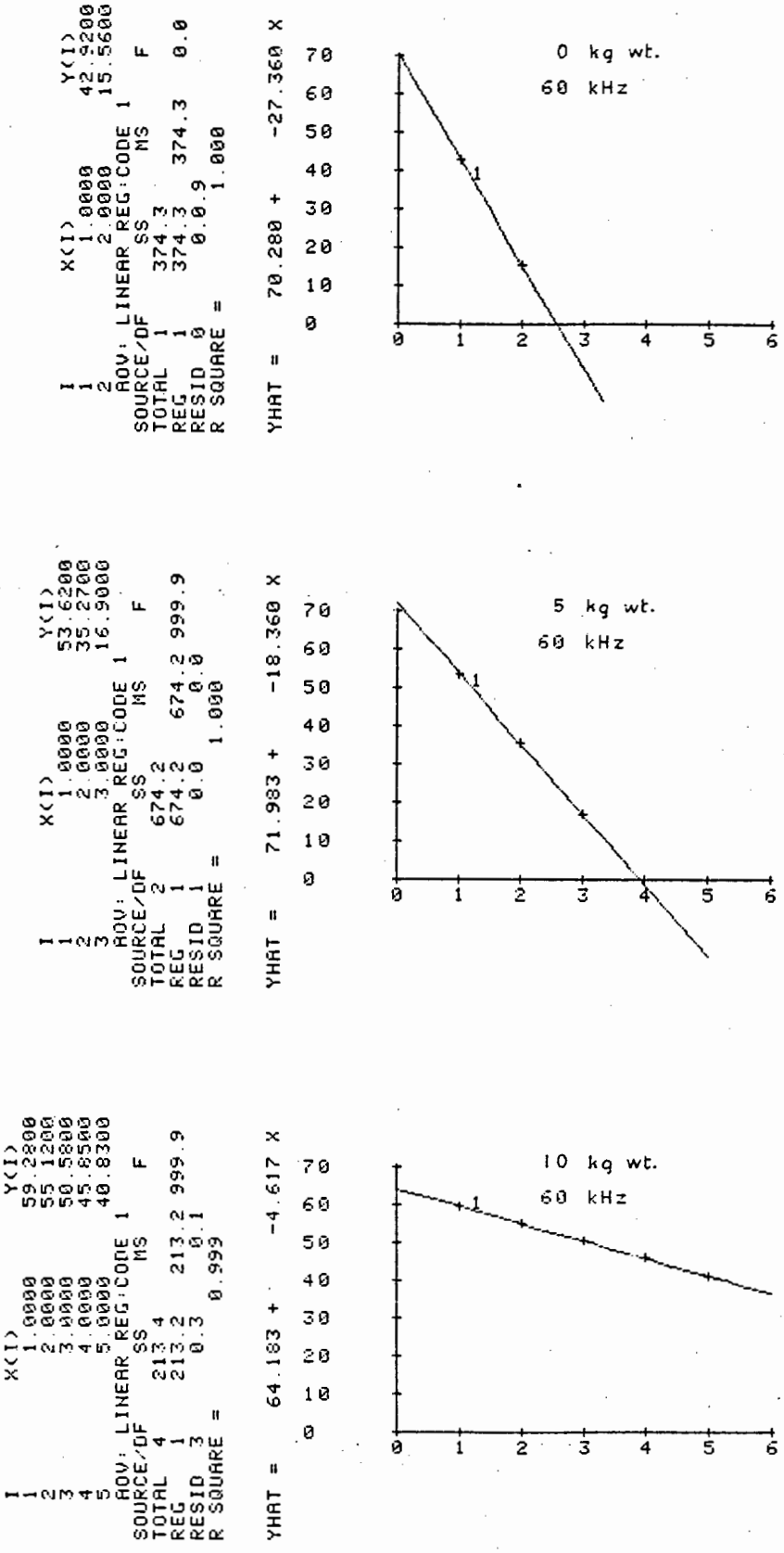

Figure 5-2-1. Examples of computer graphs of relative magnitudes of echo signals in decibels for annealed nickel wire subjected to tensile loading. The diagrams are reduced in size in the ratio of $1:\sqrt{2}$.

Note on the Curves of Figures 5-2-2 and 5-3-2

The curves of Figures 5-2-2 and 5-3-2 were drawn at about the time of the experimental work from values of attenuation derived by ordinary arithmetic from the values given in Tables 5-2-1 and 5-3-1, and were not drawn, as had been intended, and as is stated in the text, from the values in Tables 5-2-2 and 5-3-2, derived by computer.

The method of ordinary arithmetic is as follows:

If there are n readings of magnitudes of echo signals for a given setting of attenuation, and if V_1 and V_n are the voltages of, respectively, the first and last echo signals measured, then

$$\text{mean attenuation per round of travel, in decibels} = 20 \log_{10} \left(\frac{V_1}{V_n} \right)^{\frac{1}{n-1}}$$

$$= \frac{20}{n-1} \log_{10} \frac{V_1}{V_n}$$

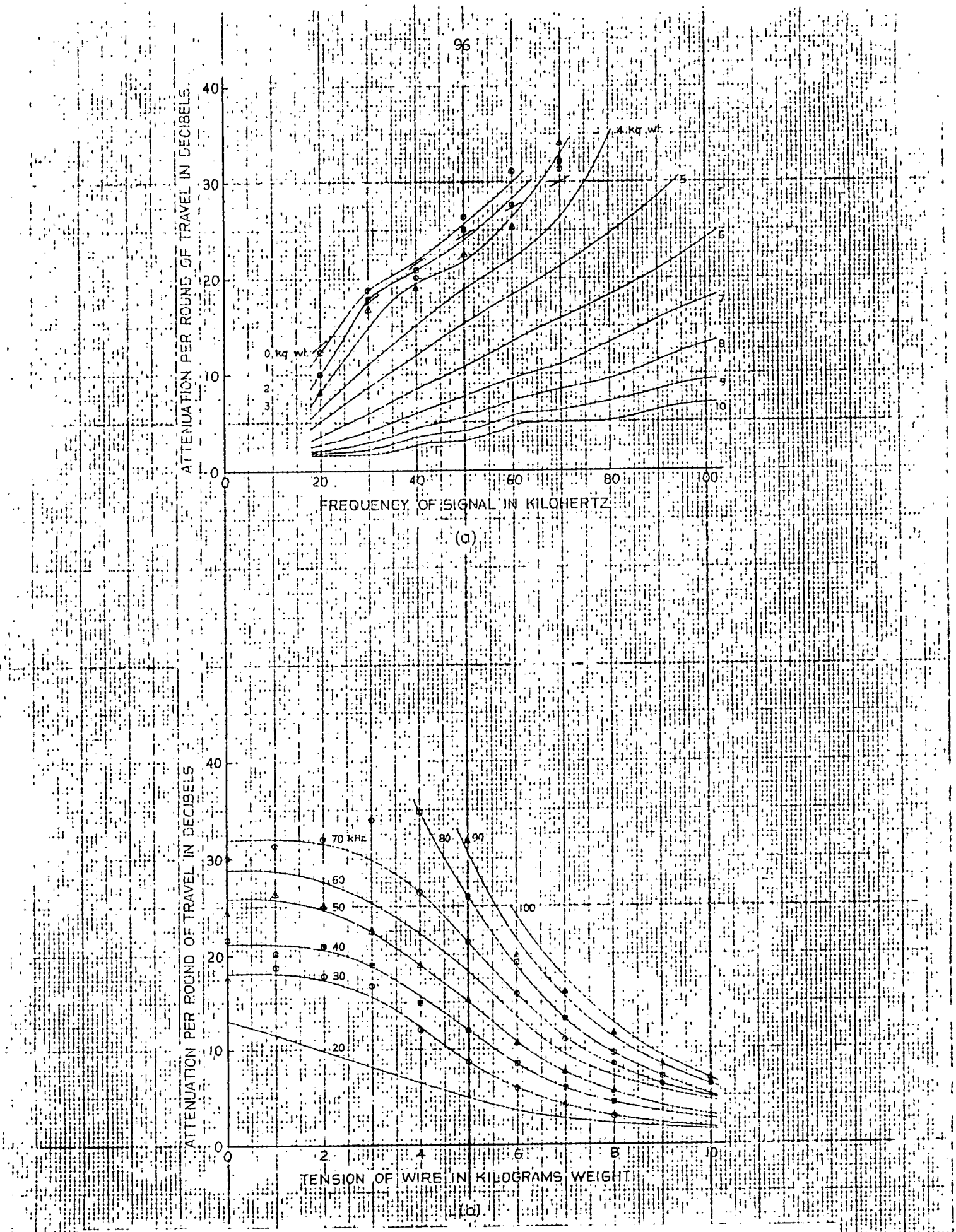

Figure 5-2-2. Curves showing the variation of attenuation of longitudinal, ultrasonic waves in annealed 1,52-mm-diameter nickel wire with signal frequency and with static tension of the wire.

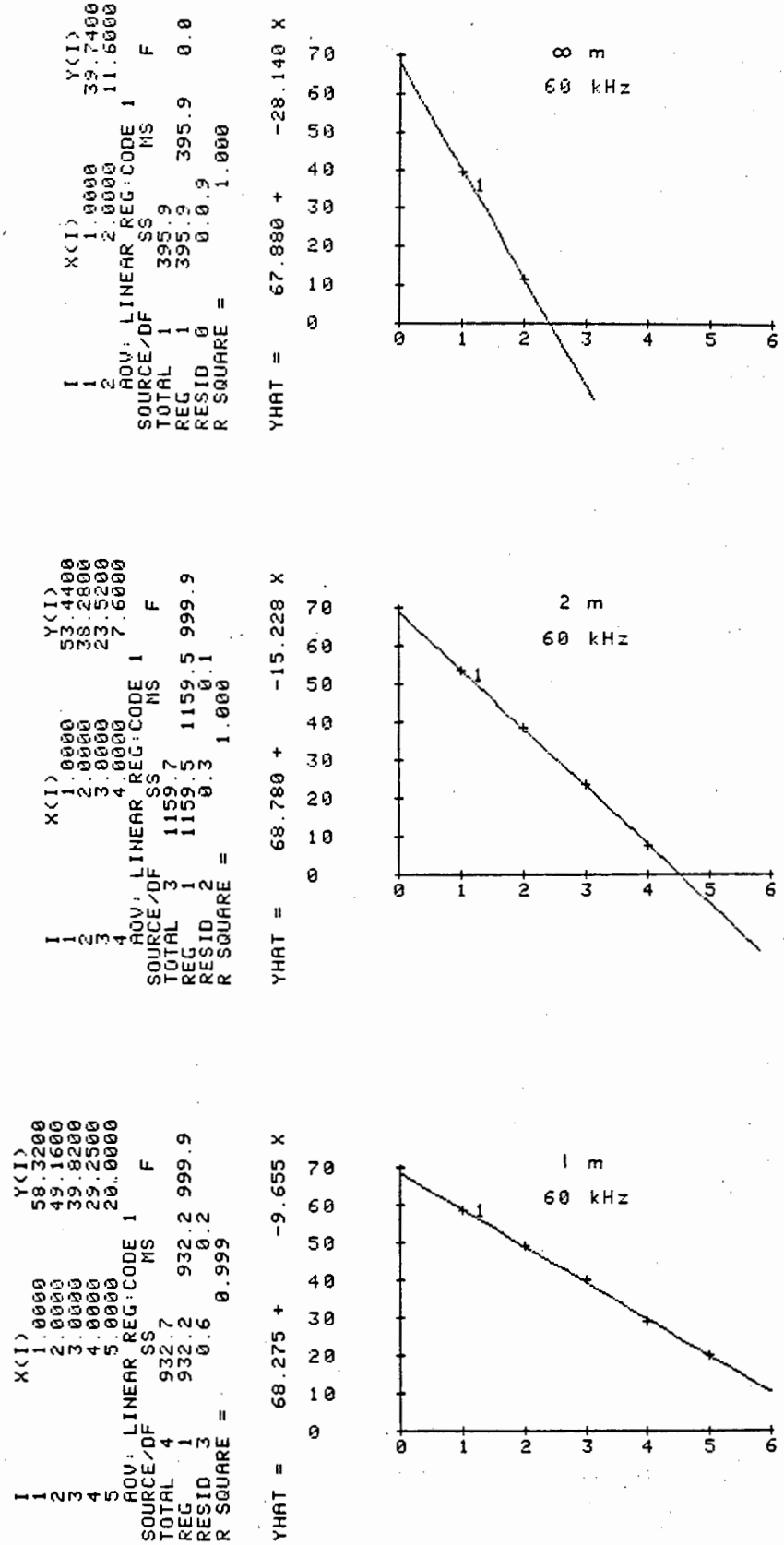

Figure 5-3-1. Examples of computer graphs of relative magnitudes of echo signals in decibels for an annealed nickel wire subjected to uniform flexure for a large part of its length; radii of curvature are shown. The diagrams are reduced in size in the ratio of $1:\sqrt{2}$.

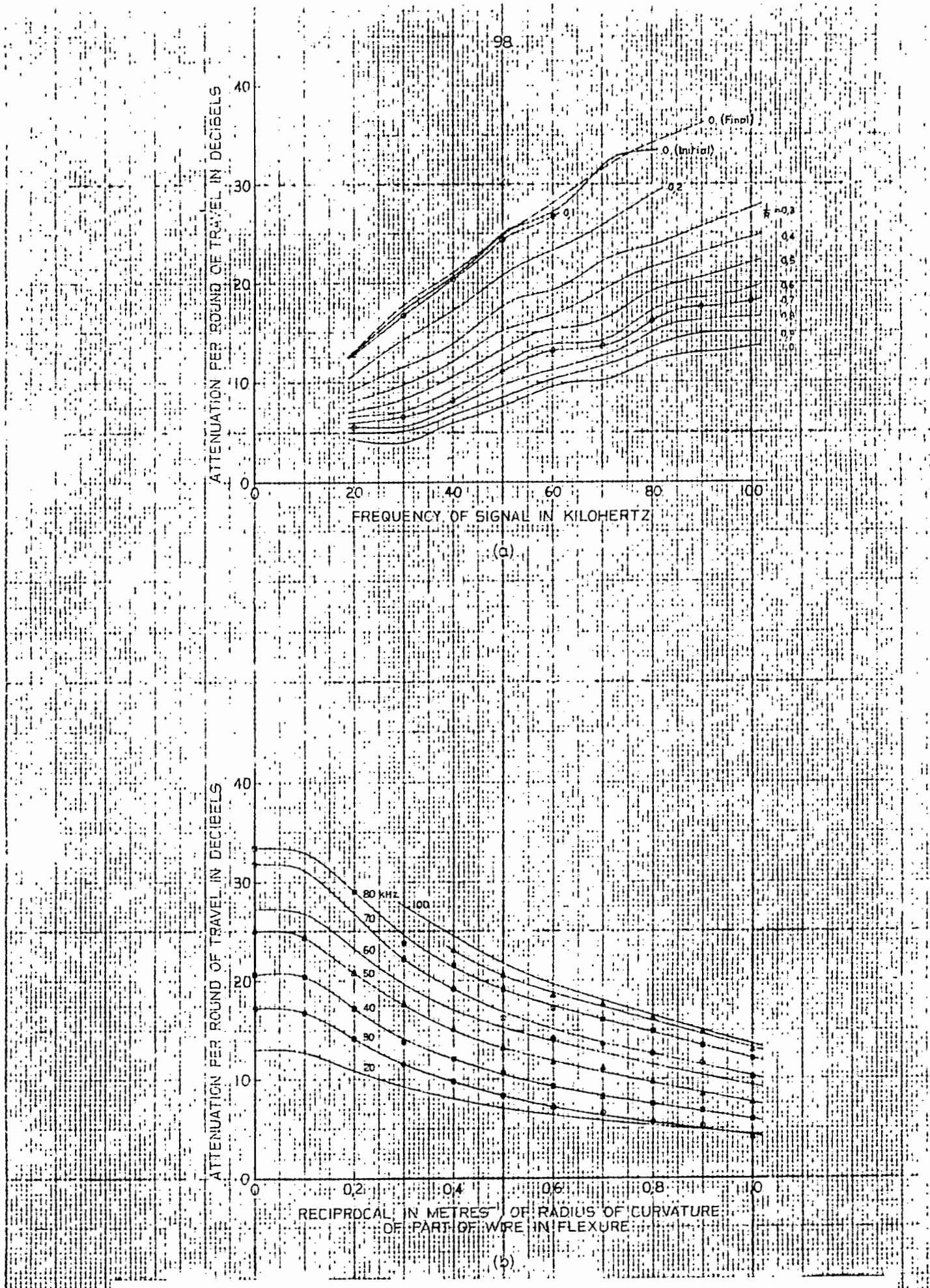

Figure 5-3-2. Curves showing the variation of attenuation of longitudinal, ultrasonic waves in annealed 1,52-mm-diameter nickel wire with signal frequency and with flexure of the wire.

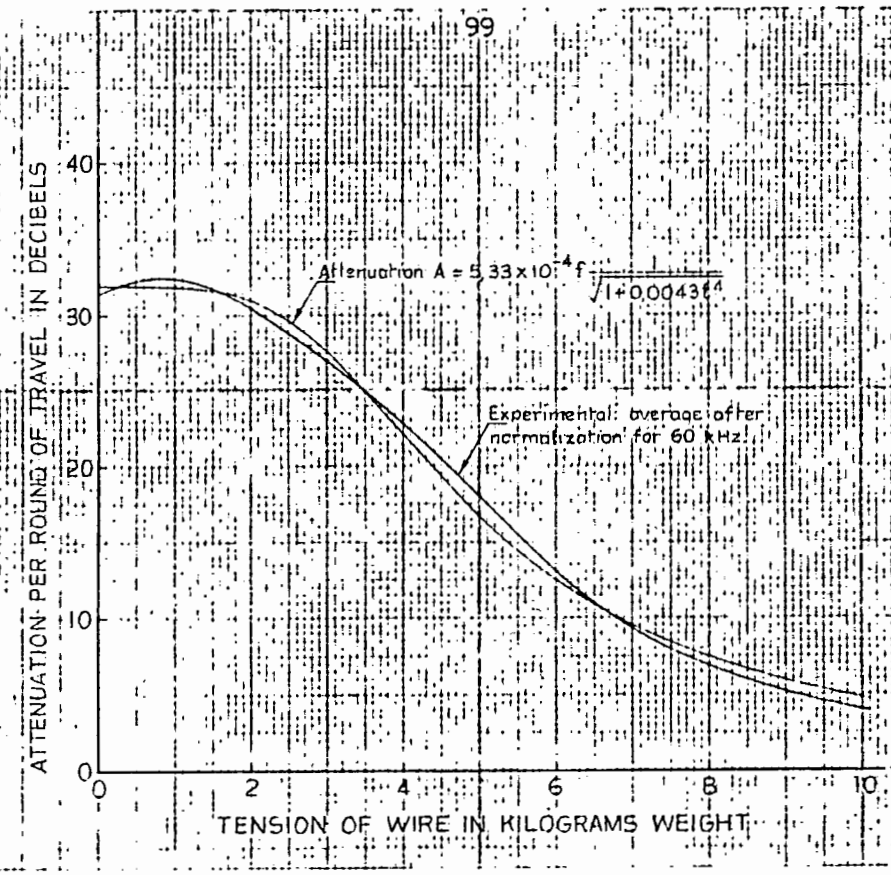

Figure 5-4-1. Experimental and fitted curves of attenuation of longitudinal, ultrasonic waves in annealed 1,52-mm-diameter nickel wire as a function of static tension of the wire.

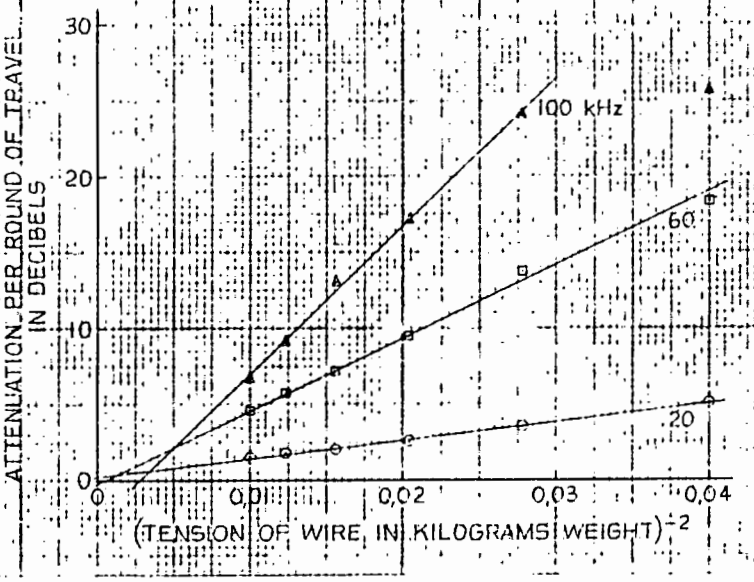

Figure 5-4-2. Graph to show the existence, for tensions of larger magnitude, of an approximately inverse-square relationship between the attenuation of longitudinal, ultrasonic waves in annealed 1,5-mm-diameter nickel wire and static tension of the wire.

Table 5-2-1

Tension of wire in kilograms weight	Peak-to-peak magnitudes of echo signals, in millivolts, and values in decibels with respect to 1 millivolt									
	For signal frequency of 20 kHz					For signal frequency of 30 kHz				
	For echo No.1	For echo No.2	For echo No.3	For echo No.4	For echo No.5	For echo No.1	For echo No.2	For echo No.3	For echo No.4	For echo No.5
0	760	160	38			560	70	10		
	57,62	44,08	31,60			54,96	36,90	20,00		
1	700	155	35	10		520	65	7		
	56,90	43,81	30,88	20,00		54,32	36,26	16,90		
2	640	182	50	17	6	600	85	10		
	56,12	45,20	33,98	24,61	15,56	55,56	38,59	20,00		
3	770	270	100	42	18	640	120	21	2	
	57,73	48,63	40,00	32,46	25,11	56,12	41,58	26,44	6,02	
4	660	311	150	73	34	775	200	50	12	
	56,39	49,86	43,52	37,27	30,63	57,79	46,02	33,98	21,58	
5	730	400	238	128	68	840	295	125	38	15,5
	57,27	52,04	47,53	42,14	36,65	58,49	49,40	41,94	31,60	23,81
6	630	405	278	183	120	850	410	208	107	58
	55,99	52,15	48,88	45,25	41,58	58,59	52,26	46,36	40,59	35,27
7	558	402	307	230	170	700	433	268	160	108
	54,93	52,08	49,74	47,23	44,61	56,90	52,73	48,56	44,08	40,67
8	485	381	307	243	188	621	441	309	208	161
	53,71	51,62	49,74	47,71	45,48	55,86	52,89	49,80	46,36	44,14
9	400	328	270	214	177	499	380	288	219	178
	52,04	50,32	48,63	46,61	44,96	53,96	51,60	49,19	46,81	45,01
10	339	281	240	199	170	390	325	261	220	184
	50,60	48,97	47,60	45,98	44,61	51,82	50,24	48,33	46,85	45,30

Table 5-2-1 (continued)

Tension of wire in kilograms weight	Peak-to-peak magnitudes of echo signals, in millivolts, and values in decibels with respect to 1 millivolt									
	For signal frequency of 40 kHz					For signal frequency of 50 kHz				
	For echo No.1	For echo No.2	For echo No.3	For echo No.4	For echo No.5	For echo No.1	For echo No.2	For echo No.3	For echo No.4	For echo No.5
0	360	30				265	16			
	51,13	29,54				48,46	24,08			
1	310	25	3			208	10			
	49,83	27,96	9,54			46,36	20,00			
2	365	30	3			252	14			
	51,25	29,54	9,54			48,03	22,92			
3	475	56	6			345	26			
	53,53	34,96	15,56			50,76	28,30			
4	620	110	20			492	56	6,5		
	55,85	40,83	26,02			53,84	34,96	16,26		
5	850	225	60	15,5	3,5	690	128	22	3,5	
	58,59	47,04	35,56	23,81	10,88	56,78	42,14	26,85	10,88	
6	985	370	143	54	20	912	273	80	24	7
	59,87	51,36	43,11	34,65	26,02	59,20	48,72	38,06	27,60	16,90
7	1 040	527	272	142	71	1 036	420	179	72	32
	60,34	54,44	48,69	43,05	37,03	60,31	52,46	45,06	37,15	30,10
8	920	561	348	216	123	1 000	523	282	149	80
	59,28	54,98	50,83	46,69	41,80	60,00	54,37	49,00	43,46	38,06
9	730	488	340	232	148	876	540	340	208	159
	57,27	53,77	50,63	47,31	43,41	58,85	54,65	50,63	46,36	44,03
10	572	421	320	250	171	768	538	378	270	188
	55,15	52,49	50,10	47,96	44,66	57,71	54,62	51,55	48,63	45,48

Table 5-2-1 (continued)

Tension of wire in kilograms weight	Peak-to-peak magnitudes of echo signals, in millivolts, and values in decibels with respect to 1 millivolt									
	For signal frequency of 60 kHz					For signal frequency of 70 kHz				
	For echo No.1	For echo No.2	For echo No.3	For echo No.4	For echo No.5	For echo No.1	For echo No.2	For echo No.3	For echo No.4	For echo No.5
0	140	6				95	3			
	42,92	15,56				39,55	9,54			
1	108	3				74	2			
	40,67	9,54				37,38	6,02			
2	120	5				80	2			
	41,58	13,98				38,06	6,02			
3	185	10				150	3			
	45,34	20,00				43,52	9,54			
4	305	24				158	7,5			
	49,69	27,60				43,97	17,50			
5	480	58	7			350	30			
	53,62	35,27	16,90			50,88	29,54			
6	712	147	33	6		540	88	14		
	57,05	43,35	30,37	15,56		54,65	38,89	22,92		
7	790	260	90	27	10	758	215	58	17	
	57,95	48,30	39,08	28,63	20,00	57,59	46,65	35,27	24,61	
8	778	335	148	65		796	300	116	44	
	57,82	50,50	43,41	36,26		58,02	49,54	41,29	32,87	
9	892	470	245	125		796	396	188	90	46
	59,01	53,44	47,78	41,94		58,02	51,95	45,48	39,08	33,26
10	920	570	338	196	110	990	555	316	182	104
	59,28	55,12	50,58	45,85	40,83	59,91	54,89	49,99	45,20	40,34

Table 5-2-1 (continued)

Tension of wire in kilograms weight	Peak-to-peak magnitudes of echo signals, in millivolts, and values in decibels with respect to 1 millivolt									
	For signal frequency of 80 kHz					For signal frequency of 90 kHz				
	For echo No.1	For echo No.2	For echo No.3	For echo No.4	For echo No.5	For echo No.1	For echo No.2	For echo No.3	For echo No.4	For echo No.5
0	60									
1	45									
2	50									
3	75 37,50	3 9,54				44				
4	110 40,83	2 6,02				68				
5	240 47,60	12 21,58				155 43,81	4 12,04			
6	340 50,63	37 31,36				245 47,78	22 26,85	2,5 7,96		
7	573 55,16	128 42,14	26 28,30	6 15,56		408 52,21	68 36,65	10 20,00		
8	720 57,15	238 47,53	76 37,62	24 27,60	9 19,08	535 54,57	145 43,23	38 31,60	10 20,00	
9	782 57,86	340 50,63	148 43,41	68 36,65	30 29,54	695 56,84	258 48,23	103 40,26	38 31,60	15 23,52
10	900 59,08	488 53,77	262 48,37	147 43,35	83 38,38	826 58,34	402 52,08	196 45,85	97 39,74	47 33,44

Table 5-2-1 (continued)

Tension of wire in kilograms weight	Peak-to-peak magnitudes of echo signals, in millivolts, and values in decibels with respect to 1 millivolt				
	For signal frequency of 100 kHz				
	For echo No.1	For echo No.2	For echo No.3	For echo No.4	For echo No.5
0					
1					
2					
3					
4					
5	95 39,55	5 13,98			
6	160 44,08	10 20,00			
7	301 49,57	42 32,46			
8	400 52,04	98 39,82	20 26,02		
9	535 54,57	182 45,20	70 36,90	23 27,23	7,5 17,50
10	652 56,28	292 49,31	142 43,05	72 37,15	28 28,94

Table 5-2-2

Tension of wire in kilograms weight	Mean attenuation of echo signal per round, in decibels								
	For signal frequency, in kilohertz, of								
	20	30	40	50	60	70	80	90	100
0	13,01	17,48	21,59	24,38	27,36	30,01			
1	12,36	18,71	20,15	26,36	31,13	31,36			
2	10,17	17,78	20,86	25,11	27,60	32,04			
3	8,14	16,54	18,99	22,46	25,34	33,98	27,96		
4	6,41	12,07	14,92	18,79	22,09	26,47	34,81		
5	5,11	8,72	11,87	15,30	18,36	21,34	26,02	31,77	25,57
6	3,57	5,83	8,44	10,57	13,75	15,87	19,27	19,91	24,08
7	2,55	4,11	5,80	7,57	9,56	11,03	13,26	16,11	17,11
8	2,04	3,00	4,33	5,48	7,18	8,37	9,61	11,53	13,01
9	1,79	2,27	3,42	3,79	5,69	6,24	7,06	8,33	9,21
10	1,50	1,64	2,55	3,05	4,62	4,88	5,18	6,21	6,68

Table 5-3-1

Radius of curvature of wire in metres	Peak-to-peak magnitudes of echo signals, in millivolts, and values in decibels with respect to 1 millivolt									
	For signal frequency of 20 kHz					For signal frequency of 30 kHz				
	For echo No.1	For echo No.2	For echo No.3	For echo No.4	For echo No.5	For echo No.1	For echo No.2	For echo No.3	For echo No.4	For echo No.5
∞	500	115	25,8	6,2	1,3	345	45	6,5	0,9	
	53,98	41,21	28,23	15,85	2,28	50,76	33,06	16,26	-0,92	
1	946	724	373	215	130	964	752	415	225	150
	59,52	57,19	51,43	46,65	42,28	59,68	57,52	52,36	47,04	43,52
10/9	940	672	340	170	95	952	666	338	172	88
	59,46	56,55	50,63	44,61	39,55	59,57	56,47	50,58	44,71	38,89
1,25	932	625	288	136	67	950	604	283	140	71
	59,39	55,92	49,19	42,67	36,52	59,55	55,62	49,04	42,92	37,03
10/7	920	576	248	138		920	520	227	105	45
	59,28	55,21	47,89	42,80		59,28	54,32	47,12	40,42	33,06
10/6	884	520	210	90		805	378	156	66,5	31
	58,93	54,32	46,44	39,08		58,12	51,55	43,86	36,46	29,83
2	852	440	170	74		824	343	120	46	17,5
	58,61	52,87	44,61	37,38		58,32	50,71	41,58	33,26	24,86
2,5	800	350	123			783	265	84	27	
	58,06	50,88	41,80			57,88	48,46	38,49	28,63	
10/3	732	266	86			678	185	49,5	12,7	
	57,29	48,50	38,69			56,62	45,34	33,89	22,08	
5	584	165	50			498	95,4	19		
	55,33	44,35	33,98			53,94	39,59	25,58		
10	466	103	24			370	52	7,8		
	53,37	40,26	27,60			51,36	34,32	17,84		
∞	434	96	19	4,8		320	40,8	5,2	0,7	
	52,75	39,65	25,58	13,62		50,10	32,21	14,32	-3,10	

Table 5-3-1 (continued)

Radius of curvature of wire in metres	Peak-to-peak magnitudes of echo signals, in millivolts, and values in decibels with respect to 1 millivolt									
	For signal frequency of 40 kHz					For signal frequency of 50 kHz				
	For echo No.1	For echo No.2	For echo No.3	For echo No.4	For echo No.5	For echo No.1	For echo No.2	For echo No.3	For echo No.4	For echo No.5
∞	247	22,3	2,1	0,2		158	9,7	0,5		
	47,85	26,97	6,44	-13,98		43,97	19,74	-6,02		
1	952	584	273	134	62	908	435	173	73	27
	59,57	55,33	48,72	42,54	35,85	59,16	52,77	44,76	37,27	28,63
10/9	936	496	218	104	41	872	350	128	47,5	17,8
	59,43	53,91	46,77	40,34	32,26	58,81	50,88	42,14	33,53	25,01
1,25	920	430	177	78	29	806	275	92	29,5	9,4
	59,28	52,67	44,96	37,84	29,25	58,13	48,79	39,28	29,40	19,46
10/7	884	355	130	51	20,5	776	224	65	19,5	4,8
	58,93	51,00	42,28	34,15	26,24	57,80	47,00	36,26	25,80	13,62
10/6	815	278	90	33,7	11,2	715	180	48	12,8	3,2
	58,22	48,88	39,08	30,55	20,98	57,09	45,11	33,62	22,14	10,10
2	795	225	66	20	6	610	128	28,6	6,3	
	58,01	47,04	36,39	26,02	15,56	55,71	42,14	29,13	15,99	
2,5	630	152	36,5	9,7		483	83	14,8		
	55,99	43,64	31,25	19,74		53,68	38,38	23,41		
10/3	547	109	21	4,5		392	51,5			
	54,76	40,75	26,44	13,06		51,87	34,24			
5	379	50,7	7,2			246	22,2	2,1		
	51,57	34,10	17,15			47,82	26,93	6,44		
10	275	26,3	2,5			174	10,5			
	48,79	28,40	7,96			44,81	20,42			
∞	243	20,8	1,9			148	8,5			
	47,71	26,36	5,58			43,41	18,59			

Table 5-3-1 (continued)

Radius of curvature of wire in metres	Peak-to-peak magnitudes of echo signals, in millivolts, and values in decibels with respect to 1 millivolt									
	For signal frequency of 60 kHz					For signal frequency of 70 kHz				
	For echo No.1	For echo No.2	For echo No.3	For echo No.4	For echo No.5	For echo No.1	For echo No.2	For echo No.3	For echo No.4	For echo No.5
∞	105	4,4	0,2			58,2	1,5			
	40,42	12,87	-13,98			35,30	3,52			
1	824	287	98	29	10	686	207	61	19	6,4
	58,32	49,16	39,82	29,25	20,00	56,73	46,32	35,71	25,58	16,12
10/9	792	252	80	24,5	7,8	592	154	39	9,8	2,8
	57,97	48,03	38,06	27,78	17,84	55,45	43,75	31,82	19,82	8,94
1,25	678	184	51,2	14,2	3,9	528	124	26,8	6,5	1,6
	56,62	45,30	34,19	23,04	11,82	54,45	41,87	28,56	16,26	4,08
10/7	622	138	32,6	7,5	1,5	460	92	18,3	3,7	0,9
	55,88	42,80	30,26	17,50	3,52	53,26	39,28	25,25	11,36	-0,92
10/6	575	137	25,6	5,2	1	408	72	12,7	2,5	0,6
	55,19	42,73	28,16	14,32	0,00	52,21	37,15	22,08	7,96	-4,44
2	470	82	15	2,4		328	47	6,7	1,2	
	53,44	38,28	23,52	7,60		50,32	33,44	16,52	1,58	
2,5	363	51,5	7,6			252	27,8	3,0		
	51,20	34,24	17,62			48,03	28,88	9,54		
10/3	282	31	3,3			187	14,6			
	49,00	29,83	10,37			45,44	23,29			
5	168	11,6				102				
	44,51	21,29								
10	113	5,2				63				
	41,06	14,32								
∞	97	3,8				53				
	39,74	11,60								

Table 5-3-1 (continued)

Radius of curvature of wire in metres	Peak-to-peak magnitudes of echo signals, in millivolts, and values in decibels with respect to 1 millivolt									
	For signal frequency of 80 kHz					For signal frequency of 90 kHz				
	For echo No.1	For echo No.2	For echo No.3	For echo No.4	For echo No.5	For echo No.1	For echo No.2	For echo No.3	For echo No.4	For echo No.5
∞	37,5	0,8				18,8				
	31,48	-1,94								
1	487	128	30,5	8	1,9	337	74	17	3,9	
	53,75	42,14	29,69	18,06	5,58	50,55	37,38	24,61	11,82	
10/9	438	100	22,5	5,0	0,9	280	51,5	10	1,7	
	52,83	40,00	27,04	13,98	-0,92	48,94	34,24	20,00	4,61	
1,25	383	71,4	13,3	2,2		243	38	6,1	0,9	
	51,66	37,07	22,48	6,85		47,71	31,60	15,71	-0,92	
10/7	312	51,5	8,2	1,2		200	26,5	3,5		
	49,88	34,24	18,28	1,58		46,02	28,46	10,88		
10/6	266	37,6	5,7	0,7		170	20	2,4		
	48,50	31,50	15,12	-3,10		44,61	26,02	7,60		
2	206	22,8	2,5			134	11,9	1,2		
	46,28	27,16	7,96			42,54	21,51	1,58		
2,5	157	13	1,1			94	6,6			
	43,92	22,28	0,83			39,46	16,39			
10/3	114	7,4				66,2				
	41,14	17,38								
5	65	2,3				32				
	36,26	7,23								
10	39,6					21,2				
∞	34,4	0,6				17	0,3			
	30,73	-4,44				24,61	-10,46			

Table 5-3-1 (continued)

Radius of curvature of wire in metres	Peak-to-peak magnitudes of echo signals, in millivolts, and values in decibels with respect to 1 millivolt				
	For signal frequency of 100 kHz				
	For echo No.1	For echo No.2	For echo No.3	For echo No.4	For echo No.5
∞	11,3				
1	212	43,5	9,5	2,0	
	46.53	32,77	19,55	6,02	
10/9	178	30,5	5,7	1	
	45,01	29,69	15,12	0,00	
1,25	150	22,2	3,3	0,5	
	43,52	26,93	10,37	-6,02	
10/7	122	15,2	1,9		
	41,73	23,64	5,58		
10/6	106	11,3	1,2		
	40,51	21,06	1,58		
2	79	6,1	0,5		
	37,95	15,71	-6,02		
2,5	56	3,3			
	34,96	10,37			
10/3	40,8	1,7			
	32,21	4,61			
5	18,6				
10	12,3				
∞	10,7				

Table 5-3-2

Radius of curvature of wire in metres	Mean attenuation of echo signal per round, in decibels For signal frequency, in kilohertz, of								
	20	30	40	50	60	70	80	90	100
∞	12,88	17,18	20,60	25,00	27,20	31,78	33,42		
1	4,50	4,28	6,02	7,66	9,66	10,20	12,04	12,90	13,48
10/9	5,18	5,31	6,79	8,50	10,05	11,70	13,35	14,72	14,96
1,25	5,90	5,77	7,49	9,67	11,19	12,64	14,90	16,18	16,52
10/7	5,68	6,63	8,22	10,96	13,00	13,63	16,09	17,57	18,08
10/6	6,74	7,17	9,28	11,70	13,88	14,25	17,12	18,51	19,47
2	7,20	8,44	10,59	13,22	15,23	16,31	19,16	20,48	21,99
2,5	8,13	9,77	12,11	15,14	16,79	19,25	21,55	23,07	24,59
10/3	9,30	9,77	13,94	17,63	19,32	22,15	23,76		27,60
5	10,68	14,18	17,21	20,69	23,22		29,03		
10	12,89	16,76	20,42	24,39	26,74				
∞	13,15	17,75	21,07	24,82	28,14		35,17	35,07	

Table 5-4-1. Normalized Values of Attenuation

Tension of wire in kilograms weight	Mean attenuation of echo signal per round, in decibels, normalized for a signal frequency of 60 kHz									
	For original signal frequency, in kilohertz, of									Average value
	20	30	40	50	60	70	80	90	100	
0	39,03	34,96	32,39	29,26	27,36	25,72				31,45
1	37,08	37,42	30,23	31,63	31,13	26,88				32,40
2	30,51	35,56	31,29	30,13	27,60	27,46				30,43
3	24,42	33,08	28,49	26,95	25,34	29,13	20,97			26,91
4	19,23	24,14	22,38	22,55	22,09	22,69	26,11			22,74
5	15,33	17,44	17,81	18,36	18,36	18,29	19,52	21,18	15,34	17,96
6	10,71	11,66	12,66	12,68	13,75	13,60	14,45	13,27	14,45	13,03
7	7,65	8,22	8,70	9,08	9,56	9,45	9,95	10,74	10,27	9,29
8	6,12	6,00	6,50	6,58	7,18	7,17	7,21	7,69	7,81	6,92
9	5,37	4,54	5,13	4,55	5,69	5,35	5,30	5,55	5,53	5,22
10	4,50	3,28	3,83	3,66	4,62	4,18	3,89	4,14	4,01	4,01

BIBLIOGRAPHY

Bell, J.F.W. Transmission of Plane Longitudinal and Torsional Waves. Notes.

Brailsford, F. 1960. Magnetic Materials. Third edition. London : Methuen.

Brailsford, F. 1968. An Introduction to the Magnetic Properties of Materials. Separate edition. London : Longmans.

Bratina, W.J. 1966. Internal Friction and Basic Fatigue Mechanisms in Body-Centred Cubic Metals, Mainly Iron and Carbon Steels in Mason, W.P. editor. Physical Acoustics, volume III, part A. (1st edition). New York : Academic Press.

Crawford, A.E. 1955. Ultrasonic Engineering. (1st edition). London : Butterworths.

Gordon, R.S. 1982. Digitally Controlled Signal Burst Generator. B.Sc. thesis in electrical engineering. University of Cape Town. (November 1982).

Granato, A.V. and Lücke, K. 1966. The Vibrating String Model of Dislocation Damping in Mason, W.P. editor. Physical Acoustics, volume IV, part A. (1st edition). New York : Academic Press.

Hueter, F.T. and Bolt, R.H. 1955. Sonics. (1st edition). New York : John Wiley and Sons.

Kinsler, L.E. and Frey, A.R. 1950. Fundamentals of Acoustics. (1st edition). New York : John Wiley and Sons.

Mason, W.P. 1958. Physical Acoustics and the Properties of Solids. (1st edition). Princeton : van Nostrand.

Mason, WP. 1968. editor. Physical Acoustics. (1st edition). New York : Academic Press.

Morley, A. 1940. Strength of Materials. 9th edition. London : Longmans, Green and Co.

Niblett, D.H. 1966. Bordoni Peak in Face-Centred Cubic Metals in Mason, W.P. editor. Physical Acoustics, volume III, part A. (1st edition). New York : Academic Press.

Papadakis, E.P. 1968. Ultrasonic Attenuation Caused by Scattering in Polycrystalline Media in Mason, W.P. editor. Physical Acoustics, volume IV, part B. (1st edition). New York, Academic Press.

Pollard, H.F. 1977. Sound Waves in Solids. (1st edition). London : Pion Limited.

Sharp, J.C.K. 1974. A Theoretical and Experimental Investigation into the Spectra of Selected Resonators. Ph.D. thesis. University of Aston.

Smith, P.H. 1939. Transmission Line Calculator. Electronics, volume 12, p. 29, January, 1939.

Smith, P.H. 1944. An Improved Transmission Line Calculator. Electronics, volume 17, p. 130, January, 1944.

van Vlack, L.H. 1970. Materials Science for Engineers. (1st edition). Reading, Mass.: Addison-Wesley.